

**Covalent gold nanoparticle—antibody conjugates
for sensitivity improvement
in LFIA**

**A dissertation submitted to the Mathematics, Informatics and Natural Sciences
Faculty of
Hamburg University**

by Michael Ijeh

**in partial fulfillment of the
requirements for the degree of
Doctor of Philosophy
Chemistry**

December 2011

Reviewers:

1. Prof. Dr. Horst Weller
2. Prof. Dr. J.A.C. Broekaert

Date of Disputation: 15.12.2011

Dedicated to:

my mom Catherine, my wife Margret

and my children

Noah and Alicia

*What you get by achieving your goals is not as important as what you become
by achieving your goals.*

- Goethe

CONTENTS

ABSTRACT	1
<hr/>	
1. INTRODUCTION	4
<hr/>	
2. OBJECTIVES	9
<hr/>	
3. THEORITICAL BACKGROUND	11
<hr/>	
3.1 Optical Properties of gold nanoparticle (AuNP)	11
3.2 Dielectric functions and Extinction coefficient of AuNP	13
3.3 Extinction cross section and optical density	15
3.4 Antibody (IgG)	18
3.5 Lateral Flow Immunochromatography Assay (LFIA)	21
3.6 Synthesis of metallic nanoparticles	24
3.7 AuNP-IgG conjugate	26
3.7.1 AuNP-IgG Coupling	
3.7.1.1 Physical interaction (electrostatic coupling)	
3.7.1.2 Chemical interaction (covalent coupling)	
3.8 Analytical methods	29
3.8.1 Transmission Electron Microscopy (TEM)	
3.8.2 UV-Vis	
3.8.3 Dynamic Light Scattering (DLS)	
3.8.4 Zeta Potential, ζ.	
3.8.4.1 The DLVO theory	
3.8.5 Densitomerical analysis.	

4.	EXPERIMENTAL WORK	36
<hr/>		
4.1	Materials and Equipments	36
4.2	AuNP Synthesis	36
	4.2.1 Citrate-stabilised 10-13 nm AuNPs	
	4.2.2 Citrate-stabilised AuNPs (Seed-Growth Method)	
	4.2.3 AuNP concentration determination	
4.3	AuNP coupling and analysis	41
	4.3.1 Oxidation of antibodies	
	4.3.2 Purpald test	
	4.3.3 Attachment of oxidized antibodies to PEG linkers	
	4.3.4 Ligand Exchange reactions	
	4.3.5 Bradford protein analysis	
4.4	ImmunTest	45
5.	RESULTS AND DISCUSSION	47
<hr/>		
5.1	Citrate stabilized AuNP and AuNP-RIgG conjugates	47
	5.1.1 Sizes, Shapes and optical absorption of AuNP	
	5.1.2 Dynamic light scattering (DLS)	
	5.1.3 UV-Vis Spectroscopy	
5.2	Antibody oxidation	55
5.3	Ligand exchange products	57
	5.3.1 UV-Vis absorption measurements of exchange reaction products	
	5.3.2 DLS measurements of exchange reaction products	
5.4	Conjugate's stability	60
	5.4.1 Effects of solution's ionic strength	
	5.4.2 Conjugate's absorption behaviour with storage time	
	5.4.3 Effects of ligand length	
	5.4.4 LCC (Lowest Coagulation Concentration)	

5.4.5	<i>Bulky Cap Packaging effect</i>	
5.4.6	<i>Effects of particle size and ligand length on AuNP Properties</i>	
5.5	AuNP surface coverage	87
5.5.1	<i>DLS based calculation</i>	
5.5.2	<i>LCC method</i>	
5.5.2.1	<i>Particle core size and ligand length</i>	
5.5.3	<i>Bradford method</i>	
5.5.4	<i>LCC vs Bradford</i>	
5.6	Functionality tests of AuNP-RIGG conjugates	103
5.6.1	Immuno Blot Assays	
5.6.2	Effect of particle size on sensitivity	
5.6.3	Liquid phase reactivity of conjugates	
5.6.3.1	<i>DLS analysis</i>	
5.6.3.2	<i>TEM analysis</i>	
6.	CONCLUSION	111
<hr/>		
7.	REFERENCES	113
<hr/>		
	APPENDIX	121
<hr/>		
	Risk and Safety Information	
	Acknowledgements	
	Publications	
	Curriculum Vitae	
	Declaration	

ABSTRACT

The early part of this work involves the synthesis of citrate stabilized gold nanoparticles. Protocols which enabled the preparation of approximately 10 nm – 100 nm spherical particles with narrow size distribution were used. The obtained particles were successively characterized using TEM, DLS and UV-Vis spectroscopy. The ability to prepare particles having varying sizes enabled investigation of size effect on conjugate properties. Prior to the attachment to AuNPs, thiolated polyethylene glycol (PEG) ligands were linked to specific region of the antibodies to confer conjugate stability and antibody orientation on particle surface. The obtained conjugates from AuNP and antibodies were characterized with UV-Vis spectroscopy, Zeta Potential and DLS measurements. Consequent to the conjugate preparation, series of extensive investigations were carried out on their stability, surface coverage and reactivity. The influence of PEG ligand (length) and nanoparticle core size on the stability of the conjugates was investigated.

The conjugates were found to be stable in buffer media and in salt solution with high ionic strengths. They showed antibody reactivity by specifically localizing target antigens on nitrocellulose membranes. The nanoparticles properties depended on the ligand length, particle size and surface coverage on antibody attachment.

Comparison of covalently coupled AuNP antibody conjugates with their electrostatically coupled counterpart revealed higher stability for the former. The stability could be influence by varying the polymer length of the linking PEG chain. The number of antibodies per particle (coverage) was similar for ligands with PEG weights of 5 kDa and 10 kDa molecular weights. Conjugates prepared with 3 kDa PEG ligands exhibited lower coverage values. Larger particles had more antibodies per particle (higher coverage) compared to the conjugates prepared with smaller sized particles. Similar ligand packaging on particles ($d \geq 20$ nm) was observed irrespective of size.

Finally, conjugates exhibited antibody reactivity in presence of their target antigens. TEM imaging and DLS measurement of particles also provided evidence of the antibody interactions. Sensitivity of the conjugates for the detection of antigens was shown to be influenced by variation of core metallic particles' sizes of the conjugates. The best candidates for the purpose of analyte detection were conjugates with core particles diameters within 30 nm – 45 nm.

ABSTRACT

Der erste Teil dieser Arbeit behandelt die Synthese von Citrat-stabilisierten Gold-Nanopartikeln. Hierzu wurden Verfahren angewendet, die eine Darstellung von Partikeln mit einer Größe zwischen 11-100 nm und einer engen Größenverteilung erlauben. Die erhaltenen Partikel wurden durch TEM, DLS und UV-Vis Spektroskopie charakterisiert. Weiterhin wurden Partikeleigenschaften untersucht, die sich von der Partikelgröße beeinflussen lassen.

Thioliertem Polyethylenglycol-Liganden (PEG) wurden an die Antikörper vor ihrer Immobilisierung auf die Partikeloberfläche angebunden. Diese dienen zur Partikelstabilisation und einer gezielten Orientierung der Antikörper. Konjugaten, die aus Gold-Nanopartikeln und Antikörpern hergestellt wurden. Die Charakterisierung erfolgte durch TEM, DLS und UV-Vis Spektroskopie und Zeta-Potential-Messungen. Außerdem wurden die Stabilität, die Oberflächenbelegung und die Reaktivität der Konjugate ausführlich untersucht.

Der Einfluss der PEG-Liganden und der Partikelgröße auf die Stabilität der Konjugate, sowie auf ihre allgemeine Leistungsfähigkeit, wurden ermittelt.

Die kovalent gebundenen Konjugaten blieben in Puffer- und Salzlösungen mit hoher Ionenstärke stabil. Sie zeigten Antikörperreaktivität, die durch spezifische Wechselwirkung mit Antigenen auf eine Nitrozellulose-Membran dokumentiert werden konnten. Die Eigenschaften der Konjugate waren abhängig von der Länge des Linkers, der Partikelgröße und der Oberflächenbelegung.

Der Vergleich von elektrostatisch und kovalent verbundenen Au-NP/Antikörper-Konjugaten zeigt eine höhere Stabilität der kovalent verknüpften Konjugate.

Die Partikeloberflächenbelegung ist vergleichbar und Ligandenunabhängig. Bei PEG-Liganden mit einem Molekulargewicht von 5 kDa und 10 kDa wird die Belegung außerdem durch die Partikelgröße beeinflusst.

Schließlich konnte die Reaktivität der Antikörper bezüglich der passenden Antigene nachgewiesen werden. Damit wurde die Kombination der beiden Komponenten demonstriert. TEM und DLS Messungen bestätigten diese Reaktivität.

Die Sensitivität der Konjugate für die Detektion der Antigene wurde durch die Größe der Kerngröße der metallischen Komponente beeinflusst. Für die Verwendung in LFIA-Anwendungen eignen sich besonders Partikel mit Durchmessern zwischen 30-45 nm.

1. INTRODUCTION

Nanotechnology is one of the fastest growing technologies of our time. Having made huge impact in the development and design of novel products, their application in medical fields has become revolutionary. Researchers are continued to be driven by the search for new materials, which have unique properties at the nano-scale regime. Their efforts are centered on the unique characteristic phenomena in this regime, which is governed by the principles of fundamental and applied science.

A nanoparticle is a material with dimensions in the nanometer scale usually less than 100 nm in its dimension. They contain a number of constituent atoms or molecules but can neither be treated as bulk nor as group of isolated atoms or molecules. The unique behaviors exhibited by materials at this dimension include some special chemical and physical properties. These may be of electronic, optical, magnetic or catalytic nature, which are highly valuable to life. For instance, solution of metallic nanoparticle of gold or silver shows unique optical property that has no existence in bulk [1, 2]. This unusual behavior is attributed to the large surface to volume ratio of the materials. For AuNP under the influence of an interacting incident light, the surface phenomenon, termed surface plasmon resonance (SPR), has been related to their unique optical properties [3]. The nanoparticle surface related properties are easily affected by size, shape and their surrounding dielectric environment [4].

In addition to their optical property, gold nanoparticles are resistant to oxide formation under ambient conditions. The nature of their surface chemistry promotes easy and controlled attachment of other molecules especially those with thiol functionalities. Following their exciting properties (chemical, electronic and optical) and the controllable morphology, gold nanoparticle based bioconjugates are found to be good candidates for biomedical applications. Their biocompatibility, high stability and ease of characterization [5-8] are some of their special properties that promote their diverse application. A number of diagnostic methods including selective cell and nuclear targeting, site-specific diagnosis and treatment of ailments involve the use of AuNPs as labels and vectors. Biosensor based on gold nanoparticles has been designed previously [9, 10]. The principle governing such methods is the interactions of biomolecule functionalized AuNPs with their targets resulting in aggregation. This has been used as means of identifying analytes in solutions. Aggregation causes changes in the optical absorption behavior of the particles. These changes could easily be monitored by eye.

Similarly, AuNP based immunoassays have been performed based on antigen-antibody interactions using AuNP antibody conjugates. Interaction of these conjugates with antigen caused shifts in the plasmon absorption peak [11].

Lateral Flow Immunochromatography assays (LFIAs) are useful innovation in nanotechnology, which are also based on AuNP antibody conjugates. They have shown wide applicability in medicine and research fields [12].

Unfortunately, there are some basic limitations of the present generation of handheld LFIA kits. For instance, assays have varying sensitivity levels with respect to their target agents [13]. Storage time of test results is limited due to poor stability of AuNP conjugates used for the fabrication. They are fabricated using AuNP antibody conjugates prepared by electrostatic coupling strategy. Electrostatic coupling strategy provides little room for innovation of AuNP conjugate systems. There is lack of possibility to vary surface properties of conjugates during preparation via the electrostatic attachment, which could be avoided by simply using covalent coupling for conjugate preparation. Some of the advantages of covalent attachment method over electrostatic method involve the possibility to use surface chemistry and do important investigations for product modification. Useful changes towards improvement of AuNP antibody conjugates performances in LFIA, should include conjugate modification using new coupling methods as suggested and demonstrated in this work.

An important advancement in the past was the replacement of the common organic dyes used in LFIA fabrication for gold nanoparticles. They have been easy-to-handle tools used to analyse varieties of bio-molecular binding interactions and used for point-of-care detection of analytes including pathogens and toxins [14-16].

The preparation of gold nanoconjugates in this thesis involved coupling of AuNPs to antibodies using chemical functionalities (glycan) present on specific regions of the molecules. A large number of conjugation protocols exist for preparation of bioconjugates [16-20] and figure 1.1 summarizes some of the most important strategies for labeling gold nanoparticle.

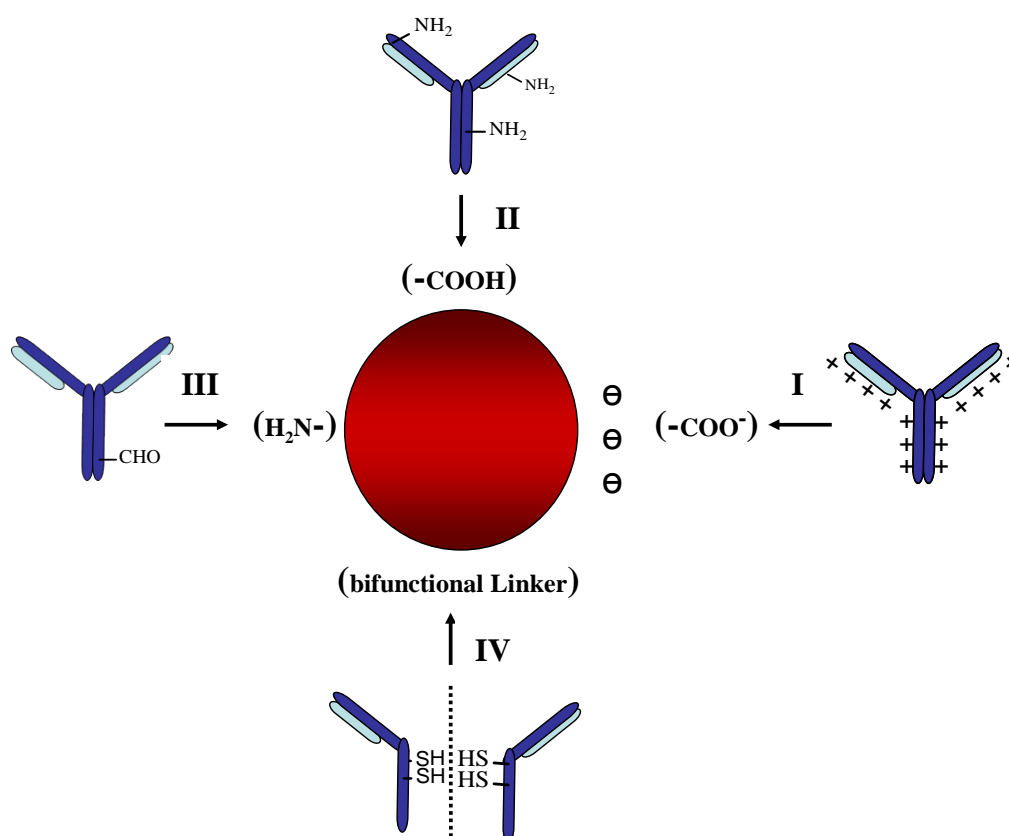


Figure 1.1: Coupling strategies (I) ionic interaction (II) EDC/NHS method (III) imine strategy (IV) antibody disulfide bond cleavage.

Starting with the most common strategy for gold nanoparticle bioconjugation, the ionic coupling strategy (route I, in figure 1.1), charged surfaces of two reacting partners are used for the binding of both components together in a conjugate. The surface charges of antibodies (IgG) for instance are positive at most coupling conditions and since the as-prepared citrate stabilized AuNP are negative, this becomes an advantage. Both reactants can easily interact electrostatically when the solutions are mixed. This method is very simple and time saving, and thus popular in laboratories. But the stability of the product conjugates is poor, since ionic interactions could easily be influenced by factors like pH, ionic strength, concentration and nature of solvent. In addition to stability, there are some problems facing the orientation of the antibodies on the nanoparticle surface for conjugates obtained by the ionic interaction strategy. An optimal orientation of the molecule on the particle surface is of vital importance. The region of the molecule (Fab regions, see figure 3.4) necessary for interaction with analyte should be directed away from the particle surface and free for interactions with targets in

solution. An electrostatic coupling event is of random nature and this has some drawbacks. If the Fab ends of IgGs are not free from hindrances, reactivity of the antibody becomes disadvantageously influenced. This becomes the case when the Fab regions of the antibody is oriented towards the particle surface hindering target recognition. Another event that could be another source of drawback is the alteration of particle's surface charge on attachment of IgG to particle surface. The particles could hereby suffer aggregation due to insufficient ionic repulsion with changes of the surface charge. This is a process that possibly ends in particle losses. The measures often taking in the electrostatic coupling strategy to avoid such particle losses is by using high excesses of antibody during the conjugate process and additional post-synthetic treatments which further stabilise the systems. These are cost intensive and intricate procedures which could be avoided especially for the fact that risks exists, that post treatment agents could even interact or compete with the antibody for spaces on the particle surface.

The other strategies suffer similar drawbacks like the electrostatic coupling method for AuNP antibody conjugates preparation. The EDC/NHS strategy poses the problem of orientation also, since the terminal lysine amine groups used for attachment to carboxyl group of reaction partner are located at varying positions on the surface of the antibody.

The cleavage of the antibody with enzymes like papain (route I, in figure 1.1) could cause changes in the tertiary structure of the antibody. In other words, cleavage could mean reduced reactivity, an aftermath of conformational changes in the molecule's tertiary structure.

Generally, the most promising strategy is the imine strategy (route III in figure 1.1). An interesting feature herein is the possibility to effect attachment on the Fc region of the antibody. The glycan moieties on the Fc region of the antibody could be oxidized to aldehyde (figure 1.2) using the common oxidizing agents like periodates (NaIO_4) [21]. The oxidation product could easily be reacted with amine functionality of any reacting partner.

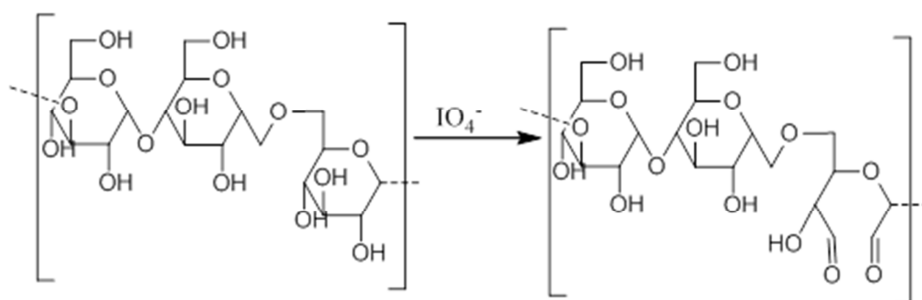


Figure 1.2: The oxidization of polysaccharide moiety using oxidizing agent like periodate (NaIO_4).

The reaction of the aldehyde group with amine produces Schiff's bases, which are unstable double bonds. These bonds could be transformed to more stable single bond amine (figure 1.3) by simple reduction reaction with mild reducing agents like the cyanoborohydrides [21].

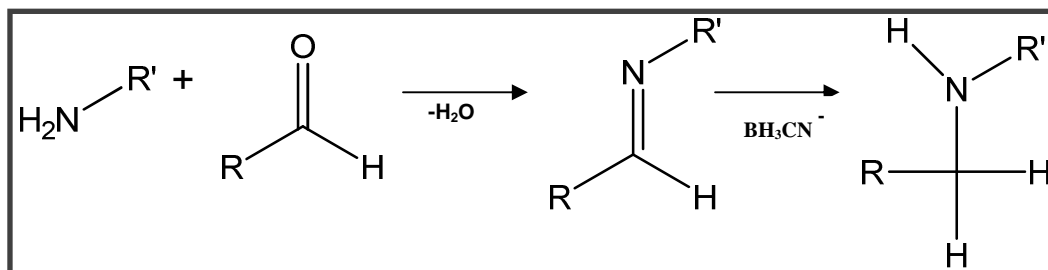


Figure 1.3: Schiff base formation (condensation reaction) between an amine functionality and aldehyde group and the transformation of the double bond to stable single bond by reduction reaction.

2. OBJECTIVES

The goal of this work is the synthesis of gold nanoparticles having sizes ranging between 10 nm – 65 nm. The synthesized particles are to be used for the preparation of AuNP antibody conjugate. The conjugate strategy shall involve the attachment of antibodies to the particles for covalently coupled systems having preferred orientation of the antibody on the particle surface. The idea is to optimize the reactivity of the conjugates by site selective attachment. This requires generating aldehydes by oxidizing the glycan moieties of the antibodies, after which the aldehyde functionalities are used to anchor PEG ligands, previously introduced onto the AuNP surface, via their amine caps. On the other hand, focus shall be directed towards improving the optical transduction of the interactions at molecular level by tuning the particle size and improving conjugate stability. These are aimed to achieve efficient conjugate nanoparticles which could help increase the performance of LFIA systems.

Important factors involving PEG ligand as materials for the enhancement of conjugate stability and solubility shall be focuses in this thesis.

Summarily, steps taken in this work to help improve the performance of the traditional LFIA are:

1. Investigating covalent attachment of antibodies to AuNP following a strategy that allows site specific coupling and a defined orientation of the molecule on the particle surface. Controlling the direction of antibodies on the particle surface with increased coupling efficiency helps to reduce the loss of biological reactivity after conjugation processes.
2. Exploring the size of gold nanoparticles used for the conjugate synthesis by systematically varying this factor and observing the corresponding changes of their properties. Extinction coefficient of gold nanoparticles is affected by their sizes and shapes. Large particles have higher extinctions which could contribute to improving the visual effect of the transducer (AuNP) in the systems. The influence of particle size on important properties of the conjugate using particles having diameters between 10 nm and 60 nm shall be investigated
3. Improving stability of conjugates systems by introducing steric factors. Materials or non-reactive polymers like PEG are used as means to boost the stability of the conjugate systems while maintaining high conjugate solubility in aqueous medium.

Preparation of conjugates having PEG layers between particles surface and attached antibodies reduces non-specific interaction of the system. The effect of the PEG polymer length (molecular weight) on the conjugates stability shall be investigated, by simply varying the size of the polymer (between 3 kDa and 10 kDa) used for coupling.

4. Characterizing the obtained conjugates using UV-Vis spectroscopy, DLS and Zeta-Potential to follow the coupling reaction, stability and hydrodynamic sizes of products. The reports shall present important information that extensively describes the system in detail.
5. Determination of the number of antibodies coupled per AuNP using lowest coagulation concentration (LCC) method, Bradford assay and calculations involving shell increase after ligand attachment to particles.
6. Investigation of the immunological reactivity of prepared conjugates by means of Immunoblotting and further proving of this event by means of DLS measurements and TEM images.

3. THEORITICAL BACKGROUND

3.1 Optical Properties of gold nanoparticle (AuNP)

The optical properties of metals are usually discussion based on the absorption and scattering of electromagnetic radiation by the materials. This happens at the metal's electronic states where changes involving interaction with external energies occur. The 5d electrons of gold can be excited into the 6s orbitals and on the other hand, the conduction band electrons could be collectively excited by interacting fields [23]. Figure 3.1 shows an absorption curve of gold nanoparticle. In this case of nano-sized material, the optical property results basically from the excitation of the conduction band electrons.

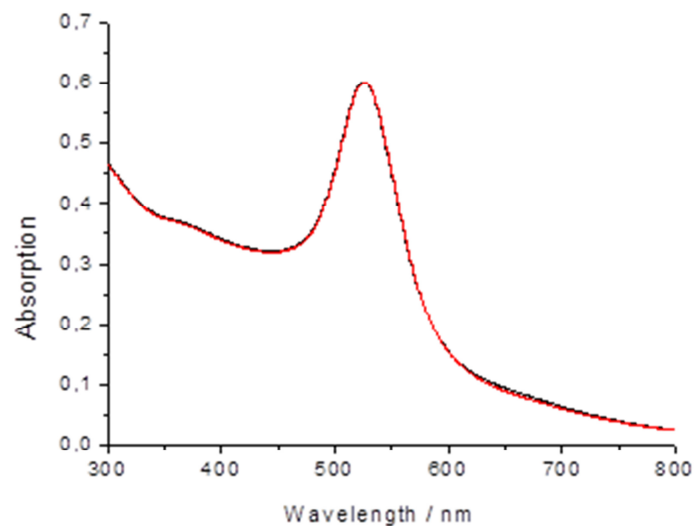


Figure 3.1: Absorption curves showing the absorption mode of gold nanoparticles at wavelengths between 300 and 800 nm wavelengths: the curve is obtained for the excitation of the conduction band electrons.

The conduction band electrons' excitation is induced by interacting electromagnetic field leading to a coherent oscillation of the electrons [24]. This process is illustrated in figure 3.2. An interacting electromagnetic wave (light) causes an excitation of the conduction electrons of the particles resulting in their coherent oscillation. This phenomenon is generally called surface plasmon resonance (SPR). For gold nanoparticles, this occurs within the visible region of the electromagnetic spectrum.

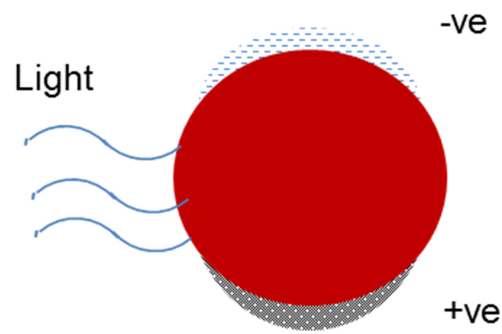


Figure 3.2: An interacting electromagnetic field (light) induces excitation of the Au nanoparticle conduction band electrons leading to a coherent oscillation of the electrons

As a consequence of the plasmon oscillation, a dipolar mode is generated with a huge enhancement of the local electric field at the nanoparticle surface. This electric field leads to a strong light absorption and scattering at the SPR frequency by the particle [24, 25].

The SPR frequency is dependent on several factors, which includes the metal dielectric constant, the particle's size and shape [26-29], as well as the dielectric properties of the surrounding medium [30,31] and inter-nanoparticle coupling interactions [32–36].

3.2 Dielectric functions and Extinction coefficient of AuNP

Gustav Mie related the optical properties of Nanoparticles with their dielectric functions. He was the first scientist to explain the optical phenomenon of metals theoretically by solving Maxwell's equation for the absorption and scattering of electromagnetic radiation by spherical particles [24, 37-40]. According to his theory, which assumes the conduction band electrons to be in the quasi-static regime, the extinction coefficient σ of particles with N electrons and radius, R could be represented by [41],

$$\sigma_{ext} = \frac{24\pi NR^3 \epsilon_m^{3/2}}{\lambda} \frac{\epsilon_2}{[\epsilon_1 + 2\epsilon_m]^2 + \epsilon_2^2} \quad (3.1)$$

λ is wavelength of the absorbed radiation and ϵ_m the dielectric constant of the surrounding medium. ϵ_1 and ϵ_2 represent the real and imaginary parts of the material dielectric function respectively. These additively make up a whole as in equation 3.2.

$$\epsilon(\omega) = \epsilon_1(\omega) + i\epsilon_2(\omega) \quad (3.2)$$

where ω is the angular frequency of the light. If ϵ_2 is small or weakly dependent on ω , then the resonance condition for the plasmon absorption is fulfilled when $\epsilon_1(\omega) = -2\epsilon_m$. Also the plasmon bandwidth mainly depends on $\epsilon_2(\omega)$.

Two terms arising from the electronic system of the materials contributes to the dielectric constant of gold nanoparticles. Their origins are related to the excitation modes of the metals, which involve 5d- and 6s-electrons summarized as [24, 42 - 44],

$$\epsilon(\omega) = \epsilon_{IB}(\omega) + \epsilon_D(\omega) \quad (3.3)$$

$\epsilon_{IB}(\omega)$ represents the term contributed by the excitation of the 5d electrons known as the interband term and $\epsilon_D(\omega)$ is the term contribution of the conduction electrons known as the Drude's term. In the Drude model, the electrons are treated as a gas of independent quasi-free particles interacting with external electric field, which experience retardation effects through collisions with the crystal ions. The Drude's term $\epsilon_D(\omega)$ can be expressed by relating the eigenfrequency of an electron gas as a function of its dielectric constants as in the free electron model given by [45, 46]:

$$\varepsilon_D(\omega) = 1 - \frac{\omega_p^2}{\omega^2 + \omega_0^2} \quad (3.4)$$

and

$$\varepsilon_{IB}(\omega) = \frac{\omega_p^2 \omega_0}{\omega(\omega^2 + \omega_0^2)} \quad (3.5)$$

ω_p is the Plasmon frequency of the electrons and $\omega_0 = 1/\tau_s$

$\tau_s = 3 \times 10^{-14}$ s for bulk gold [45]

$$\omega_p = (4\pi N_e e^2 / m^*) \quad (3.6)$$

N is the electron density, e is the electron charge and m_{eff} the electron effective mass.

3.3 Extinction cross section and optical density

For nanometer sized spherical metallic nanoparticles, the dielectric constant is directly related to the square of the refractive index, η (i.e. $\epsilon = \eta^2$). The extinction and scattering cross section σ_{ext} and σ_{sca} of a particle with radius R embedded in a medium with dielectric function ϵ_m at a wavelength λ were given by the equations [45-47],

$$\sigma_{abs} = \frac{8\pi^2}{\lambda} R^3 \left[\frac{\epsilon_p - \epsilon_m}{\epsilon_p - 2\epsilon_m} \right]^2 \quad (3.7)$$

and

$$\sigma_{sca} = \frac{128\pi^5}{\lambda^4} R^6 \left[\frac{\epsilon_p - \epsilon_m}{\epsilon_p - 2\epsilon_m} \right]^2 \quad (3.8)$$

the term in bracket is referred to as the polarizability, α which is also given by the equation [24, 48],

$$\alpha = 3\epsilon_0 V \left[\frac{\epsilon_p - \epsilon_m}{\epsilon_p - 2\epsilon_m} \right] \quad (3.9)$$

ϵ_0 is the vacuum permittivity

The extinction cross section, σ_{ext} of a spherical particle is the summation of the scattering cross section σ_{sca} and the absorption cross section, σ_{abs} [45, 46] represented by,

$$\sigma_{ext} = \sigma_{abs} + \sigma_{sca} \quad (3.10)$$

The extinction efficiency, Q_{ext} of a particle with radius R is normalized extinction cross section of an area,

$$Q_{ext} = \sigma_{ext} / \pi R^2 \quad (3.11)$$

Equation 3.12 relates the extinction efficiency to an experimentally obtained absorption A of a sample of particles.

$$A = \frac{\pi R^2 Q_{ext} l N}{2.303} \quad (3.12)$$

N is the number density of particles per unit volume and the length of the cuvette l is usually 1 cm.

El-Sayed [29] related particles optical absorption and scattering to the particle size. He theoretically demonstrated that the spectra properties (absorption efficiency Q_{abs} , scattering efficiency Q_{sca} and extinction efficiency Q_{ext}) for gold nanospheres are characteristically influence by size. Particle diameters of 20, 40, and 80 nm and polystyrene nanospheres with diameter of 300 nm were used for this purpose and the results are seen in figure 3.3 below.

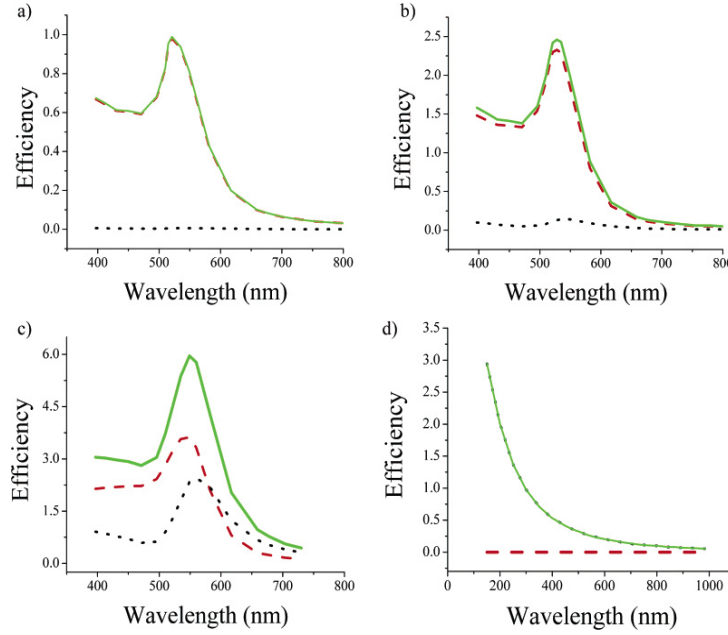


Figure 3.3: Calculated spectra of the efficiency of absorption Q_{abs} (red dashed), scattering Q_{sca} (black dotted), and extinction Q_{ext} (green solid) gold nanospheres (a) $D = 20$ nm, (b) $D = 40$ nm, (c) $D = 80$ nm, and polystyrene nanospheres (d) $D = 300$ nm. [29]

From figure 2a, the calculated spectra of the efficiency of absorption Q_{abs} (red dashed), scattering Q_{sca} (black dotted), and extinction Q_{ext} (green solid) of gold nanospheres (a) having a diameter of 20 nm, (b) having a diameter of 40 nm, (c) having a diameter of 80 nm, and polystyrene nanospheres (d) having a diameter of 300 nm, show that with increased sizes of AuNPs, scattering becomes a more evident component of extinction compared to absorption.

The degeneration of the extinction into optical absorption and scattering was shown clear in equation 3.10 and, figure 3.3 demonstrates the relative changes of these properties when varying particle size from 20 nm to 80 nm.

According to the report, it is reasonable to conclude that the particle size (diameter) optimal for optical (colour) effect of AuNP is 40 nm. This is the particle size by which AuNP shows least scattering with highest optical absorption. It was previously reported that gold nanoparticles with a diameter of 40 nm has optical cross-sections which is 4 - 5 orders larger

than those of conventionally used dyes like indocyanine green, rhodamine-6G and malachite green [29]. These findings are important fact to bear in mind when investigation the effect of particle size on the conjugate's optical properties, which is most important for the visual detection of analytes (antigens) in this work.

3.4 Antibody (IgG)

Antibodies, also known as immunoglobulin (IgG) are a group of glycoproteins which are involved in specific defence mechanisms in vertebrates. They are released from plasma cells (B lymphocytes) after activation mediated by antigen (virus, bacteria, parasite) and have different effector functions. They execute their functions by specifically binding with antigens and triggering immune response in the body by activating reaction cascade that increases the production of other IgGs. The most important functions of the antibodies are:

- removal of pathogens and toxins from infected organism
- activation of other components of the immune mechanism. For instance, IgM and IgG activate an immune reaction cascade that results in pores opening in the membrane of target cells;
- being active in opsonization and phagocytosis, cellular cytotoxicity and the responses to parasites and allergic responses e.g. IgE in allergic responses activates the mastocytes, which release their charged granules (of histamine, prostaglandins, etc.) and participates in the elimination of parasites with the help of eosinophils [49].

Looking at the structure of IgGs, they are seen as three dimensional combination of special globulin structures (formed from polypeptide chains) and “Y” shaped (figure 3.4).

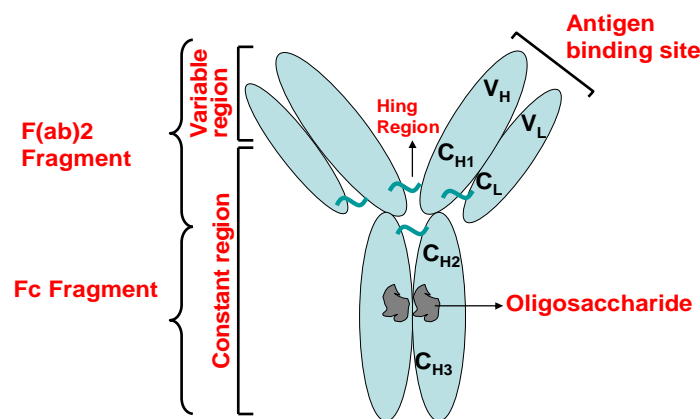


Figure 3.4: Structure of antibody (IgG)

The polypeptide chains are of two types – the heavy (H) chains having 55-70 kDa weight and the light (L) chains having 24-25 kDa weight. While there are five species of the heavy chains (α , δ , ϵ , γ and μ), the light chains are of two species (κ and λ) [50–53]. A whole IgG molecule is a combination of 2 identical H-chains bound by disulphur bridges with 2 identical L-chains. In addition to the disulphide bridges between the chains, there exist also

intracatenary disulphide bridges contributing to the stability to the molecule [54]. The existing different H-chains result in five IgG species: IgA, IgD, IgE, IgG and IgM, depending on the type of H-chain that the molecule is composed of. This structural difference relates also to their distinct functionality. The antibody can be found in monomeric forms (as in IgG), in dimers or in tetramers.

The L-chain is composed of two special regions: the variable domain (V_L), at its aminoterminal end and the constant domain (C_L). Similarly, the heavy chain contains a variable domain (V_H) and three or four constant domains (C_{H1} , C_{H2} , C_{H3} , C_{H4}) [55]. The variable regions of the L- and H-chains together, form special zones known as the divergent hypervariable regions, or complementary determining regions (CDR) important for the molecules interaction with antigen. There are three of these regions in the V_L domain and three in the V_H domain [56, 57]. These regions are separated by regions known as framework (FRW) composed of highly conserved sequences. The nature of the CDR confers the molecule with high antigen-binding specificity, which varies among antibodies. Millions of different antibodies can be generated, each one with a distinct specificity.

Among the five forms of antibodies introduced above, IgG is the most common and a major plasma glycoprotein having an N-linked oligosaccharides in the CH_2 domain.

The oligosaccharide chains (an average of two to eight carbohydrate chains) are asparagine-linked moieties located on the Fc region of the IgG molecule and they constitutes a variety of diantennary complex-type structures with some intersecting' N-acetylglucosamine or fucose residues [58, 59].

The specific interactions and the oligosaccharide heterogeneity have interested scientist in the past and studies based on the glycosylation process of IgG were carried out [60 - 62].

The biantennary oligosaccharide complexes form bridges across the domains on the Fc region using their $\alpha(1-6)$ arms for interacting with the polypeptide of adjacent domain and their $\alpha(1-3)$ arms for interaction with each other to form a bridge between the two domains.

Finally, the existence of the oligosaccharide chains on the IgG molecule and most importantly their location on the Fc region establishes a potential anchoring site for other molecules or particles. This is the turning point of the coupling strategy used in this work which shall be fully understood after going through this thesis

Kornfeld et al. [63] reported that significant differences in oligosaccharides structure exist between individual IgG proteins. This fact should be considered coupling protocols involving

the generation of aldehyde groups from these oligosaccharides, since IgG could show varying reactivity in the involved oxidation step.

The classical Y shape (figure 3.4) of IgG molecule shows a molecule with two identical domains for antigen binding known as Fab (**F**ragment for **a**ntigen **b**inding) segments, and other two identical domains with effector functions known as Fc (**F**ragment **c**ystalization) segments.

3.5 Lateral Flow Immunochromatography Assay (LFIA)

Lateral Flow Immunochromatography Assays or Lateral flow tests are simple diagnostic test kits commonly based on a nitrocellulose membrane matrix. They are used to detect the presence (or absence) of a target analyte in a sample. LFIA was first described in the 1960s [64] and the first commercial application as a pregnancy test was in 1988 [65]. Today this technique has found application in clinical, veterinary, agricultural, food industry, bio-defence and environmental laboratories. For medical diagnostics they are often used for tests at homes or in the laboratories, where they are specifically used for the investigation of a variety of bio-molecular binding interactions and for fast detection of analytes including pathogens and toxins [66-68].

Ready as simple-to-operate systems, they could be applied without extensive training or sophisticated equipment. This method of diagnostic tests has improved lives of humans, especially in resource-poor countries where they are applied for infectious disease diagnostics such as HIV, hepatitis B and E, syphilis and chikungunya.

The LFIA tests are relatively inexpensive, reliable, and could be read visually in the fields. A test runs within 15 minutes and the systems are very stable and robust, having long shelf lives with no special storage methods.

A typical LFIA test strip, which is illustrated in Figure 3.5, consists of the following components:

1. Sample pad – an absorbent pad onto which the test sample is applied
2. Conjugate or reagent pad – containing antibodies, which are specific to the target analyte and usually conjugated to coloured particles (usually AuNPs, or latex beads)
3. Reaction membrane – a hydrophobic nitrocellulose or cellulose acetate membrane onto which anti-target antibodies are immobilised in a line across the membrane as a test line. It has an additional control line containing antibodies specific for the conjugate antibodies also immobilised on the membrane.
4. Wicking Pad – another absorbent pad designed to draw the sample across the reaction membrane by capillary action.

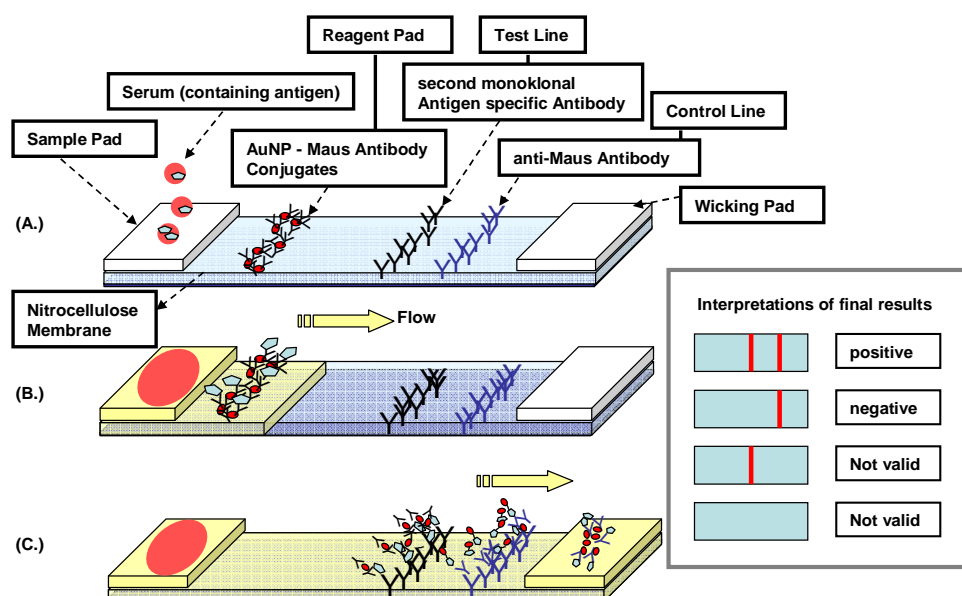


Figure 3.5: Components and functional principles of LFIA.

The components of the strip are usually fixed to an inert backing material and may be presented in a simple dipstick format or within a plastic casing with a sample port and reaction window showing the capture and control zones [69]. After the sample is applied (A in figure 3.5), the test sample flows along the nitrocellulose membrane via capillary action, on which it encounters a colored reagent e.g. AuNP-Antibody conjugates applied (B in figure 3.5) and continues through the zones containing immobilized antibodies or antigens applied (C in figure 3.5). Depending upon the analytes present in the sample the colored reagent can become bound at the test line. The membrane could have one of the four possible appearances shown on the right side of figure 3.5 after the test. The readout of the test result is positive when both the test and control lines are red as seen in the box, otherwise could be negative or not valid as demonstrated.

One common property to all immunochromatographic assays is that they are all based on antigen-antibody reactions. By this means, the detection of one of the reaction partners at low concentration are achieved. The assay format varies according to the method used for the test signal analysis. Signals could be radioactive type (Radioimmunoassay), enzyme linked (ELISA) or Lateral Flow promoted (LFIA).

LFIA are expressed in different forms, ranging from Immunochromatography Assay (IA), Lateral-Flow-Assay (LFA), Lateral Flow Device (LFD), Dipstick-Assay, Point of Care (POC) to Bed Side Test, depending on their formats. A common feature is that they are all based on accumulation concepts.

They are further classified into different groups based on their general operating system as shown in figure 3.6, namely those based on labels and those without labels.

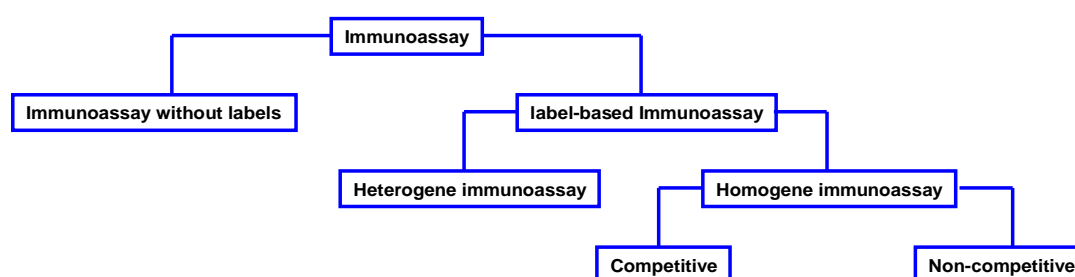


Figure 3.6: Types of immunassays based on their general operating system.

Immunoassay based on labels could be any of the heterogene and homogene types of systems. In the heterogene systems a reaction partner is immobilised on a solid support while the other partner is solubilised in solution. The heterogene systems have both reaction partners solubilised in solution. Depending on the methods for analytes detection and signal generation, the homogene systems are further grouped into the competitive and non-competitive forms.

Due to their unique properties, gold nanoparticles (AuNPs) are very attractive labelling agents and they can be visualized with the eyes as well as with a large variety of different techniques. The particles provide contrast for the observation and visualization of analytes and are transducers for read-outs. They maintain constant stability (their properties remain unchanged) through the test process. In the past, AuNPs have been used as replacement for organic dyes in labelling applications. Fluorophores or absorbing dyes have lost attractiveness to AuNPs in enzyme-linked immunosorbent assays or LFIA, which have shown excellent applicability in medical and research fields [70].

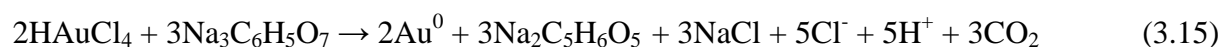
3.6 Synthesis of metallic nanoparticles

A number of useful protocols for the synthesis of colloidal nanoparticles have been published in the past [71-73]. The synthesized particles have unique surface functionalities and defined sizes ranges. Sizes and shapes of the particles could be controlled by simple variation of the conditions under which the synthesis is carried out [74, 75]. Also an important issue is the nanoparticles' stability during and after preparation since aggregation or precipitation of the synthesized particles in solution could take place. These are avoided by introducing stabilizing agents on the particle surface to confer charge or steric stability to the nanoparticles in solution.

A common synthetic route of gold nanoparticles is the aqueous reduction of HAuCl_4 by sodium citrate at boiling point [74, 76]. Other reducing agents like borohydrides and amines have been used [77, 78]. Particles synthesized by citrate reduction are nearly monodisperse spheres whose sizes could be controlled by the initial reagent concentrations [79, 80]. These particles' surfaces are covered with negatively charged citrate layers characterized by Zeta Potentials. They have optical properties characterized by their plasmon absorbance band in the visible region of the electromagnetic wave e.g. 15 nm particles have peaks at about 520 nm.

Reduction with citrates is not limited to gold nanoparticles. Silver, palladium, and platinum nanoparticles are also products of citrate reduction of their respective precursors [81-85].

In an elaborated study, Kumar [86] suggested the reaction equation involved in AuNP synthesis via citrate reduction of HAuCl_4 as seen in equation 3.15.



Nanoparticles with Core/shell structures [87, 88], organosilicon covered gold particles prepared using a molecular reactor technique [89], metallic nanoparticles capped with various shells, such as graphite [81] or CdS [90] have been previously synthesized. There are different capping methodologies used. In some cases the reductive formation of nanoparticles is performed in the presence of the shell-forming material, as in the citrate reduction of gold nanoparticles synthesis, but in other cases the capping involved post synthetic step [90].

Products' surface functionality is important when considering a synthetic procedure for nanoparticles. Desired functionalities are introduced directly on the particle surface in the

process of shell formation. The borohydride reduction of HAuCl_4 in the presence of dodecylamine gives rise to gold nanoparticles (3-5 nm) with surface alkyl functionality. Other borohydride reductions in the presence of thiols [91] produced nanoparticles with surface functionality ranging from amines to carboxylic acids. Due to solubility problems, some protocols involve two phase synthesis, as seen in the preparation of long chain alkanethiol stabilized gold colloids [92, 93]. The surface ligands could even be exchanged by simple place exchange reaction with other ligands for the purposes of improving solubility, stability as well as surface functionalities [94]. A common application of this strategy is the introduction of carboxyl capped ligands on the particles (as stabilizing agents), which are finally used to link amino groups of biological molecules [95]. The ability to easily functionalize AuNPs provides means to change the surface properties by attaching different kinds of molecules to their surfaces.

Interactions between particles in a suspension greatly affect their stability. Such interactions could either be stabilizing or destabilizing in nature. For example, van der Waals forces, being a collection of universal attractive forces between atoms and molecules, draw colloidal particles together. On the other hand, electrostatic forces, arising from a charged double layer present at each particle's surface, cause repulsion of particles from one another. If the attractive forces between particles in suspension become greater than the repulsive forces (e.g. if the distance between particles is smaller than the sum of their electric double layer distances), the particles will fuse irreversibly (flocculate) and precipitate.

3.7 AuNP-IgG conjugate

The unique properties of AuNPs, their rich surface chemistry and lack of toxicity as well as easy methods of synthesis have promoted conjugation of the particles with numerous biomolecules for site-specific delivery. Tkachenko et al. used AuNPs for specific nuclear targeting by conjugating them with bovine serum albumin [96, 97]. AuNPs were tagged with monoclonal antibodies and oncoproteins associated with human papillomavirus [98]. Mercaptoalkyl-oligonucleotide conjugated AuNPs were used in the detection of polynucleotides by plasmon band interactions with the surrounding environment [99]. Gold nanoshells with coatings of breast tumor marker Her-2 were effectively localized in the microscopic tumors present in the breast tissue [100]. In the area of imaging AuNPs conjugates are used as detectors for cells undergoing apoptosis especially in the chemotherapeutic fields.

Bioconjugation simply involves the linkage of biomolecules to nanoparticles by chemical or biological means. It includes the conjugation of antibodies, nucleic acids and liposomal components or other biologically active molecules with nanoparticles. The outcome is the combinations of useful properties. Proteins used to target analytes are combined with gold nanoparticles, for visualization purposes.

Antibodies conjugation to nanoparticles is currently undergoing a flurry of research and development activities. There important improvement on the quality of the available cross linking reactions and reagent systems for creating novel conjugates with peculiar properties.

3.7.1 AuNP-IgG Coupling

The coupling and functionalization of NPs with proteins is done by using a variety of methods. These include electrostatics interaction, ligand recognition, metal-mediated complexation, chemisorption, and covalent binding through bifunctional linkers [101–103].

Antibodies (and other proteins) contain amino acid polymers with a number of reactive side chains which could be utilized for attachment. Alternative to these intrinsic reactive groups, specific reactive moieties could be generated or introduced onto the molecule by chemical modification. These introduced groups are consequently used as "handles" for attaching other molecules or particles.

3.7.1.1 Physical interaction (*electrostatic coupling*)

This is a simple method to form AuNP IgG conjugates through electrostatic interactions of IgGs with charged particles' surfaces. Since the discovery of immunogold labeling in 1971 by Faulk and Taylor, a great deal of information is known about the nature of bonding between gold nanoparticles and antibodies [104]. It was suggested that electrostatic interaction between proteins and AuNPs depends on three separate but dependent phenomena: (a) ionic attraction between the negatively charged gold and the positively charged antibody; (b) hydrophobic attraction between the antibody and the gold surface; (c) dative binding between the gold conducting electrons and amino acid sulfur atoms of the antibody [105].

The antibody, AbVF (having a lysine and cysteine residues) was found to bind gold nanoparticles via their thiol/amine groups after a preceding electrostatic contact of both reacting partners. A weak hydrophobic interaction between gold and the antibody was claimed in addition to the presence of gold-sulfhydryl/gold-amine bond between the gold nanoparticles and cysteine/lysine residues present on the antibody [106, 107].

Playing a key role during the process of conjugation, solution pH determines the charge and stability of the conjugate. Additionally, this factor influences surface coverage and protein biofunctionality after conjugation process.

Nanoparticle IgG conjugates could be prepared through specific protein–ligand interactions. The NPs are functionalized with groups having specific affinity for certain proteins or oligonucleotides. For example, streptavidin previously attached to gold NPs have been used for the binding of biotinylated proteins [108]. Also NPs functionalized with antibodies were used for affinity binding of their respective antigen [109 - 111].

3.7.1.2 Chemical interaction (covalent coupling)

The problems facing electrostatic coupling method like conjugate instability and IgG inactivation could be solved by using covalent conjugation methods [112]. This is achieved in a number of ways like (i) chemisorption via thiol derivatives; and (ii) through the use of bifunctional linkers. The chemisorption of proteins onto a metal particle surface can proceed through cysteine residues present in the protein e.g., oligopeptide, serum albumin and IgG [113], or chemically in the presence of 2-iminothiolane (Traut's reagent) [113, 114].

Bifunctional linkers are highly diverse and they offer versatile covalent conjugation of proteins with NPs. Thiols and disulfides or phosphine ligands are often used to link or anchor molecules to Au, Ag, CdS, and CdSe. An example of a bifunctional linking process involves a carbodiimide-mediated amidation and esterification with thiol groups.

Traditional covalent immobilization techniques for proteins utilize functional groups in their amino acid side chains such as amino groups in lysines, carboxyl groups in glutamic and aspartic acid, phenolic rings in tyrosines, and sulfhydryl groups in cysteines [115].

Above pH 8.0 ($pK_a = 9.18$), lysine amines easily go into nucleophilic reactions with a variety of reagents like activated carboxyl groups to form stable bonds [116].

Thiol functionalities from cysteines, cysteine, methionine and those from the reduction of disulfide bonds of antibodies using dithiothreitol (DTT) are used for covalent attachments. Other crosslinking reagents such as Traut's reagent (2-iminothiolane), succinimidyl (acetylthio) acetate (SATA), and sulfosuccinimidyl 6-[3-(2-pyridyldithio)propionamido]hexanoate (Sulfo-LC-SPDP) are used for attaching thiol groups on antibodies [116-118, 120].

Antibodies could be chemically modified by integrating an "anchor" on the molecule, which is then utilized for attaching a wide variety of molecules or nanoparticles. The manner of attachment of antibodies on particles' surfaces could be in a random or oriented form depending on the strategy used for the conjugation [115, 121 - 123]. In this thesis, focus was centered on the orientation of the antibody on the particles, after the conjugation process. Therefore an interesting method for covalent coupling of antibodies to AuNP was used. Glycan moieties on antibodies were oxidized with sodium periodate to aldehydes [121] which reacts with amine, hydrazide, or hydrazine. Because these polysaccharides are predominantly found on the crystallisable fragment (Fc) region of the antibody, conjugation proceeds in a site-specific manner preserving the activity of the molecule. This specific approach offers the highest retention of antigen binding ability [124].

3.8 Analytical methods

3.8.1 Transmission Electron Microscopy (TEM)

Transmission electron microscopic images of the nanoparticles were taken with a JEOL JEM-1011 instrument operated at an accelerating voltage of 100 kV with a LaB₆-Cathode as electron source. The samples for TEM measurements were prepared by placing a droplet of the colloidal solution onto a carbon-coated copper grid and allowing it to dry in air.

3.8.2 UV-Vis

The absorption spectroscopic measurements were recorded on a Cary 50 single beam UV-Vis spectrometer, with cells of 1 cm path length.

3.8.3 Dynamic Light Scattering (DLS)

DLS measurements were carried out using a Malvern Zetasizer Nano ZS ZEN 3600 instrument.

Dynamic Light Scattering (DLS) or Photon Correlation Spectroscopy (PCS) is one of the most popular techniques used to determine the size of a particle.

By this method, the dynamics of a particles system in relation with the Brownian motion and fluctuations of scattered light is investigated with time. The frequency shifts, the angular distribution, the polarization, and the intensity of the scatter light are determined by the size, shapes and molecular interactions in the scattering material. Figure 3.9 shows a simple system setup for DLS.

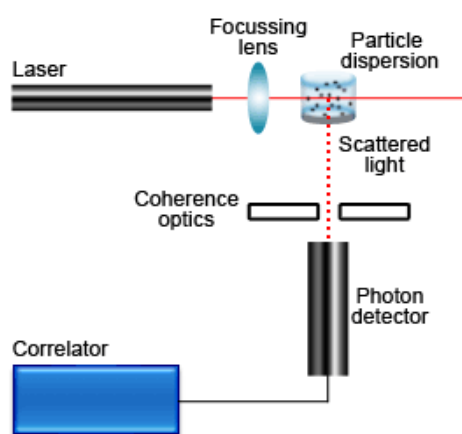


Figure 3.9: A schematic representation of the setup of DLS system.

Light from a laser is focused on a sample as seen in figure 3.9. The light scattered at a given scattering angle is collected by a square law detector – a photomultiplier or an avalanche photodiode. The output of the photomultiplier is then digitized by a photon counting system and the output sent to an autocorrelator.

In solution, particles are constantly in motion. Under this condition known as Brownian motion, the particle experiences Doppler Effect. This phenomenon is coupled with an oscillating polarization of the particles electrons when monochromatic light beam is passed through their solutions. This effect generates a secondary wave source known as the scatter light which undergoes either constructive or destructive interference by the surrounding particles as illustrated in figure 3.7 [125]. The scatter light could be characterised by wave frequency shifts, angular distribution, polarization and intensity, which are influenced by the size, shape and molecular interactions in the scattering material. By this means particle size could be deduced by the autocorrelation of the the particle's motions and its diffusion coefficient. DLS provides additional information on the particles polydispersity, establishing a useful analytical tool for quantitative assay.

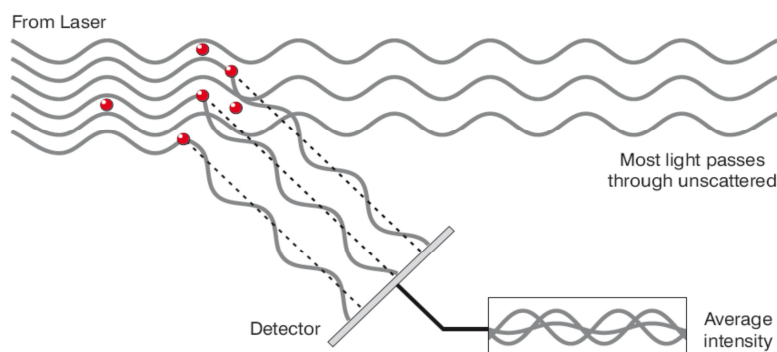


Figure 3.7: Constructive and Destructive interference of scattered light

The Intensity of the scattered light recorded with time, is plotted as seen in figure 3.8. A record of intensity fluctuation gives information about the time scale of movement of the particles.

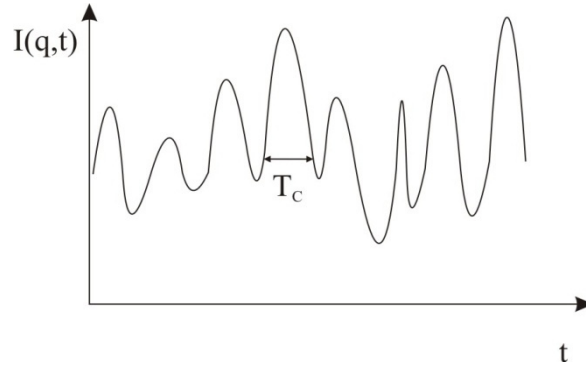


Figure 3.8: The progression of scattered light intensity at a given angle.

The normalized scattered intensity time autocorrelation function of the scattered light may be written as

$$g^{(2)}(q, \tau) \equiv \frac{\langle I(\vec{q}, 0) I(\vec{q}, \tau) \rangle}{\langle I(\vec{q}) \rangle^2} = \left\{ 1 + \gamma [g^{(1)}(q, \tau)]^2 \right\} \quad (3.17)$$

γ is a constant determined by the specific experimental setup and $g^{(1)}$ is the normalized first order (scattered electric field) time autocorrelation function.

For a dilute solution of monodisperse nanoparticles with a single exponential whose time decay is determined by the translational self-diffusion coefficient of the particle D and the length of the scattering vector q :

$$g^{(1)}(q, \tau) = \exp(-q^2 D_0 \tau) = \exp(-\Gamma \tau) \quad (3.18)$$

where, $\Gamma = q^2 D_0$ is the reciprocal decay time. D_0 is given by the STOKES-EINSTEIN equation:

$$D = k_B T / 6\pi\eta R \quad (3.19)$$

k_B is the Boltzmann's constant, T temperature, η the solvent viscosity and R the hydrodynamic radius of particle.

A graphical presentation of the time-correlation intensity function $\langle I(q, t) I(q, t + \tau) \rangle$ is demonstrated in figure 3.10.

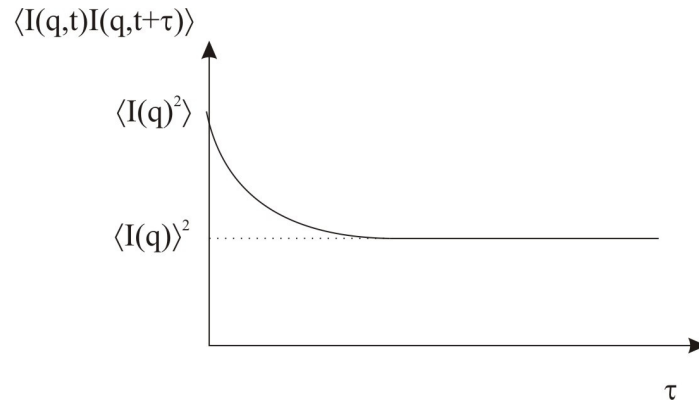


Figure 3.10: A graphical presentation of the time-correlation intensity function, $\langle I(q,t)I(q,t+\tau) \rangle$.

The time-correlation function $\langle I(q,t)I(q,t+\tau) \rangle$ has initially value of $\langle I(q)^2 \rangle$. For times very long compared to the correlation time, τ the correlation function decays to $\langle I(q) \rangle^2$.

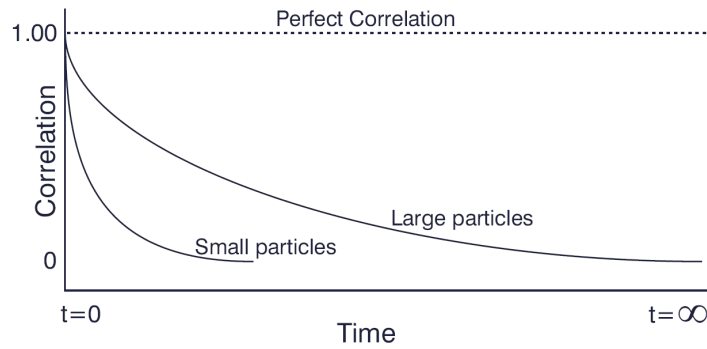


Figure 3.11: Normalised time-correlation function as related to particle sizes

The correlation curves of smaller particles falls faster than those for larger particles as demonstrated in figure 3.11. From this relationship, information on the particle's radius could be obtained.

3.8.4 Zeta Potential, ζ

The Malvern Zetasizer Nano Instrument was used for all zeta potential measurements. The instrument has a laser used as an illuminating light source, which is directed into the sample. The reference beam has intensity within 3500 and 2000 kcps. The light intensity, which fluctuates with frequencies dependent on the particle speed, is passed to a digital signal processor which analyses the data with software relating electrophoretic mobility to particle zeta potential.

Nanoparticle colloid is stabilized by electrostatic forces indicated by the zeta potential of the particles in solution. This is established with an electrical double layer on charged particles. The interactions of particles with each other in aqueous solution as relates the double layer was extensively described in the Derjaguin, Landau, Verway and Overbeek or DLVO theory [126].

3.8.4.1 The DLVO theory

DLVO theory postulates that the stability of a colloidal system arises due to an energy barrier originating from the balance between two opposing forces: the van der Waals attractive (V_A) forces and electrical double layer repulsive (V_R) forces between the particles on approaching each other. This barrier (figure 3.12) prevents two particles from agglomerating. Collisions with enough energy to overcome this barrier, brings particles in close distance at which the attractive forces exceeds causing particles to agglomerate.

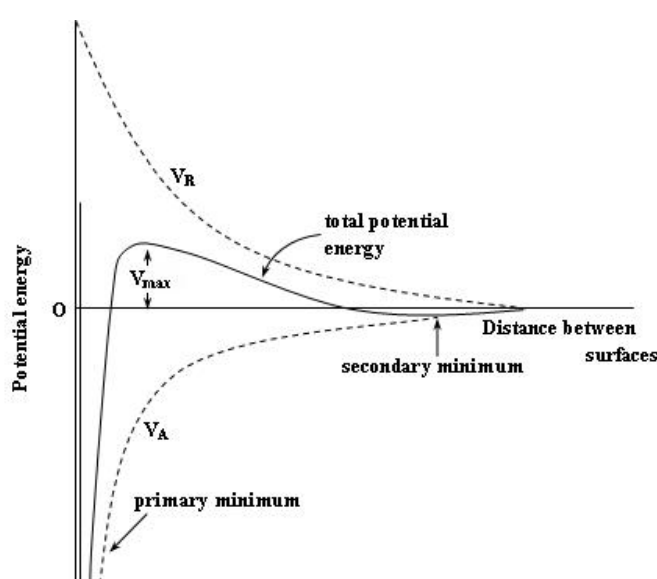


Figure 3.12: The total potential energy curve resulting from the net value between the force of attraction VR and the force of repulsion at distance between the particles.

In an aqueous solution of nanoparticles, cations and anions are attracted to particle surface forming double layer forming an inner and an outer layer. Ions in the inner layer, closer to the surface of the particle binds strongly to the surface and those on the outer diffuse layer are loosely bound. The diffuse layer is made up of two sub-layers with an imaginary plane known as slipping plane, forming a boundary between ions which move with the particle in solution and those stationary.

The electrical double layer model was first introduced by Stern in 1924 by combining the Helmholtz and the Gouy-Chapman models. It is applied in evaluating the zeta potential of particles by utilizing one of four basic types of electrokinetic principles:

- i. *Electrophoresis*, the mobility of charged colloidal particle suspended in an electrolyte and subjected to a potential gradient.
- ii. *Streaming potential*, an induced electric potential, generated by flow of liquid in a single capillary or in a system of capillaries.
- iii. *Electro-osmosis*, the induction of liquid movement in a capillary or in a system of capillaries when a potential is applied.
- iv. *Sedimentation potential*, sedimentation process established on application of gravity to a dispersion.

Using any of the above electrokinetic principles, the potential which exists between the particle surface and the surrounding medium at the slipping plane could be estimated and its value is known as the Zeta potential. This factor is influenced by the distance of the slip plan from the particle surface.

To achieve an estimation of the Zeta potential, the electrophoretic mobility, u of particle is used. This can be obtained by balancing the viscous drag force and the electric pulling force from an applied electric field at a steady state of particle velocity to obtain equation 3.21.

$$u = \frac{q}{6\pi\eta R} \quad (3.21)$$

R is the particle radius, η the viscosity of the suspending medium and q the particle charge. Considering the double-layer, given by the reciprocal of the Debye screening length k , Huckel

modified equation 3.21 to obtain the zeta potential of a particle having $R \ll 1/k$. His modification done by applying Henry's equation is presented in equation 3.22 [127].

$$\xi = \frac{3}{2} \frac{qu}{\epsilon_r \epsilon_0} \quad (3.22)$$

ϵ_r is the relative permittivity and ϵ_0 , the permittivity of vacuum.

Smoluchowski extended this theory for spherical colloid with $R \gg 1/k$ to obtain the relationship [127];

$$\mu = \frac{\epsilon_r \epsilon_0}{\eta} \xi \quad (3.23)$$

3.8.5 Densitomerical analysis

The density of particles on nitrocellulose membrane was imaged on a Molecular Imager VersaDoc MP 4000 system and their analysis was performed using Quantity One software (Biorad).

4. EXPERIMENTAL WORK

4.1 Materials and Equipment

Chemicals were purchased from Aldrich, Merck, Iris Biotech, and Roth. All chemicals and solvents were reagent grade or of higher quality and used as received. Deionized water was purified with a Millipore Simplicity system (resistivity 18.2 M Ω cm).

REAGENTS

- | | |
|---|----------------|
| • Albumin Fraction V | Pierce Biotech |
| • 1-(3-Dimethylaminopropyl)-3-ethylcarbodiimide | Sigma |
| • Gold (III) chloride trihydrate | Sigma Aldrich |
| • Methoxypoly(ethyleneoxy) Ethyl Acrylate | Monomerpolymer |
| • Normal rabbit antibody | Sigma Aldrich |
| • NaOH | Sigma Aldrich |
| • NaCNBH ₄ | Sigma Aldrich |
| • pH Paper | Aldrich |
| • Polyclonal goat anti-rabbit antibody | Sigma Aldrich |
| • Pentaerythritol tetrakis(3-mercaptopropionate) | Sigma Aldrich |
| • Purpald | |
| • Sodium bicarbonate | Sigma Aldrich |
| • Sodium carbonate | Fluka |
| • Sodium hydrogencarbonate | Sigma Aldrich |
| • Sodium citrate | Sigma Aldrich |
| • Sodium periodate | Sigma Aldrich |
| • Sodium hydrogenphosphate dihydrate | |
| • Sodium phosphate | Fluka |
| • HCl*H ₂ N-PEG-SH, 5 kDa, 5 kDa, 10 kDa | Iris Biotech |
| • sodium phosphate | Sigma Aldrich |
| • Whatman Protran Nitrocellulose Membrane | Aldrich |

4. EXPERIMENTAL WORK

Aqua regia was always prepared fresh by mixing concentrated HCl/HNO₃ in a 3:1 ratio in the fume hood. 6.25 mM chloroauric acid solution was prepared by dissolving 24.6 mg of gold (III) chloride trihydrate in 10 ml of ddH₂O.

For 2.2 mM trisodium citrate solution, 1.29 g of sodium citrate was dissolved in 2 L of ddH₂O.

Purpald solution was freshly prepared each time by dissolving 10 mg Purpald in 1N NaOH.

EQUIPMENT

- | | |
|--|-----------------|
| • Hot plate with magnetic stir bar | Eppendorf |
| • 10,000 and 100,000 MWCO centrifuge filters | Millipore |
| • 1.5-ml micro-centrifuge tubes | Eppendorf |
| • Microfuge | Beckman Coulter |

4.2 AuNP Synthesis

The synthesis of gold nanoparticles was pioneered by Turkevich [72, 73] and his work was followed up later by Frens [76] who improved the synthesis protocol yielding better dispersity of the particles. The synthesis is based on the reduction of gold chloride by sodium citrate at specific concentrations and at a temperature high enough for the sodium citrate to act as a reducing agent (around 80-100 °C), and thus causing the gold to be reduced from Au(III) to Au(0). Citrate serves a dual purpose in the synthesis; it serves to both reduce the gold and stabilize the particles. In the zero oxidation state, gold atoms start to nucleate and grow into particles. Usually a stabilizing agent is also added to prevent the particles from aggregating. Because thiol groups bind to gold surfaces with high affinity, most frequently thiol modified ligands are used as stabilizing agents which bind to the surface of the AuNPs by formation of Au-sulfur bonds [128]. Synthesis of AuNPs with various sizes and shapes can be achieved through judicious choice of experimental conditions and reagents.

4.2.1 Citrate-stabilised 10-13 nm AuNPs

10 – 13 nm citrate stabilized gold nanoparticles (AuNP) were synthesized following the method described by Frens [76]. 0,17g HAuCl₄ in 500 mL bidistilled water (1.0 mM) were introduced into a 1L Erlenmeyer flask on a stirring hot plate. A magnetic stir bar was added and the solution brought to a boil under reflux. To the boiling solution, 0,57g trisodium citrate dihydrate (Na₃C₆H₅O₇ · 2H₂O) in 50 mL bidistilled water (38.8 mM) was added. The gold sol gradually formed as the citrate reduces the gold (III). After approximately 15 minutes the heating was stopped when a deep red colour was obtained.

4.2.2 Seed-Growth Method

20 nm AuNPs and larger particles were synthesized following the method described by Bastus [129]. The seeded-growth method of AuNP synthesis is a procedure, whereby a series of AuNP samples with varying sizes could be acquired by a single preparation proceeding involving a desired number of growth circles, which are initiated by a common seed generation step. The steps involved in the seeded-growth preparation of AuNP are illustrated in Figure 4.1.

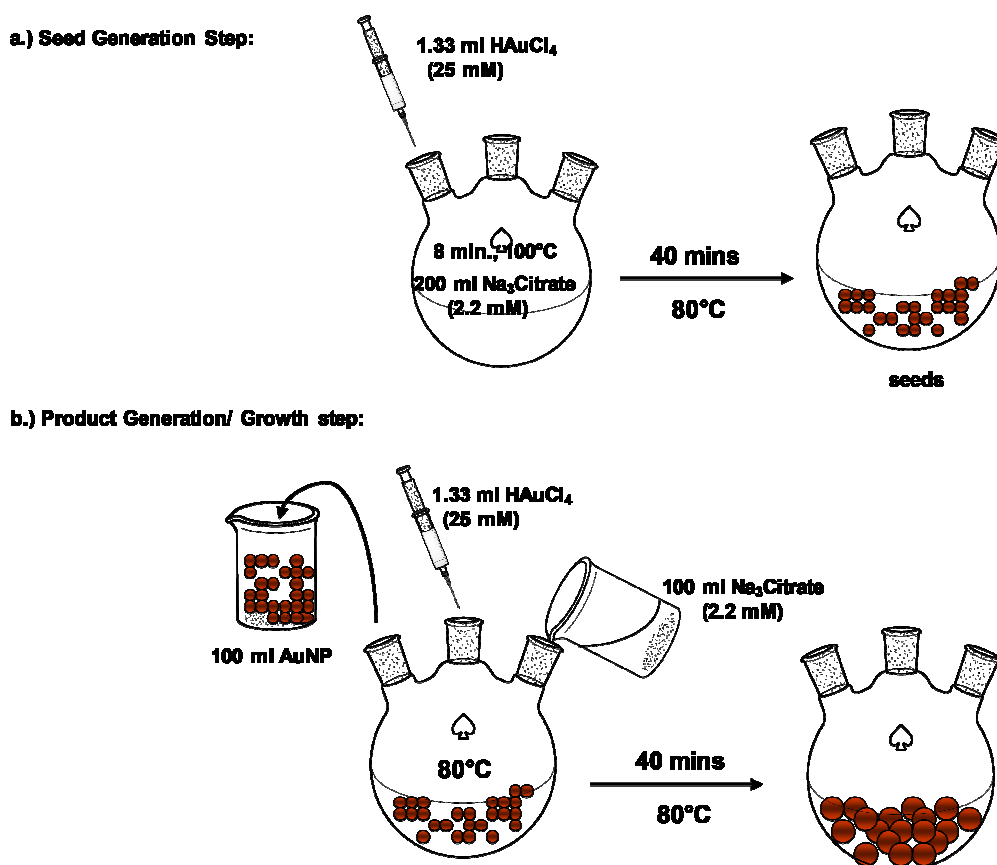


Figure 4.1: Steps involved in the seeded-growth preparation method of AuNP.

A solution containing 200 mL (2.2 mM) trisodium citrate dihydrate ($\text{Na}_3\text{C}_6\text{H}_5\text{O}_7 \cdot 2\text{H}_2\text{O}$) in a 250 mL flask was heated to 100°C with stirring under reflux. Using a syringe, 1.33 mL of 25 mM $\text{HAuCl}_4 \cdot 3\text{H}_2\text{O}$ was injected into the flask and stirred at 100°C for 8 minutes (Nucleation). The solution turned deep red. The temperature was reduced to 80°C and stirred continuously another 40 minutes. Then 100 mL aliquot was withdrawn (G0) and 100 mL of trisodium citrate dihydrate (2.2 mM) added and the temperature of the solution maintained at 80°C. At this temperature, 1.33 mL $\text{HAuCl}_4 \cdot 3\text{H}_2\text{O}$ (25 mM) was injected into the flask with a continued

stirring for another 60 minutes (Growth). After another withdrawal of 100 mL aliquot (G1) from the reaction solution, the growth procedure was repeated to acquire further samples (G2 – G5). This process could be continued with the accompanying 100 mL aliquot withdrawal after each step to acquire further samples with larger sizes (Gn where n = 6...). All steps involved the traditional addition of 100 mL trisodium citrate dihydrate (2.2 mM) and 1.33 mL HAuCl₄.3H₂O (25 mM) at 80°C with 40 minutes of stirring as described above.

4.2.3 AuNP concentration determination

All concentration determinations were done with UV-Vis measurements. The formula by Haiss et al. [130] was used for all concentration determinations. According to the relationship, the concentration N, is given by,

$$N = \frac{A_{450} * 10^{14}}{d^2 \left[-0.295 + 1.36 \exp \left\{ - \left(\frac{d - 96.8}{78.2} \right)^2 \right\} \right]} \quad (4.1)$$

N is AuNP concentration in NPs/mL, d the particle diameter and A₄₅₀, the optical absorption at 450 nm.

For the calculation of the number of surface atoms, Z₀ of a particle with radius r, the equation put together by Vossmeier from our working group, equation 4.2 was used.

$$Z_0 = 247.0 nm^{-3} \left[r^3 - (r - 0.288)^3 \right] f \quad (4.2)$$

The factor f takes account of the bulk density variation between the particle surface and the interior of the material, given by $f = (f_1 + f_2)/2$. $f_1 = 0,71$ for the (100) plane and $f_2 = 0,82$ for the (111) plane.

4.3 AuNP coupling and analysis

An efficient method was applied to confer a site-specific attachment of the PEG to rabbit IgG before coupling to AuNP surfaces (figure 4.2) [131]. This coupling method ensures a controlled immobilization of antibody on surfaces, while maintaining the orientation and activity of the bound antibody. Thiolated PEGs with amine caps were attached on IgG via oxidised glycan moieties on its Fc segment and this was brought onto the surface of the particles by taking advantage of the gold-thiol chemistry.

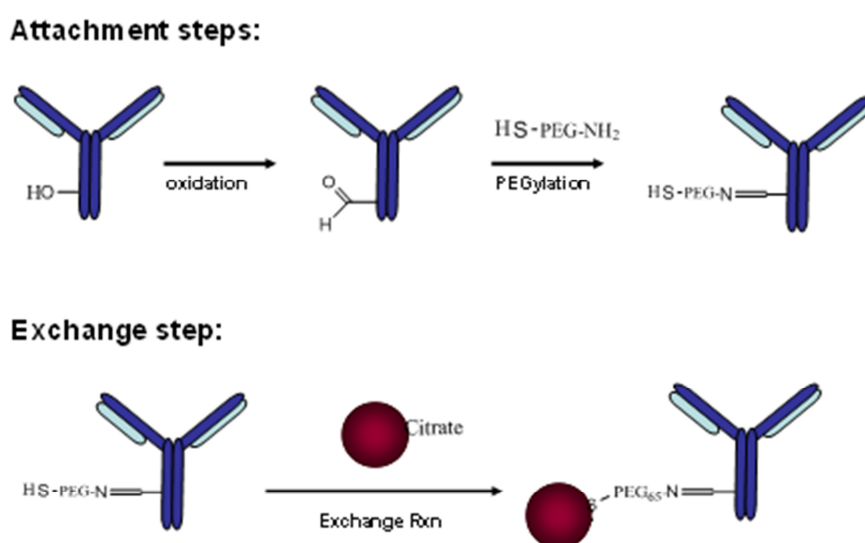


Figure 4.2: Illustration of steps in covalent coupling of RIgG to AuNP

After citrate stabilized AuNP were synthesized, exchange reaction was carried out with the HS-PEG-RIgG ligand. This enabled the covalent attachment of the RIgG onto AuNP surface. The surface coverage and stability of the AuNPs stabilised with the modified IgG were investigated. This was done by using three different strategies involving DLS, Protein analysis and Theoretical calculations and the obtained results were compared with each other. Stability analysis of the conjugates with UV Vis Spectroscopy in addition to observations of system's color change was made. The behaviour of conjugates with different types of adsorption have been compared, namely the electrostatic interaction between the positive charges on the IgG and the negatively charged gold surfaces and the attachment of thiolated PEO polymers for gold due to thiol-gold interactions. The comparison of the results from the three applied methods of estimation for AuNP surface coverage suggests a strong correlation

between ligand concentration and adlayer conformation and coverage. The impact of ligand concentration on adsorption and stability has been explored.

4.3.1 Oxidation of antibodies

The extent of oxidation of the carbohydrate residues on the Fc portion of the IgG depends on pH, periodate concentration, exposure time, and temperature [16]. The oxidation was carried out by agitating 10 mg IgG in 1xPBS buffer, pH 7.5, and 20 mM periodic acid. Exposure to light was minimized during the preparation of the periodic acid reagent as well as during the oxidation reaction. A typical concentration of IgG used for oxidation was approximately 1.0 mg/ml. 5 mL 1xPBS was added to the reaction solution and shaken for 2 min. The oxidation reactions time was 30 min at 25°C. After oxidation, undesirable oxidation byproducts such as formaldehyde were removed by centrifugal filtration (VIVASPIN; MWCO 100,000) at 2,000g.

4.3.2 Purpald test

500 µl of a Purpald solution (10mg/mL) is added to a 50 µl sample. The solution was immediately mixed and left open in contact with the atmospheric air for a few minutes (between 5 - 10 minutes in most cases) until the solution turns purple. Purple colour indicates the presence of aldehydes [132].

4.3.3 Attachment of oxidized antibodies to PEG linkers

The attachment of the HS-PEG-NH₂ linker to IgG was carried out according to a previously published protocol [131] with some modifications. For the covalent attachment of the oxidized IgG to the amine capped PEG linker, 1 mL of a 1 mg/ml IgG solution was added to 1 mL PEG linker (6.3 µmol) solution, and stirred overnight at RT. The used concentration of linker in the solution was approximately 1000 times larger than that of IgG. The product was washed by adding 6 mL 1x PBS buffer and subjected to centrifugational filtration (VIVASPIN MWCO 100,000) at 2,000g. Final volume after centrifugation was 1 mL. The washing step was repeated twice.

4.3.4 Ligand exchange reactions

The AuNP samples were used as prepared for ligand exchange reactions. For the exchange reaction, ligands dissolved in 1xPBS were mixed with the AuNP solutions at high molar excess. In a usual coupling procedure, 1.5 mL 18 nM AuNP solution is mixed with 1mL containing 1000 times excess of ligand (HS-PEG-NH₂, HS-PEG-RIgG or RIgG). The mixture was stirred for 30 minutes and purified by repeated centrifugation and resuspension in PBS buffer. Finally UV-Vis and DLS measurements of the purified products were made. The products were stored in the refrigerator at 4°C until use

4.3.5 Bradford protein analysis

A Bradford assay was performed as described in ref. [133] with modification in order to determine the amount of unbound RIgG after the exchange reaction. Briefly, protein concentration estimation was done by using Roti-Nanoquant reagent in a modified Bradford protocol.

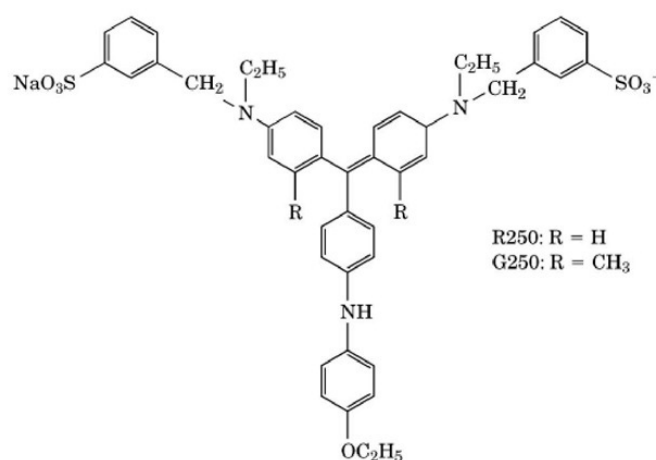


Figure 4.5: Coomassie Brilliant Blue

The Bradford assay [133] involves the use of the dye Coomassie Brilliant Blue G-250 (figure 4.5) for protein quantitation purposes. The dye goes into ionic interaction by first donating its free proton to the ionizable groups on the protein (arginine, histidine, phenylalanine, tryptophan and tyrosine) causing conformational changes that, consequently exposes the proteins hydrophobic regions with which hydrophobic interaction with the non-polar region of the dye via van der Waals forces takes place. This interaction brings about stabilization of the

blue form (the anionic form) of coomassie dye, consequently shifting the absorption peak of the dye from 465 to 595 nm [134].

Nanoquant reagent was diluted 1:5 with bidistilled water before use. Standard solutions of RIGG in the range 5–50 mg/ml in 1xPBS buffer were prepared. The standard solutions and the samples solutions (200 μ L each) were introduced into plastic disposable cuvettes and 800 μ L of the dye solution was added into each of the cuvettes, mix and incubate for 10 min at room temperature. The absorbance of the samples at 450 and 590 nm were taken and the values of the ratio OD 595 nm/450 nm plotted against concentration. The standard response curve was finally fitted and the quantity of the unknown protein was estimated.

4.4 ImmunTest

A nitrocellulose membrane (NC-membrane) sheet was dipped in a glass petri-dish containing bidist H_2O and left for a few minutes. The NC-membrane washed 3 times with 1x PBS by gradually decanting the water and adding 1xPBS. After a few minutes of swirling, the wash solution is decanted and the process repeated. The now conditioned membrane is placed on a filter paper (wicking pad).

With a glass pipette, the solution of protein to be immobilized (RIgG, GaRIgG, BSA or others) was introduced onto the wet NC-membrane on different spots and left to seep in. This involved using a glass pipe as illustrated in Figure 4.3. Thereafter, the NC-membrane was blocked by immersion in 1% BSA in 1x PBS for 30 minutes and subsequently washed 3x with 1x PBS as described above. The blocked NC-membrane was then immersed into a glass dish containing AuNP-antibody conjugate solution and left to incubate at RT for 2hr. The NC-membrane was washed with 1x PBS and inspected for red spots by visualization with the naked eyes. Figure 4.4 demonstrates steps involved in the process of the Immune test.

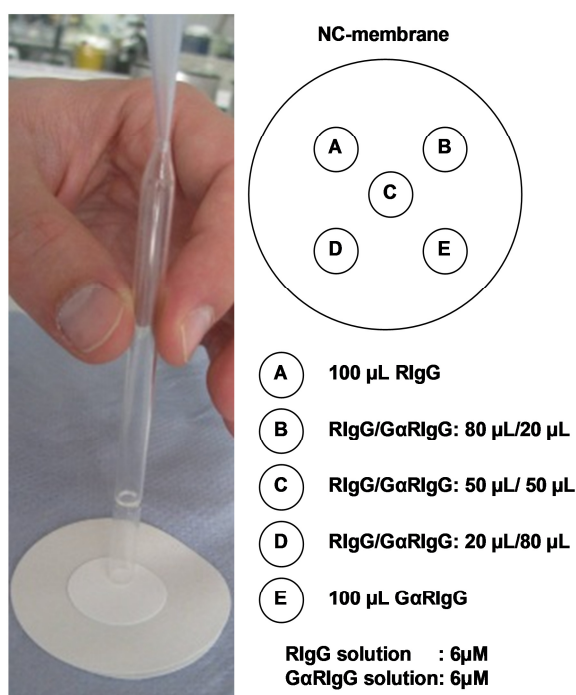


Figure 4.3: Illustration of protein immobilization on NC-Membrane

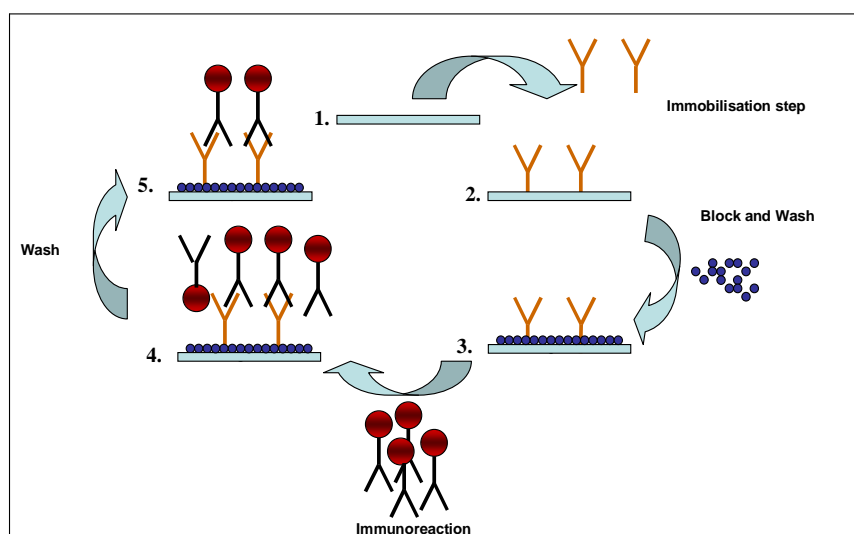


Figure 4.4: (1) Nitrocellulose Membrane, 2) Spots of desired proteins are immobilised on Nitrocellulose Membrane. 3) The Membrane with spots is treated with solution of blocking reagent. 4) The Membrane with spots treated with blocking reagent is reacted with Antibody covered AuNP 5) and finally washed with buffer solution.

The Nitrocellulose membrane (Protran BA85 from Aldrich) used in this work are round shaped sheets of 25 mm diameter having $0.45\ \mu\text{m}$ pore size and $80\ \mu\text{g}/\text{cm}^2$ binding capacity. The calculated surface area of this membrane is $4.9\ \text{cm}^2$. The surface of the spots of immobilized proteins has area size of $0.26\ \text{cm}^2$. Considering a membrane binding capacity of $80\ \mu\text{g}/\text{cm}^2$ (Producers information), the maximum capacity of the spots is $21\ \mu\text{g}\ \text{IgG}/\text{Spot}$ ($0.13\ \text{pmol}/\text{Spot}$).

5. RESULTS AND DISCUSSION

The synthesis of citrate stabilized gold nanoparticles in this work was successful. Protocols which enabled the preparation of approximately 10 nm – 100 nm spherical particles with narrow size distribution were used. The particles were characterized using TEM, DLS and UV-Vis spectroscopy. Prior to antibodies attachment to the particles, thiolated polyethylene glycol (PEG) ligands were linked specifically to the Fc region of the molecule and the resulting conjugates were characterized with UV-Vis spectroscopy, DLS measurement as well as with other analytical methods like Bradford protein analysis and lowest coagulation concentration (LCC) analysis. Investigations revealed relevant information on the conjugates stability, surface coverage, surface charge density and antibody reactivity.

5.1 Citrate stabilized AuNP and AuNP-RIgG conjugates

The gold nanoparticles (AuNPs) used in this work were synthesized by the reduction of HAuCl₄ with citrate. Procedures similar to this synthetic approach for gold nanoparticles has been demonstrated before [74-76]. While the classical synthesis method [76] with a little variation was used to prepare 12 nm AuNPs in this work, the seeded-growth method [129] was used to synthesize gold nanoparticles having sizes approximately 20 nm and above. In the later method, a controlled deposition of gold atoms on the surfaces of seed particles yielded larger particles which are uniform in sizes.

5.1.1 Sizes, Shapes and optical absorption of AuNP

The synthesized AuNPs were characterized by transmission electron microscopy (TEM) and UV-Vis absorption spectroscopy. The photograph seen in figure 5.1 is from a sample of 12 nm particles synthesized according to the procedure described in section 4.1.1. Figure 5.2 show the TEM image of the particle with the size distribution histogram and the UV-Vis spectrum.

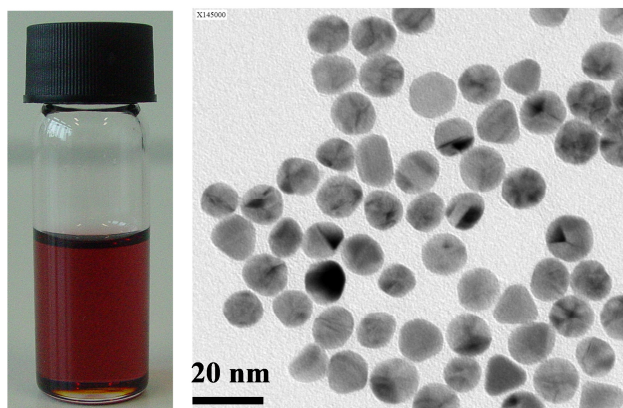


Figure 5.1: Photograph and TEM image of the 12 nm citrate stabilized AuNPs

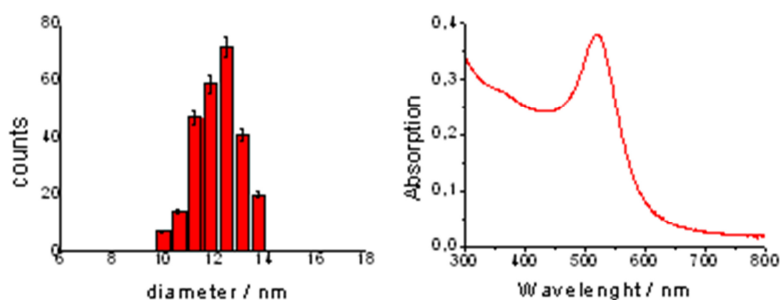


Figure 5.2: Size distribution histogram of the particles in figure V-I and the UV-Vis spectrum.

As seen in figure 5.1, the solution possesses the characteristic red colour of gold nanoparticles and the TEM image show spherically shaped nanoparticles and a few triangular or ellipsoidal shaped particles. The diameter of the nanoparticles is 12.0 ± 1.4 nm and the plasmon absorption peak is at 520 nm.

In the case of the seeded growth products synthesized, the TEM images of products from different generations are shown in Figure 5.3. The shapes of nanoparticles are quite spherical and their average diameter is as given in table 5.1 and also indicated in the respective figures. A size increase which progressing with the generation from G1 to G6 could be noted.

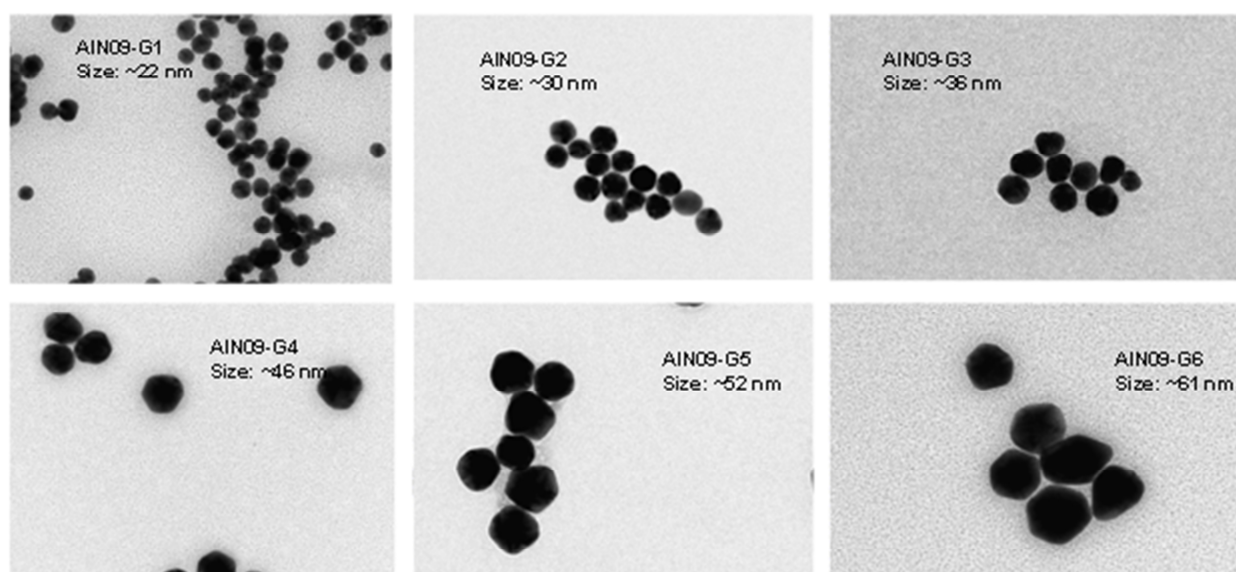


Figure 5.3. TEM images of citrate-stabilized gold nanoparticles prepared with the Seeded-Growth method. With progressive generations: G1 (Figure 2a), G2 (Figure 2b), G3 (Figure 2c), G4 (Figures 2d) G5 (Figures 2e) G6 (Figures 2f).

5.1.2 Dynamic light scattering (DLS)

The samples were further analyzed using dynamic light scattering (DLS). In DLS size information is obtained based on Stoke's law by relating the average time required for the particle to diffuse through a fixed focal volume. It is generally assumed that all particles are spherical and for nonspherical particles only an effective size (comparable to volume) is obtained.

Figure 5.4 shows the measurement results of six samples obtained from a single synthesis using the seed-growth procedure. The curves are the plots of the volume (%) distribution against calculated sizes of the particles and table 5.1 summarizes the results. The intensity and number statistics in addition to the volume statistics data for each of the measured samples are included in the table.

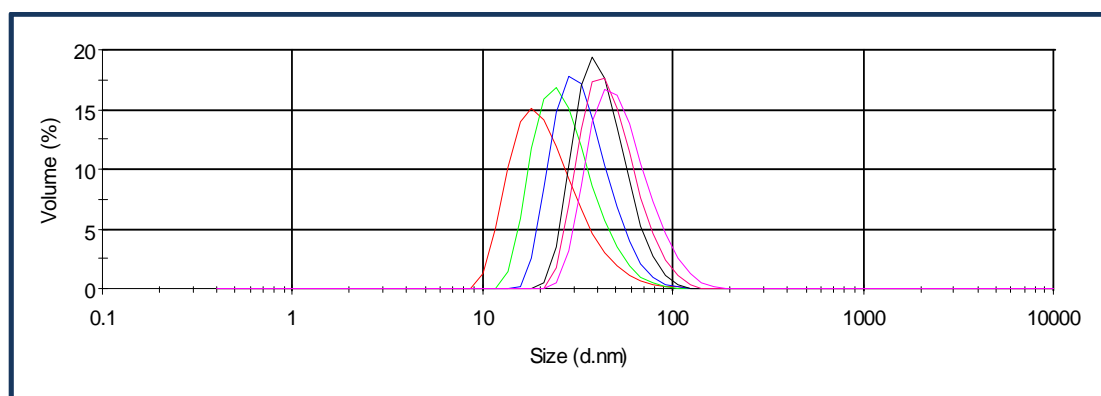


Figure 5.4: DLS measurement results of the particles from the generation series G1 to G6. The table also shows the measured value using the TEM images.

Table 5.1: Hydrodynamic diameter from DLS measurement of AuNP-G1 to -G6. The table also shows the obtained diameter from the TEM images.

Sample	TEM	DLS			
	Values (nm)	Intensity (nm)	Volume (nm)	Number (nm)	PDI
AuNP-G1	22	45,51	23,67	16,50	0,23
AuNP-G2	30	42,21	28,60	21,83	0,20
AuNP-G3	36	47,35	34,91	27,49	0,18
AuNP-G4	46	54,59	43,58	35,62	0,16
AuNP-G5	52	62,29	48,25	38,14	0,18
AuNP-G6	61	73,14	55,17	42,08	0,20

The intensity, volume or number values show increasing hydrodynamic size of the particles through the generation from G1 to G6 as seen in table 5.1. It must be noted that the intensity distributions are the fundamental analysis results obtained from direct measurements of the sample by the instrument. This intensity values were consequently converted into volume and number distribution by using Mie theory. The DLS size values are expected to be larger than those of the TEM values due to the double layer which goes into the calculations of the hydrodynamic radius of the particles in solution. This factor is absent in the dried state of the samples imaged by TEM. Obviously, the hydrodynamic diameters are reduced on comparing the volume and number values to the TEM results. This is attributed to discrepancies

originating from smaller particles present in sample which constitutes statistical errors in the analysis. Comparably though, the values of the volume distribution show closer agreement with the TEM values. The Polydispersity Index (PDI) value of approximately 0.2 for each of the investigated samples suggests similar Polydispersity of the particles in each of the generations. This is supported by the TEM images in Figure 5.3 and strongly indicates monodisperse AuNPs. This suggests individual existence of particles in a stable form in solution, free from aggregation of any kind for every sample regardless of the generation step from which it was obtained .

5.1.3 UV-Vis Spectroscopy

Characteristically, AuNPs show surface plasmon absorption in the UV-visible absorption spectrum. The absorption peak positions are dependent on the medium surrounding of the particles. A change in the nature of constituent surrounding ligand shell results to shift of the peak.

Characterization of the prepared citrate stabilized AuNPs was done by determination of their extinction coefficients as well as observing their absorption peaks and absorption curve appearances. Figure 5.5 shows the resulting absorption spectra of the analysed AuNP samples, each having absorption maximum falling within the spectral range of 520 nm to 535 nm wavelength. Their maximum peaks, λ_{max} values are summarised in table 5.2 and a plot of these values against the particle sizes (TEM) was done as seen in figure 5.6. The extinction coefficient, ξ for each of the samples was estimated by calculations using the Lambert-beer's law and the optical absorption values of dilution series. Subsequently, the obtained values were plotted against the particles' sizes as shown in figure 5.7.

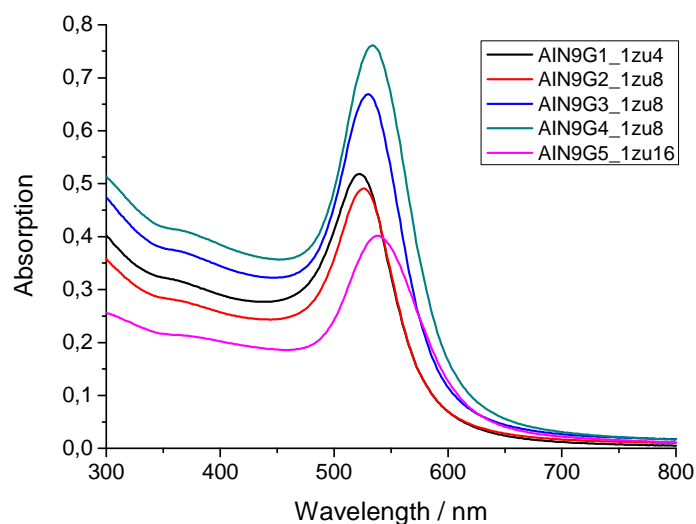


Figure 5.5: Absorption spectrum of the gold nanoparticles with their Plasmon band maxima

Table 5.2: Values and results obtained from the analysis of the absorption curves seen in figure 5.5. The λ_{\max} values are the maximum peak positions of each sample with their maximum optical density, OD_{\max} . The calculated extinction coefficient, ξ and solution concentration after synthesis, **Conc. (nM)** are also shown.

Sample	UV-Vis			
	λ_{\max} (nm)	OD_{\max}	$\xi * 10^9$ ($\text{M}^{-1}\text{cm}^{-1}$)	Conc. (nM)
AuNP-G1	522	0,37	1,37	1,95
AuNP-G2	526	1,04	3,84	0,84
AuNP-G3	530	1,96	7,27	0,72
AuNP-G4	533	4,37	16,20	0,34
AuNP-G5	538	6,49	24,06	0,27

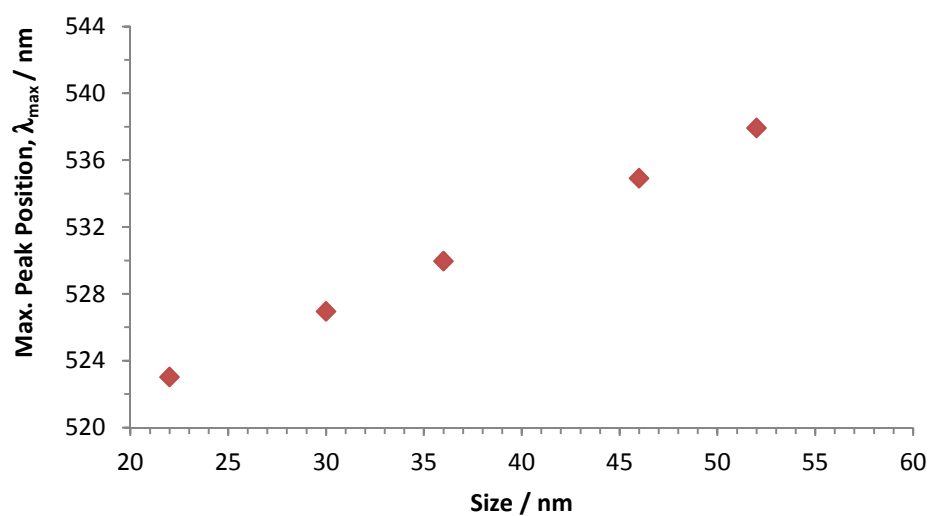


Figure 5.6: The maximum peak positions λ_{max} plotted against the TEM sizes of the particles AuNP-G1 to AuNP-G5.

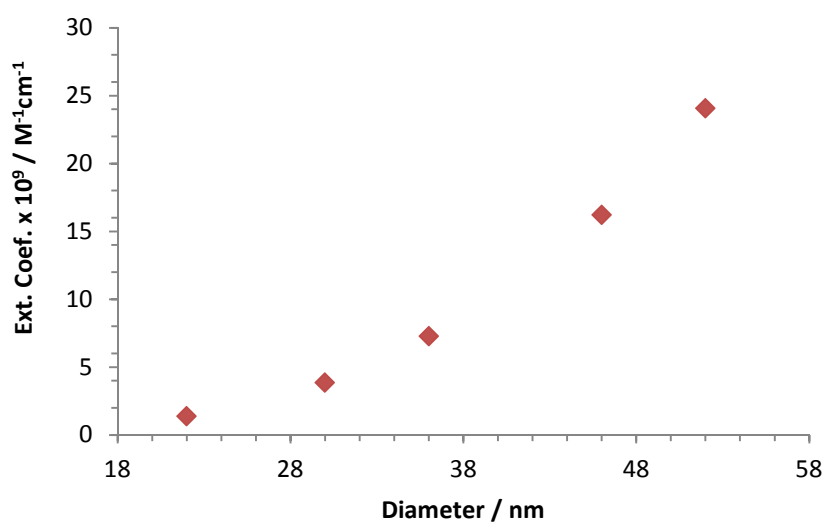


Figure 5.7: The Extinction coefficient plotted against the TEM sizes (diameters) of the particles AuNP-G1 to AuNP-G5.

The solution concentrations of the particles were calculated according to Haiss [130] as described in section 4.2.3. The resulting values are shown in table 5.2. The solution concentrations reduced to approximately half values compared to those of samples from succeeding generation steps of the synthesis. This is expected, since intermediate product reduced to half volumes at the end of each generation cycle before being used as seeds for the succeeding generation of products.

From table 5.2, the optical density of the gold nanoparticles increases with particle size. This behaviour becomes clearer on plotting the extinction coefficient against the diameter as shown in figure 5.7. The curve shows the characteristic behaviour in agreement with theory [135] as expected.

According to the observation made in figure 5.5, the maximum peak shifts to longer wavelength (red-shift) with increasing particle size. This behaviour confirms the previous report on the size dependent peak shifts of gold nanoparticles [23]. It was made clear then, that the plasmon position and the extinction coefficient of gold nanoparticles in the larger size regime ($d \geq 20$ nm) depended on the particle size because higher order terms plays some important roles in this regime. Consequently, the dipole approximation applied in calculations for the smaller regime becomes invalid. For the larger particles, whose radius becomes comparable to the interacting light's wavelength, polarization by electromagnetic field becomes inhomogeneous. This event leads to excitations at multipole modes with consequent peaks at different energies [136].

5.2 Antibody oxidation

An important feature of the imine coupling strategy, which is chosen for the conjugate preparations in this work, is the existing sugar moiety utilized for the attachment of conjugate partner on the Fc region of antibodies. This has the advantage, that the steric hindrances of the antigen interacting region of the antibody are minimized, which otherwise causes reduction in antibody reactivity efficiency. This is a common problem with other coupling strategies.

An important step in the procedure for coupling antibodies with AuNPs is the generation of the aldehyde group by the Fc glycan (sugar) oxidation. This was done in 1xPBS with NaIO₄ as described in section 4.3.1. To confirm the oxidation, the presence of the aldehyde groups was monitored by using the purpald test [137]. Purpald reacts readily with aldehydes to form an intermediate product which turns purple on exposure to atmospheric oxygen. Figure 5.8 demonstrates the steps involved in the reaction.

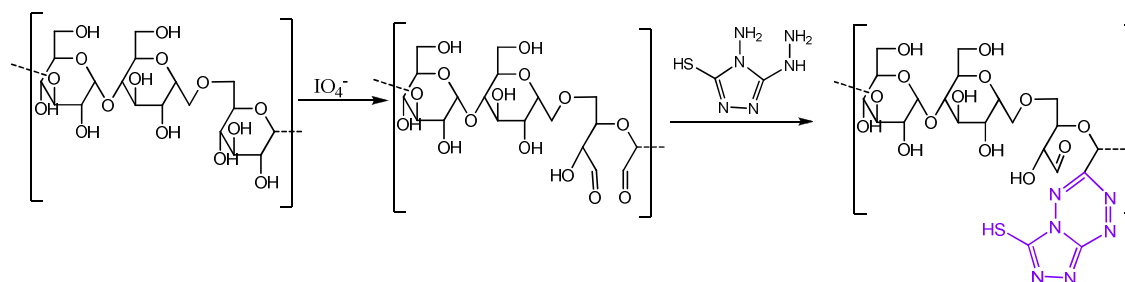


Figure 5.8: The generation of aldehyde groups by oxidation of sugar and its subsequent reaction with purpald to form the product (tetrazine) which turns purple on exposure to atmospheric oxygen.

The purpald reaction is an indication of the presence of the aldehyde groups after the oxidation of the Fc glycan. A control experiment for this test was done by using the unoxidized antibody. While the oxidized antibody samples were subjected to this reaction, they were similarly treated after the attachment of amine capped PEG ligands. The photographs in figure 5.9 show solutions of the purpald treated samples.

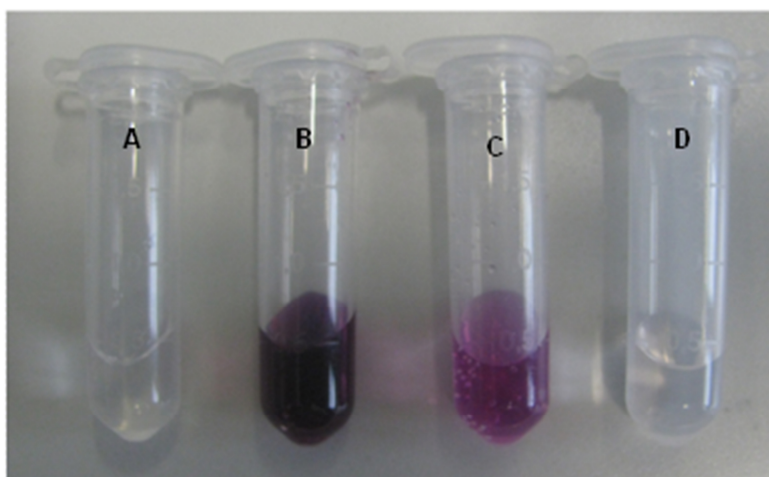


Figure 5.9: Samples after treatment with purpald reagent: (A) aliquot taken before oxidation; (B) aliquot taken after the oxidation reaction; (C) aliquot taken a few minutes after addition of amine capped linker; (D) aliquot taken 12 hours after addition of amine capped linker.

Figure 5.9 shows the aliquots after the treatments with purpald reagent. 20 mL aliquots of the RIgG solution was taken before oxidation (A), after the oxidation reaction (B), few minutes after addition of amine capped linker (C) and 12 hours after addition of amine capped linker (D). The aliquots taken after oxidation behaved in a similar way with those taken a few minutes after addition of linkers. These samples turned purple with purpald reagent. On the other hand, there was no colour appearance in aliquots taken before RIgG oxidation and samples taken 24 hours after addition of amine linker. The reason for this behaviour is the absent of aldehyde groups in both samples. The generated aldehyde groups when free, reacted with the purpald molecules resulting in the purple colour as seen in figure 5.9 B. Reduced colour intensity in figure 5.9 C was as a result of the diminished availability of the aldehyde groups with time as they are continuously lost on reacting with the linkers to form Schiff's base. After 12 hours all aldehyde groups have been used up and the solution could show no evidence of any aldehyde groups present. These results suggests the generation of the aldehyde groups from the glycan moiety on the Fc region of the RIgG and their complete exhaustion on reaction with amine groups of the Linker to for Schiff's bases.

5.3 Ligand exchange products

The synthesized citrate stabilized AuNPs were used for preparation of conjugates. These conjugate systems were achieved by simple exchange reaction of the citrate molecules with ligands, especially thiolated PEGs, RIgGs and PEGylated RIgGs, on the particle surfaces. The changes in optical absorption due to the changes on the particles' surface were monitored with a combination of UV-Vis absorption measurement and dynamic light scattering (DLS) analysis.

5.3.1 UV-Vis absorption measurements of exchange reaction products

After the attachment of the linkers to the oxidized RIgGs, the products, PEGylated RIgGs were used for exchange reactions with citrates molecules on the AuNP surfaces. As control experiments, two similar exchange reactions were carried out using thiolated PEG ligands resulting in the product AuNP-PEG-NH₂ and by using unoxidized RIgG to obtain conjugates coupled by ionic interaction, AuRIgG. UV-Vis measurements of all three products as well as that of citrate stabilised AuNP were made. The measurement results are plasmon bands shown in Figure 5.10.

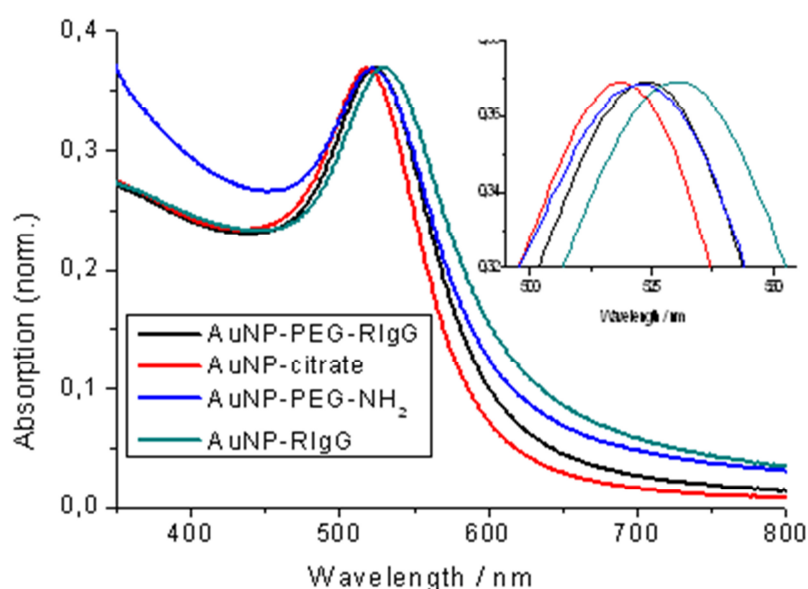


Figure 5.10: UV-Vis spectra of samples of citrate stabilised AuNP particles (AuNP-citrate) and those obtained from exchange reactions carried out using free thiolated PEG ligands (AuNP-PEG-NH₂), PEGylated RIgG (AuNP-PEG-RIgG) and unoxidized RIgG (AuNP-RIgG)

The figure, 5.10 shows normalized UV-visible absorption spectra for the samples and their enlarged forms. Slight shifts in the absorption peak were observed. These peak-shifts suggest changes occurring on the particle surfaces. They indicate the replacement of the citrate coverage of the particles by the ligands during the exchange reaction. The products resulting at the end of this process different characteristic absorption position [137]. On comparing the individual curves, the samples resulting from using RIgG for citrate exchange showed the largest peak-shift. PEGylated RIgG ligands show similar shift as the PEG ligands. The similarity observed for the latter cases indicates that the ligand moieties directly interacting with the nanoparticle's surface are similar for both samples. This behavior suggests covalent interaction of the thiol groups of both ligands, **HS**-PEG-NH₂ and **HS**-PEG-RIgG with the AuNP surfaces. The unoxidized RIgG shows a different form of interaction since the type of interaction involved here is different from the covalent form attributed to Au-thiol interaction. This unique interaction which is mostly ionic in nature results in conjugates showing larger peak-shift.

5.3.2 DLS measurements of exchange reaction products

AuNPs are extraordinary light scatterers, a property which is used when characterizing their hydrodynamic diameters by DLS. Using citrate stabilized AuNPs, four samples shown in figure 5.11, with different surface coatings were prepared via place exchange reactions:

- a) HS-PEG-NH₂ (MW, 3kD) was used to obtain sample AuNP-PEG-NH₂.
- b) A mixture of HS-PEG-NH₂ and RIgG was used to obtain sample RIgG/AuNP-PEG-NH₂.
- c) PEGylated RIgG (HS-PEG-RIgG) was used to obtain AuNP-PEG-RIgG.
- d) RIgG was adsorbed electrostatically to obtain AuNP-RIgG.

The products were analysed by DLS measurements after purification.

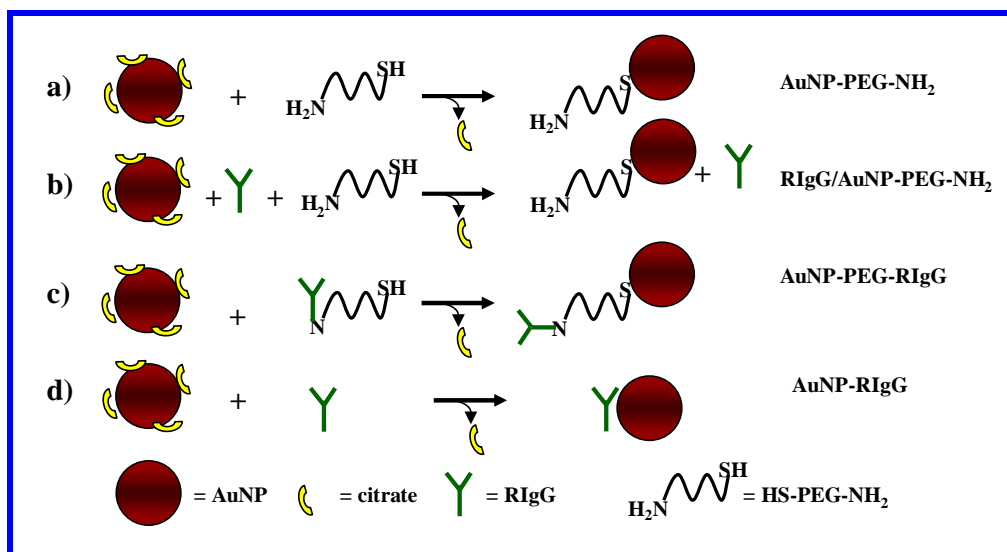


Figure 5.11: AuNP conjugates prepared via place exchange reactions using citrate stabilized AuNPs. Four samples a) AuNP-PEG-NH₂ from HS-PEG-NH₂ (MW, 3kD), b) RIgG/AuNP-PEG-NH₂ from mixture of HS-PEG-NH₂ and RIgG, c) AuNP-PEG-RIgG using PEGylated RIgG (HS-PEG-RIgG), d) AuNP-RIgG using RIgG which was adsorbed electrostatically to the particle surface.

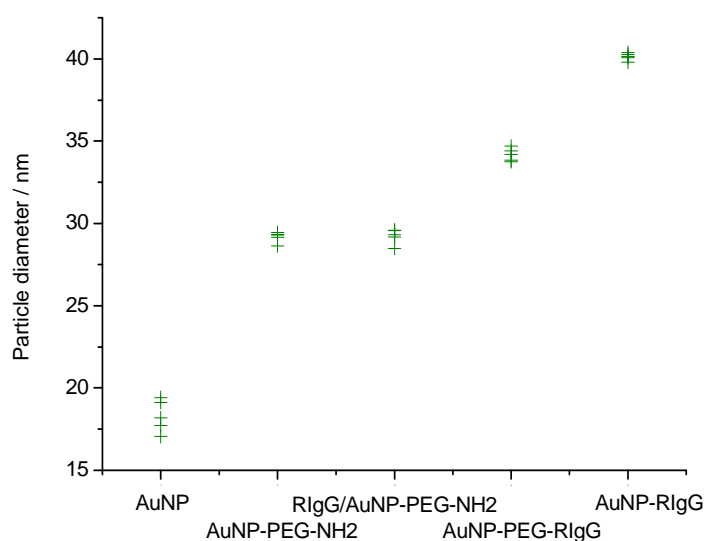


Figure 5.12: DLS sizes of the samples shown in Scheme 5a. The sample AuNP refers to citrate stabilized AuNPs.

Figure 5.12 shows the plot of the DLS hydrodynamic diameter against the AuNP systems synthesized as schematized in figure 5.11. Each sample was prepared and measured 5 times. The initial core size of the citrate-protected AuNPs was 12 nm as determined by TEM and their hydrodynamic size was ~18 nm as determined by DLS. The DLS-sizes of samples AuNP-PEG-NH₂ and RIgG/AuNP-PEG-NH₂ were both ~29 nm. This result indicates that the

nature of the moiety covering AuNP-surface was similar in both samples. In the latter case it seems that the surface covering was strongly dominated by the HS-PEG-NH₂ ligands from the mixture of PEG ligands and RIgGs. This is a behavior attributed to the high affinity of the thiol group to the gold atoms. This interaction is stronger than the electrostatic interaction between the antibody and the gold surface. On the other hand, the much smaller PEG ligands could reach the surface of the AuNP faster than the larger RIgG molecules. From the aforementioned, a cumulative effect results in a binding preference of the PEG ligands to the particle surfaces.

The particle size increase from the citrate stabilized AuNPs on exchange with the PEG-ligand, is ~11 nm. This increase in size, which corresponds to a PEG shell thickness of ~ 6 nm, is in reasonable agreement theoretical calculations [138].

In contrast to the AuNPs samples prepared from PEG-linkers (AuNP-PEG-NH₂), the covalently coupled conjugates prepared from HS-PEG-RIgG (AuNP-PEG-RIgG) and their electrostatically coupled counterparts prepared from RIgG (AuNP-RIgG) exhibited larger DLS-measured sizes with values at ~ 34 nm and ~ 40 nm, respectively. The conjugate, AuNP-PEG-RIgG showed an average size increase of about 16 nm compared to citrate stabilized AuNPs, while AuNP-RIgG exhibited a size increase of ~22 nm.

5.4 Conjugate's stability

The influence, most especially on their stability, which adsorbed macromolecules or polymer layers deposited on nanoparticle surfaces could exert on nanoparticle properties, has been studied in the past [139 - 142]. Consequently, the idea of steric stabilization of nanoparticles was suggested. Following this, Abuchowski et al. investigated covalently attached PEG coatings to proteins [143]. Their work was elaborated to include the biomedical applications of the particle systems. Based on those works, this section and the proceeding ones elaborate on the contribution of PEG linkers to AuNP antibody conjugate's stability, their absorbance properties and coverage.

Shifts in plasmon band and changes of the absorption value on aging of AuNP systems could be linked to changes or state of their stability. Insufficient stabilization could cause aggregation of particles. This could lead to the agglomeration of the particles. Aggregation causes decreased optical absorption when particles are lost to agglomeration during this process. Increased interaction between the individual particles leading to agglomerations and precipitation of particles ends in loss of the characteristic red colour of their solutions. This process could be easily monitored with eye or instrumental absorption measurements.

5.4.1 Effect of solution's ionic strength

For biological applications, the AuNPs systems must withstand electrolytic environments such as buffer solutions and cell culture medium over a long period of time. Citrate stabilized AuNPs do not meet this requirement because they irreversibly aggregate even at very low salt concentrations (≤ 0.03 M NaCl). These are values even below the physiological concentration of 150 mM NaCl [139, 140].

The stability of the gold nanoparticle antibody conjugate system prepared by electrostatic interaction was compared with the behaviour of the covalently coupled counterpart by observing their behaviors when introduced in media of varying ionic strength.

For this investigation, electrostatically coupled conjugates and covalent conjugates were prepared by using thousand fold excess of RIgG (200 μ L, 6 μ M) and H₂N-PEG-RIgG respectively for exchange with citrate AuNP (1 mL, 1.2 nM). The prepared samples were then subjected to different media of varying ionic strength by introducing known concentrations of NaCl solutions to the conjugate solution to obtain salt concentrations varying from 0.1M to 4M. Figure 5.13 and Figure 5.14 show the UV-Vis absorption spectra of the salt solutions of

both systems: the ionically coupled as well as covalently coupled conjugates systems respectively. The absorption spectra shown in figure 5.14 shows the behaviour of the electrostatically coupled conjugates recorded repeatedly over short time interval of 5 minutes from the preparation. Figure 5.14 shows the spectra from the first and last measurements of the covalently coupled conjugates made over a time period of 4 hours.

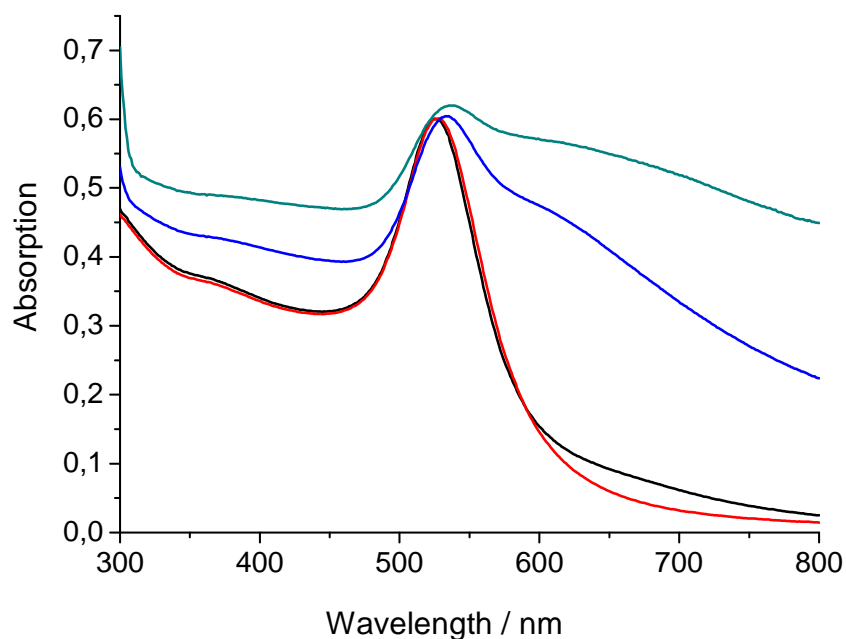


Figure 5.13: Normalized absorption spectra of the ionically coupled AuNP RIgG conjugate in 1xPBS solution. Measurements were taken in 5 minutes intervals after preparation starting with the red spectrum, black, blue and finally the green spectrum.

As can be seen from figure 5.13, the absorbance at wavelengths between 600 nm to 800 nm increased continuously over the period of investigation until a total loss of the red colour of the solution due to particle loss by aggregation could even be seen by the eye. The figure reveals the aggregation of AuNPs after introducing them in solutions with different NaCl concentrations within short time intervals.

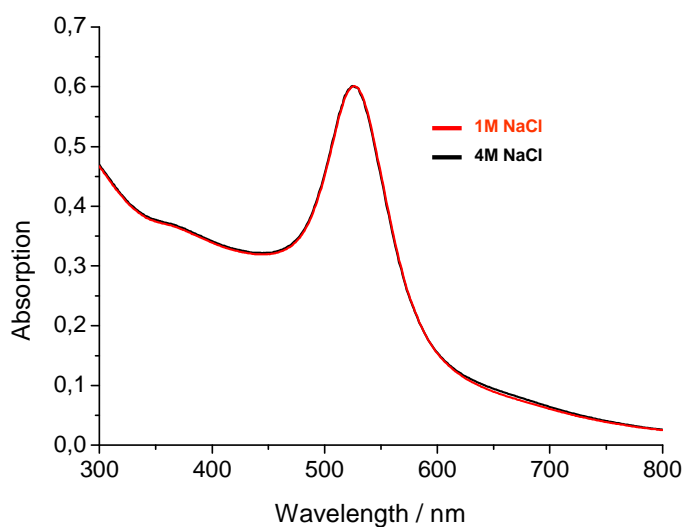


Figure 5.14: The spectra of the covalently coupled system, representing the first (red curve) and last (black curve) measurement made over 4 hours are shown.

This covalently coupled conjugates exhibited similar behaviour in all the tested salt concentrations varying from 0.1M to 4M. Figure 5.14 shows a stable behavior of the HS-PEG-RIGG coated AuNPs even in high ionic environment. The absorption behaviour in media with ionic strength of 4 M NaCl remained unchanged even after 4 hours of storage.

In conclusion of the above observation from both tested systems, ionically coupled AuNP-RIGG conjugates and the covalently coupled AuNP-PEG-RIGG conjugates in different ionic media, it is obvious that the covalent system are more stable. This demonstrates again the superior stability of the covalent conjugate systems over the ionic conjugate systems while serving as an evident of the important role played by the PEG polymer in stabilizing the conjugates. In most of the electrostatic coupling protocols, post synthetic step are included to introduce PEG ligands or other stabilization factor to help the stability of the systems.

5.4.2 Conjugate's absorption behaviour with storage time

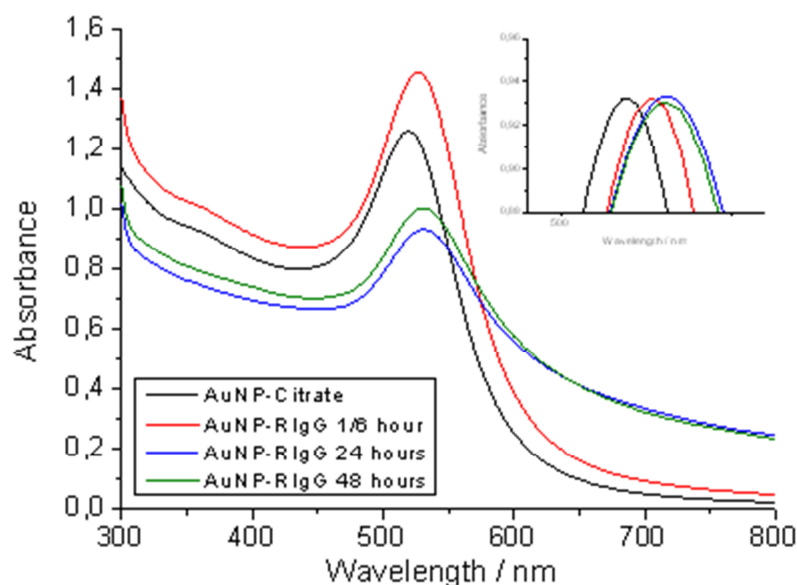
The stability of AuNP systems on storage can be related to the variation of their optical behaviour over the storage time.

To compare the stability of different AuNP systems, the samples AuNP-PEG-RIGG (covalent), AuNP-RIGG (ionic) and AuNP-PEG-NH₂ (covalent) were prepared and their stabilities were monitored over 48 hours by recording their UV-Vis spectra at time intervals.

For a proper result analysis, the obtained spectra were normalized and enlarged (inset) as shown in each of the figures 5.15.

Figure 5.15 *I* show the spectra for AuNP-RIGG. The absorption curves from all measurements of citrate stabilized AuNP and for all three samples taken at intervals between 1/6 hours and 48 hours are shown in figure 5.15 *II*. The spectra were similarly analyzed like that in 5.15 *I* and for simplicity a summary of the results is presented in table 5.3.

I.



II.

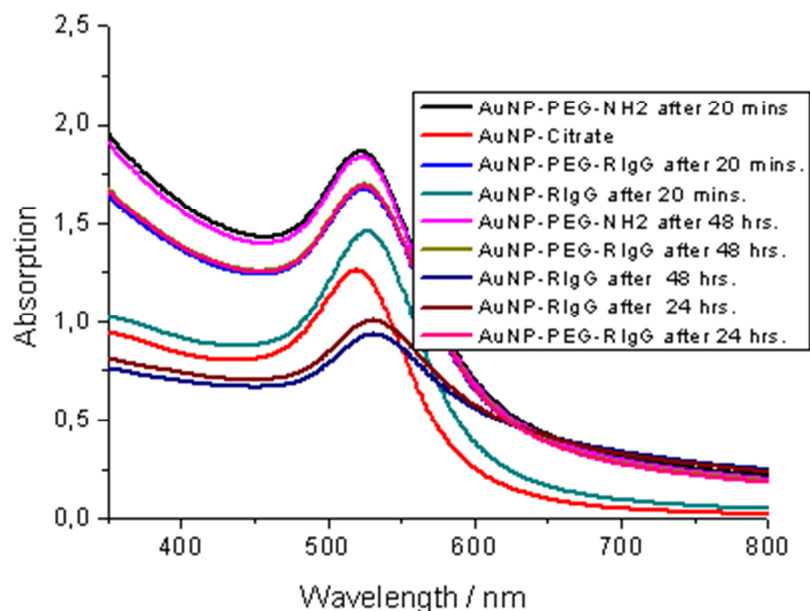


Figure 5.15: The absorption peaks showing changes of peaks peak positions summarized in table 5c.

Table 5.3: summarized result obtained from absorption peaks of the data in figure 5l.

Capping Agent	Citrate	PEG	Shift (nm)	RlgG (covalent)	Shift (nm)	RlgG (ionic)	Shift (nm)
Max. Absorption peak (nm) (20 mins)	519	523	4	524	5	526	7
Max. Absorption peak (nm) (40 mins)		523	4	524	5	527	8
Max. Absorption peak (nm) (24 hrs)		523	4	524	5	530	11
Max. Absorption peak (nm) (48 hrs)		523	4	524	5	530	11

The table (5.3) enables an uncomplicated comparison of the absorption behaviours of the exchange products obtained using AuNP-PEG-NH₂ (initial absorption peak at 523 nm), AuNP-PEG-RlgG (initial peak at 524 nm) and AuNP-RlgG (ionic, having initial peak at 526 nm). The UV-Vis measurements were initially done after 20 minutes exchange. The peak of the citrate stabilized AuNPs, AuNP-Citrate is at 519 nm. On comparison, it becomes obvious that the peak positions of all sample systems shifted (dark grey columns) after

functionalization (exchange reaction). AuNP-PEG-NH₂ and AuNP-PEG-RIgG showed similar behaviours with shift of 4 nm and 5 nm respectively. For the AuNP-RIgG system, peak-shift up to 7 nm was observed 20 minutes after preparation. This shows different behaviour due to differences in the attaching mode (surface interacting moieties) between electrostatically coupled AuNP-RIgG system and the covalent coupled AuNP-PEG-RIgG and the AuNP-PEG-NH₂ systems. This similarity in the latter two systems (covalent systems) is a behaviour attributed to their similar surface interacting moiety of thiol capped PEG ligands.

The stabilising effect of PEG polymer becomes obvious, when peaks from particles covered with covalently coupled PEG ligands (including PEG attached to IgG) showed minimal shifts. Over the period of 48 hours the PEGylated RIgG nanoparticle conjugate (AuNP-PEG-RIgG) remained outstandingly stable with no observable peak-shifts. The peak of the less stable AuNP-RIgG system shifted continuously over 24 hours and could only remain constant after this time.

5.4.3 Effects of ligand length on particle stability

For the investigation in this section, first the AuNP systems were synthesized according to the procedures described in section 4.3 and figure 5.16 shows representative illustration of the products obtained by conjugating AuNP (size ~12 nm) with thiolated PEG polymers: HS-PEG-NH₂, MW: 3 kDa, 5 kDa and 10 kDa and with thiolated PEG-RIgG previously synthesized using similar PEG polymers: HS-PEG-NH₂ with PEG having MW: 3 kDa, 5 kDa and 10 kDa.

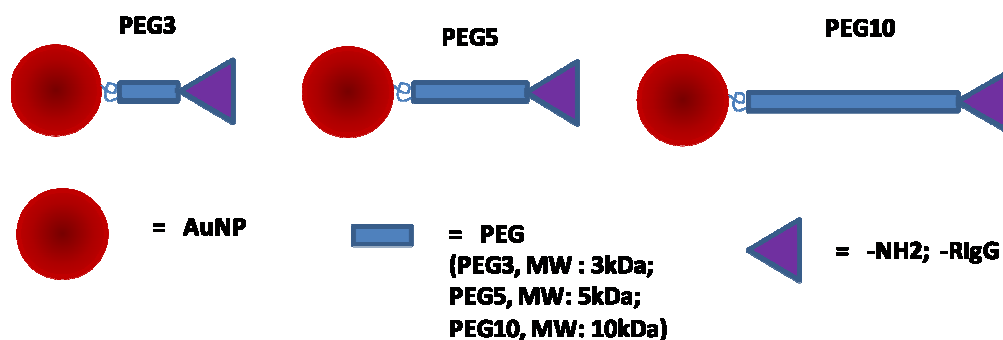


Figure 5.16: The systems achieved by conjugating thiolated PEG polymers (MW: 3 kDa, 5 kDa and 10 kDa) or thiolated PEG-RIgGs with AuNPs

Consequent to the ligand exchange procedure using thiolated PEG polymers, three AuNP systems: AuNP-PEG3-NH₂, AuNP-PEG5-NH₂ and AuNP-PEG10-NH₂ were obtained respectively. The resulting conjugates were characterised by UV-Vis absorbance measurements. This method was used to monitor the absorbance behaviour of conjugates over a period of 96 hours by taking measurements at ¼ hour, 24 hours and 96 hours after conjugation. Figure 5.17 shows the absorption spectra obtained for the three samples. The figures 5.17.1 – 5.17.3 represent the result for the repeated measurements and the normalised absorption spectra (insets). The spectrum of the citrate stabilized AuNPs which is used as reference sample is also shown in each case. Figure 5.17.4 shows a bar diagram representation of the samples' absorbance.

(I)

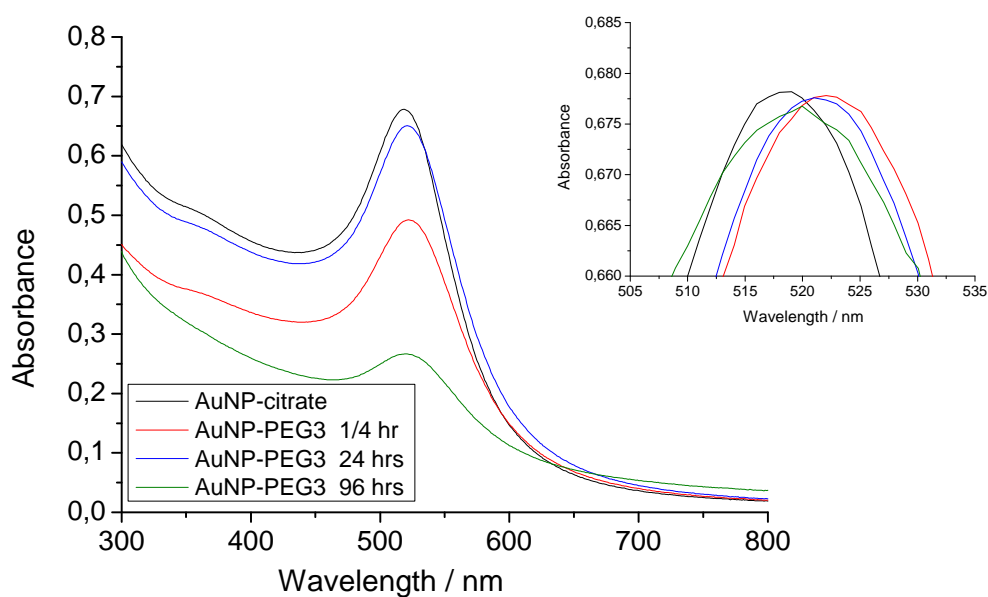


Figure 5.17.1: The normalised absorption spectra of the samples prepared using PEG3 including that of the citrate stabilized AuNPs which is used as reference sample.

(II)

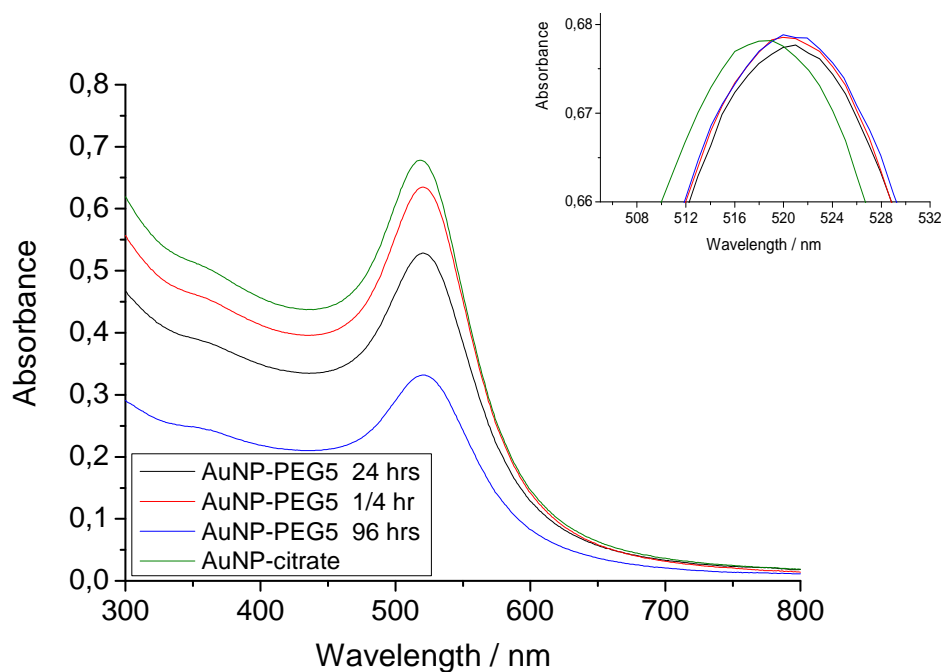


Figure 5.17.2: The normalised absorption spectra of the samples prepared using PEG5 including that of the citrate stabilized AuNPs which is used as reference sample.

(III)

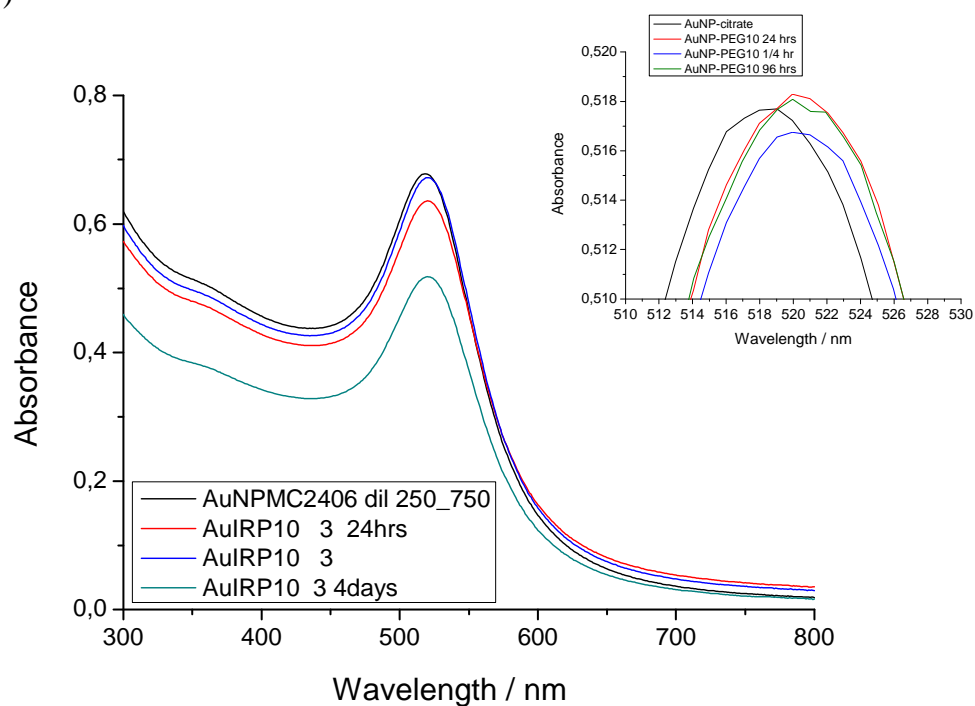


Figure 5.17.3: The normalised absorption spectra of the samples prepared using PEG10 including that of the citrate stabilized AuNPs which is used as reference sample.

(IV)

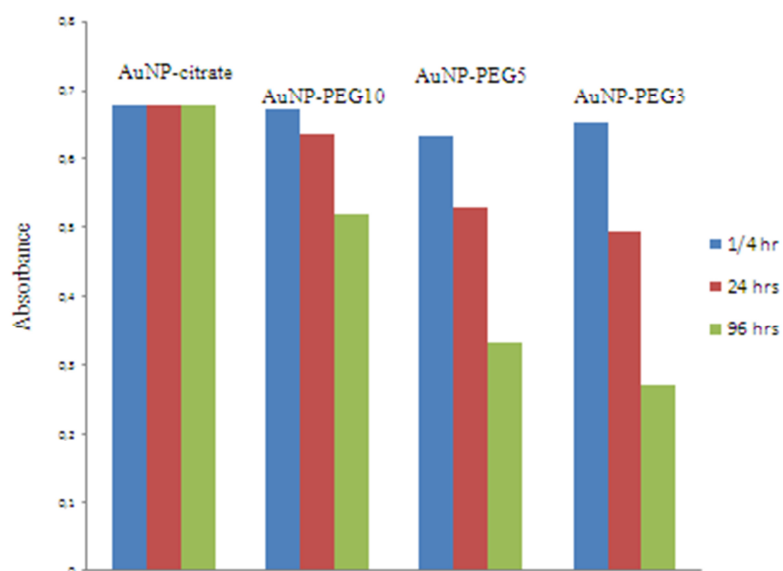


Figure 5.17.4: Bar diagram showing changes of absorbance from curves in diagrams (I) - (III) over the 96 hours period of investigation.

The usual peak shifts were observed on a careful examination of the curves, ¼ hour after the ligand attachments. This is due to the presence of the PEG ligands on the AuNP surfaces. System prepared with the smallest ligand, AuNP-PEG3-NH₂ showed remarkably progressive decrease in absorbance through the 4 days of investigation. At this time scattering is observed to be enhanced due to aggregation. This effect is attributed to particle-particle interaction as they become linked and closer to each other. This could be due to electrostatic interaction between citrate molecules (through carboxyl groups) in solution with the amine functionality of the ligands on the particle surfaces. The extent of interaction between the particles could be affected by the length of the PEG ligand. For the 3 kDa ligand this interaction is evidently stronger and enough to cause precipitation of the particles, leading to reduced absorption. The system with the 5 kDa PEG ligand, AuNP-PEG5-NH₂ showed no scattering effect after 96 hours, although a progressive decrease in absorption within the period of investigation was also observed. This effect is less pronounced compared to that from the AuNP-PEG3-NH₂ system. Similar to the AuNP-PEG5-NH₂ system, sample obtained using the 10 kDa PEG ligand, AuNP-PEG10-NH₂ showed no scattering effect after 96 hours, but after 24 hours little decrease in absorbance was observed, which was progressive over 96 hours. This effect is significantly less pronounced when compared to the AuNP-PEG3-NH₂ and the AuNP-PEG5-NH₂ systems.

In conclusion, even when the systems with larger PEG polymers, AuNP-PEG10-NH₂ are most stable over the investigation period, all the systems were initially not perfectly stable, as they do show decrease in absorption. Nonetheless, the stability of these AuNP systems decorated with HS-PEG-NH₂ increases with increasing length of the PEG polymer chain as indicated by the observed scattering exhibited by the system having -PEG3-NH₂ with less pronounced decrease in absorbance on aging when -PEG10-NH₂ is used.

The experiments described above were analogically repeated with RIgGs previously modified with similar ligands (HS-PEG-NH₂, MW: 3 kDa, 5 kDa and 10 kDa). The modification was done by the IgG glycan oxidation method described in the experimental section of this work. After the attachment of ligand to RIgG, the conjugates were then prepared by exchange reaction of citrate stabilised AuNPs (size ~12 nm) with the PEGylated RIgG to obtain three samples (AuNP-PEG3-RIgG, AuNP-PEG5-RIgG and AuNP-PEG10-RIgG) respectively.

The resulting conjugates were also characterised by UV-Vis absorbance measurements and their behaviours monitored over a period of 96 hours like done above. Figure 5.18 shows the

absorption measurement results for the three samples. The figures, 5.18.1 – 5.18.3 represent the result for repeated measurement over 96 hours and the corresponding normalised absorption spectra (insets). The citrate stabilized AuNPs was used as reference sample. Figure 5.18.4 shows a bar diagram representation of the samples' absorbance.

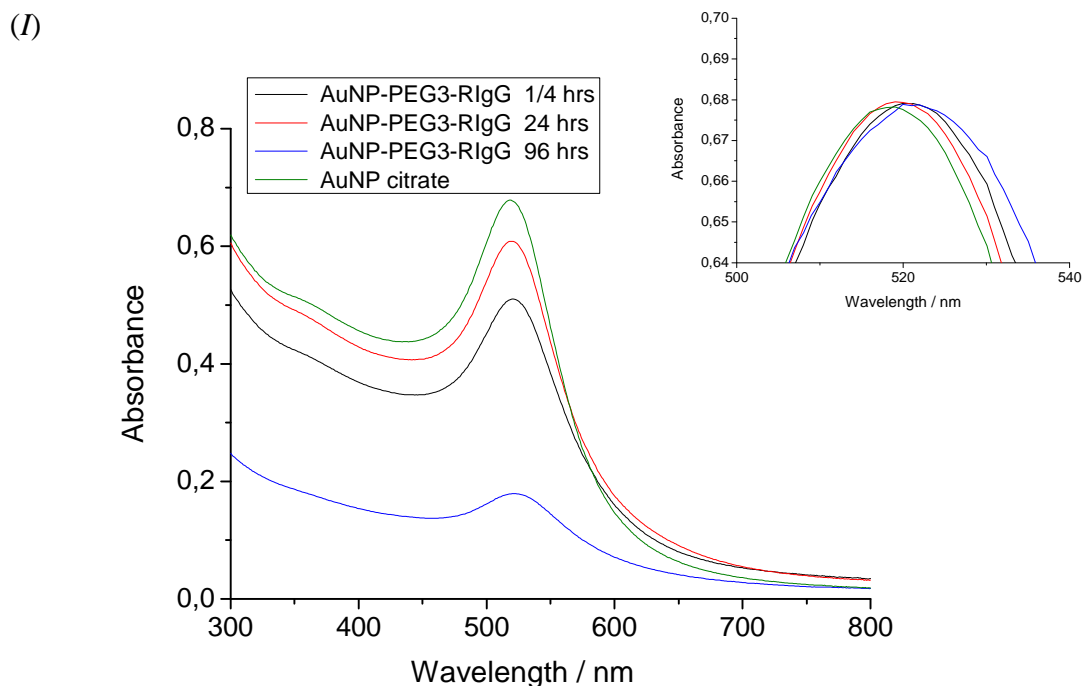


Figure 5.18.1: The absorption spectra and their normalised forms (inset) of the AuNP-PEG-RIgG conjugates prepared using PEG3 including that of the citrate stabilized AuNPs used as reference sample.

(II)

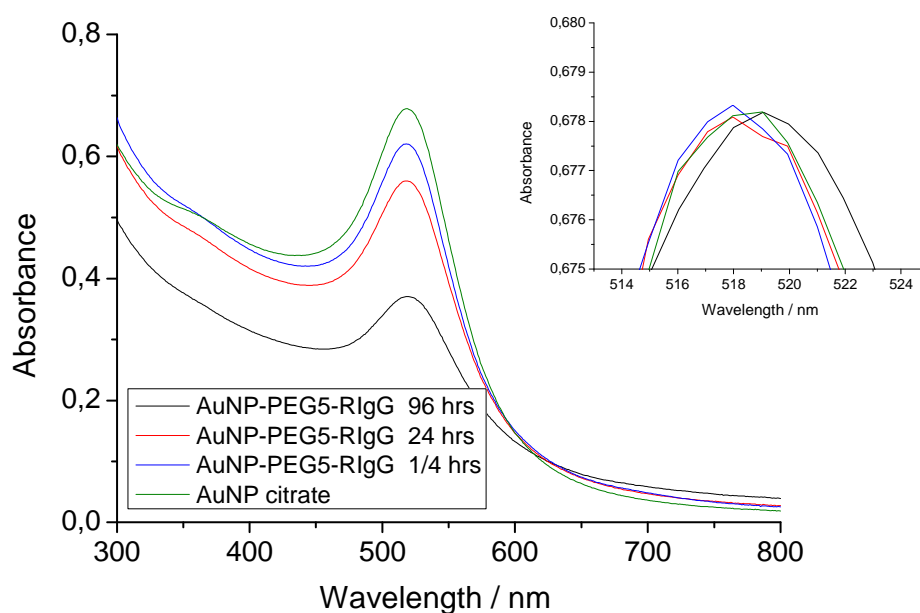


Figure 5.18.2: The absorption spectra and their normalised forms (inset) of the AuNP-PEG-RIgG conjugates prepared using PEG5 including that of the citrate stabilized AuNPs used as reference sample.

(III)

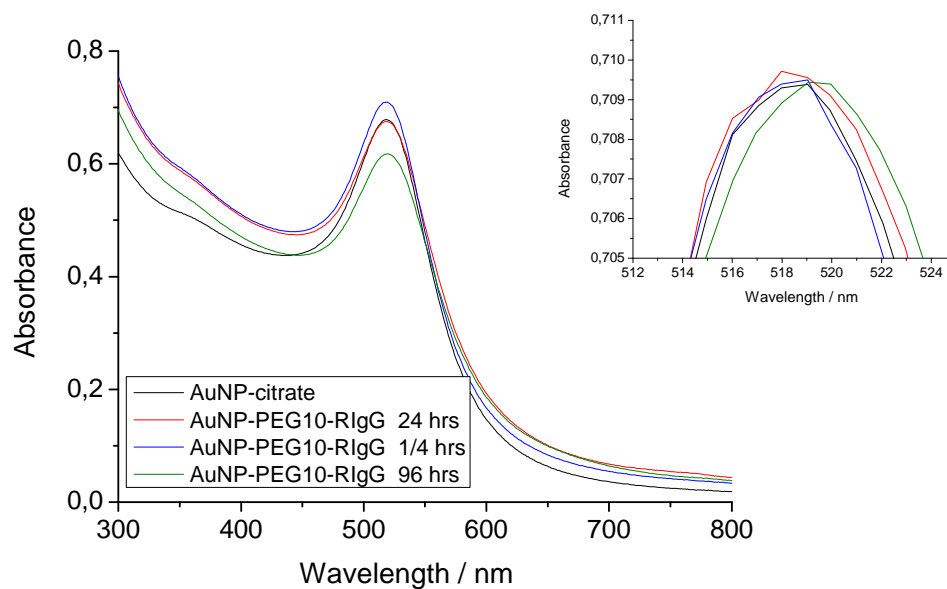


Figure 5.18.3: The absorption spectra and their normalised forms (inset) of the AuNP-PEG-RIgG conjugates prepared using PEG10 including that of the citrate stabilized AuNPs used as reference sample.

(IV)

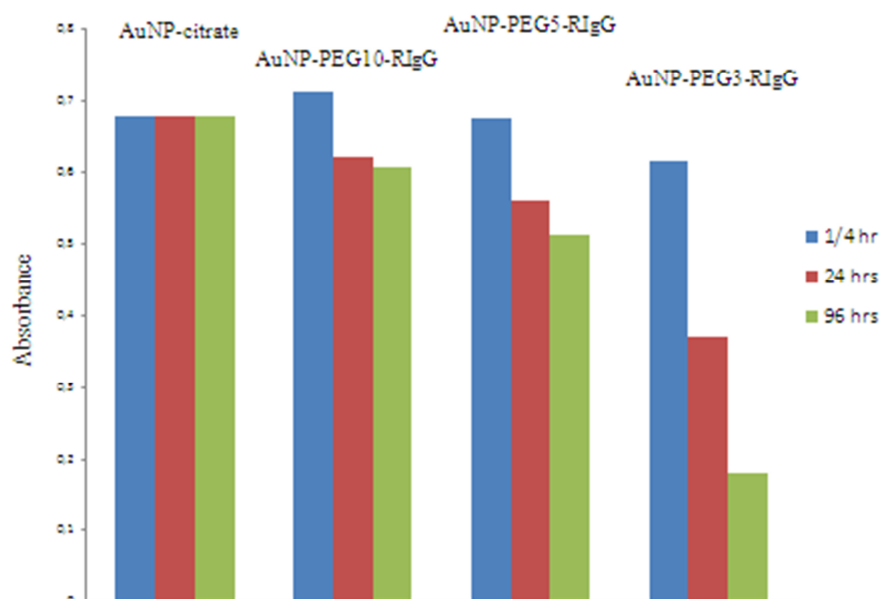


Figure 5.18.4: Bar diagram showing changes of absorbance from the curves in diagrams (I) - (III) over the 96 hours period of investigation.

The results obtained here show some analogy to those obtained in the preceding discussion.

The usual peak shifts were also observed on a careful look at the curves, $\frac{1}{4}$ hour after the ligand attachments. This is due to the presence of the PEG-RIgG ligands on the AuNP surfaces.

The system with the smallest ligand, AuNP-PEG3-RIgG showed remarkably progressive decrease in absorbance through the 4 days of investigation, which could be attributed to particle-particle interaction as discussed already in the preceding paragraphs. For the 3 kDa attached RIgG this interaction is evidently strong with reduced absorption. The system with the 5 kDa PEG ligand, AuNP-PEG5-RIgG showed some scattering effect also after 96 hours and a progressive decrease in absorption within the period of investigation was also observed. These effects are less pronounced when compared to the AuNP-PEG3-RIgG system but the scattering effect is in contrary to the observation made by the AuNP-PEG5-NH₂ system without attached RIgG molecule. Unlike the AuNP-PEG5-RIgG system, the 10 kDa PEG ligand, AuNP-PEG10-RIgG showed no scattering effect after 96 hours, but after 24 hours little decrease in absorbance was observed, which was progressive over 96 hours. This effect

is significantly less pronounced when compared to the AuNP-PEG3-RIgG and the AuNP-PEG5-RIgG systems.

In conclusion, similar to the systems without RIgG molecule (AuNP-PEG3-NH₂, AuNP-PEG5-NH₂ and AuNP-PEG10-NH₂) the larger PEG polymers showed comparably most stable behaviour over the investigation period even when all the systems were not perfectly stable initially. The stability of AuNP systems decorated with HS-PEG-RIgG increases with increasing length of the PEG polymer chain as indicated by the observed scattering exhibited by the systems AuNP-PEG3-RIgG, AuNP-PEG5-RIgG and a less pronounced decrease in absorbance with aging of samples prepared with HS-PEG10-RIgG.

5.4.4 LCC (*Lowest Coagulation Concentration*)

After a successful conjugation of nanoparticles with proteins such as antibodies, the stability in high salt content of buffer solutions are guaranteed. This idea has been used as one method to confirm the successful conjugation of proteins to AuNPs [144-146].

Another logical parameter explored to determine the stabilizing strength of the ligands here is the LCC method. This is a means of determining the minimum concentration of the ligands (which are HS-PEG-NH₂, HS-PEG-RIgG and RIgG), necessary to stabilize the particles in PBS buffer after ligand exchange. PEG ligand (HS-PEG-NH₂) with molecular weight of 3kD was used for the investigations in this section and consequently for all preparations and attachments. The PBS buffer used contained approximately 0.14 M NaCl, which is higher than the biological salt concentration of about 0.10 M. The salt content of PBS is sufficient to cause agglomeration, making this buffer an efficient candidate for use in testing the stability of gold nanoparticle. Therefore agglomeration takes place in this condition, for gold nanoparticles that are electrostatically stabilized as well as for those with insufficient ligand coverage.

Briefly, varied concentrations of the respective ligands solutions prepared in 1x PBS were used for exchange reactions with 100 μ L AuNP (16 nM, 12 nm diameter). Basically, the reaction solution is 1x PBS, since the AuNP in citrate buffer was introduced in a comparably minimal volume. The experiment was started with high ligand concentration (a large ligand excess) and then repeated with a dilution series of this initial concentrations until the lowest ligand concentration that can stabilize the same AuNP concentration (the LCC) was obtained.

Figures 5.19.1, 5.19.2 and 5.19.3 show photographs and UV-Vis absorption spectra of 700 μL AuNP solution with ligand concentration shown in table 5.18 (Experiment 1, 2 and 3). Accordingly, the final salt concentration was 0.12 M, pH 7.0 and 1.6 pmol AuNP (12 nm) concentration were used in each case. Samples concentrations within the minimum stability range are shown in figures 5.19.1 – 5.19.3.

Table 5.4: Ligands concentrations used in LCC experiments with results in figures 5.19.1 - figure 5.19.3.

Exp.	Ligand	A. (nmol/mL)	B. (nmol/mL)	C. (nmol/mL)	D. (nmol/mL)	AuNP (nmol/mL)	Ligand/ Particle
1.	HS-PEG3-NH ₂	2.6×10^{-1}	2.6	2.6×10^1		2.3×10^{-3}	11304
2.	RlgG	2.6×10^{-2}	5.2×10^{-2}	2.6×10^{-1}		2.3×10^{-3}	113
3.	HS -PEG3-RlgG	1.3×10^{-4}	2.6×10^{-4}	2.6×10^{-3}	2.6×10^{-2}	2.3×10^{-3}	11

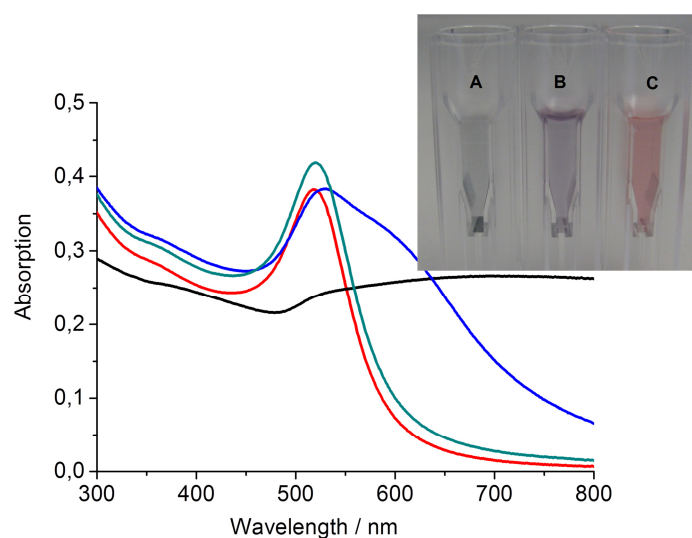


Figure 5.19.1: UV-Vis spectra and photograph of AuNP conjugates. The spectrum (red line) is from the citrate stabilized AuNPs while the others are those of the samples in the cuvettes in the photograph from right to left (green, blue and black line) respectively. The photograph is that for samples prepared using ligand concentrations as given in table 5.4 (Experiment 1). For the attachment, 1.8 pmol AuNP were used in each case.

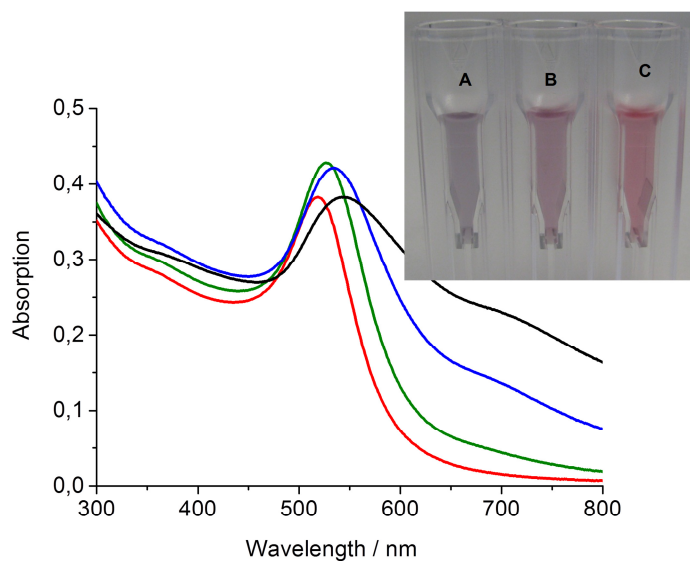


Figure 5.19.2: UV-Vis spectra and photograph of AuNP conjugates. The spectrum (red line) is from the citrate stabilized AuNPs while the others are those of the samples in the cuvettes in the photograph from right to left (green, blue and black line) respectively. The photograph is that for samples prepared using ligand concentrations as given in table 5.4 (Experiment 2). For the attachment, 1.8 pmol AuNP were used in each case.

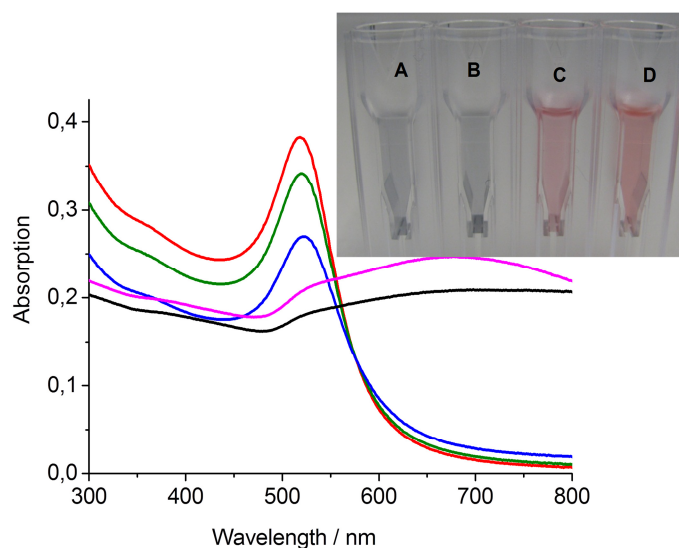


Figure 5.19.3: UV-Vis spectra and photograph of AuNP conjugates. The spectrum (red line) is from the citrate stabilized AuNPs while the others are those of the samples in the cuvettes in the photograph from right to left (green, blue and black line) respectively. The photograph is that for samples prepared using ligand concentrations as given in table 5.4 (Experiment 3). For the attachment, 1.8 pmol AuNP were used in each case.

The transitions from stable solutions (higher ligand concentration) to aggregated particles (lowest ligand concentration) were recognized by the color changes in the photographs (figures 5.19.1, 5.19.2 and 5.19.3). UV-Vis spectrum of citrate stabilized particles is included as reference (red curve) in each case. The photographs show the samples with ligand concentration that could confer stability are those that retained their red color and could be visually distinguished from the unstable samples which turned blue. However, this optical distinction seen from the samples UV-Vis spectrum are clearer. This allows a finer cut to be made between the stable and the unstable samples. On a closer examination of the optical absorption forms and their optical densities, the ligand concentrations printed bold in table 5.4 for samples in cuvette C in each of the photographs are the lowest coagulation concentration of ligands for the respective samples. The calculated ligand excess values for these samples having the LCC are: 11,304.00 for HS-PEG-NH₂, 113.00 for RIgG and 11.00 for HS-PEG-RIgG. This can synonymously be assumed to be the lowest ligand concentrations that can sufficiently stabilize a 100 mL (1.6 pmol, 12 nm diameter) AuNPs in 1xPBS solution. The surface atoms of a 12 nm AuNP were calculated as 5562 and therefore for HS-PEG-NH₂, there are about 1 atoms/2 ligands, for RIgG 49 atoms/ligand and for HS-PEG-RIgG 506 atoms/ligand.

The results show that HS-PEG-RIgG is the most effective particle stabilizer than HS-PEG-NH₂ and RIgG. This is possible due to the advantage of the combined steric effect from both the PEG and RIgG molecules and the covalent bonding effect from the thiolated attachment to the particle surface via the thiol cap of the ligand.

5.4.5 Bulky Cap Packaging effect

AuNP systems with 52 nm Au core were prepared using PEG ligands HS-(PEG) n -RIgG having 72, 113 or 227 PEG units. The obtained samples are AuNP-PEG3-RIgG, AuNP-PEG5-RIgG AuNP-PEG10-RIgG respectively. These samples were investigated by using the LCC method to obtain the minimum ligand concentrations from which the surface coverages were estimated. The coverage was obtained by either dividing the concentration of the ligand (HS-PEG-RIgG) at LCC by the AuNP concentration or by dividing the total particle surface atoms by the ligand concentration at LCC. The results obtained for the coverage using 52 nm AuNP core particles are seen in table 5.5.

Table 5.5: The number of RIgG linked to each nanoparticle obtained by LCC analysis method, for HS-PEG3-RIgG, HS-PEG5-RIgG, HS-PEG10-RIgG.

	RIgG/AuNP	Surface atoms/RIgG	Particle Core size, TEM (nm)
AuNP-PEG3-RIgG	37	2931	52
AuNP-PEG5-RIgG	74	1465	52
AuNP-PEG10-RIgG	74	1465	52

In table 5.5, ligand length promoted changes could be observed. Ligands having PEG molecular weights of 3 kDa ($n = 72$) has 37 ligands/AuNP and those with 5 kDa PEG ($n = 113$) has 74 ligands/AuNP. This shows a clear difference in their coverages due to the ligand length. There was no difference between systems with 5 kDa PEG and those with 10 kDa PEG ligand, both having 74 ligands per particle. This behavior is similar to that observed by Bradford analysis, which shall be discussed later. In that experiment, 12 nm AuNP instead of 52 nm AuNP and similar PEG ligands to those used in this section, were used. This unique behavior can be explained by the “Bulky Cap” effect schematized in figure 5.20.

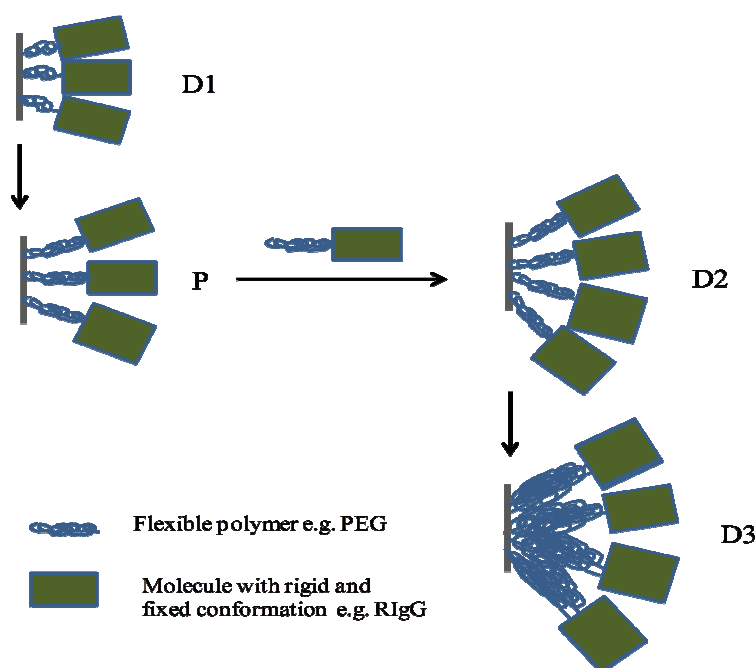


Figure 5.20: The bulky cap packaging effect. At small PEG length, the IgG is a limiting factor to coverage and with longer ligand length the diagonal size of the PEG becomes the limiting factor to coverage.

Consider a ligand consisting of two polymer segments – a flexible neutrally charged (PEG) segment and a three dimensional rigid and bulky segment (e.g. IgG), attached to a specified surface area on AuNP via a thiol capped PEG spacer, whose length is variable. With short PEG lengths, the rigid moieties are close to each other near the particle surface. This arrangement brings bulky caps close to each other, so that they become limiting factor to the coverage (figure 5.20 D1 and D2). This situation may also be caused by charged ligand or PEG caps experiencing electrostatic repulsions when close to neighboring groups on the particle surface. If the ligand length is increased, the rigid moiety are placed some few distance away from the surface, resulting in additional free space that allows insertion of more ligands on the surface (P). When the PEG length is again increased, it caused the the rigid cap to be driven further away from the surface. At a particular length, the diagonal size of the flexible moiety reaches a limit, where there is a direct contact of the PEG with their nearest neighbors (figure 5.20 D3). The ligands become densely packed via the PEG segment at the

particles surface. A repeated PEG length increase only contributes to a one dimensional movement of the ligand in the direction away from the surface since the empty spaces close to the particle surface are fully occupied by the ligand. Addition of more ligands onto the particle surface becomes impossible and the surface coverage remains constant even when the ligand length is increased.

5.4.6 Effects of particle size and ligand (length) on AuNP Properties

Following the discussions made in the preceding sections, the nanomaterial properties, such as size, plasmon-peak shift, surface coverage, stabilizing strength are affected by the type and length of PEG ligand deposited on the particle surface. In this section, detailed discussion on the changes of particle size and surface charge density due to the nature of the ligand and the size of the Au core is continued.

The size of nanoparticles changes significantly with variations of the particle shell thickness, which is often determined by the length of the PEG ligand and the surface packaging.

Using citrate stabilized AuNPs having TEM size of 12 nm, three samples with PEG (HS-PEG-NH₂: MW; ~3 kDa, ~5 kDa and ~1 kDa) coatings were prepared via place exchange reactions. After preparation, the samples were analysed by DLS measurements. Results obtained were plotted against the length of the ligands as seen in figure 5.21.

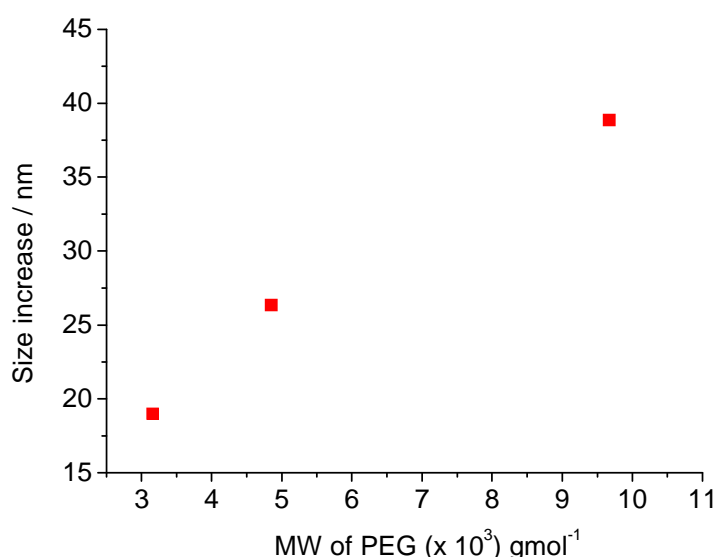


Figure 5.21: Results obtained by plotting the obtained DLS values for each ligand against the length of the ligands.

From figure 5.21, the size of the particle showed a linear increase proportional to the length of the PEG ligand used for its preparation. This result is in good agreement with the results reported for the hydrodynamic thickness of PEG coating terminally anchored to spherical liposomes by Hill [148]. They found that hydrodynamic size and electrophoretic mobility of liposomes are influenced by the molecular weights (chain lengths) of terminally anchored PEG.

In a manner similar to the above investigation, a study of particle surfaces having different Au core sizes and similar ligand was made. Like that investigation with PEG polymers, the PEG polymers this time were also previously attached to RIgG (PEGylated RIgG) before use for exchange reactions. The products were obtained from preparations involving gold nanoparticles with varying sizes; AuNP4 ($d = 36$ nm), AuNP5 ($d = 42$ nm), AuNP6 ($d = 61$ nm) and PEG ligands with MW of 5 kDa. The results of the DLS measurements of the products are shown in table 5.6 f.

Table 5.6: The results of the DLS measurements samples prepared with gold nanoparticles, AuNP4 (36 nm), AuNP5 (42 nm), AuNP6 (61 nm) and PEG ligands (MW: 5000). The average values are printed in blue.

Sample	DLS				Increase (nm)
	Intensity	Volume	Number	PDI	
AuNP4	54.59	43.58	35.62	0.16	
AuNP4-PEG5	78.01	60.71	50.00	0.14	22 (11)
AuNP4-PEG5-RIgG	90.63	63.88	43.51	0.17	29 (14.5)
AuNP5	62.29	48.25	38.14	0.18	
AuNP5-PEG5	86.75	66.32	48.31	0.14	22 (11)
AuNP5-PEG5-RIgG	102.66	78.88	39.22	0.17	33 (16.5)
AuNP6	73.14	55.17	42.08	0.20	
AuNP6-PEG5	92.42	70.28	49.53	0.14	21 (10.5)
AuNP6-PEG5-RIgG	101.52	80.17	55.41	0.15	29 (14.5)

The size (diameter) increase due to ligand deposition on the particle surface is printed in green as shown in table 5.6. These values were obtained by subtracting the size of the AuNPs before exchange reaction from those of the ligand covered particles. The thicknesses of the particles (in brackets) were then obtained as half the diameter increases. An average increase in thickness of ~ 22 nm/2 i.e. 11 nm for the PEG ligands and ~ 30 nm/2 i.e. 15 nm for the PEGylated RIgG ligands were estimated. This value obtained for 5 kDa PEG ligand is in agreement with literature values for PEG thickness on nanoparticles [148, 153].

The results above allowed an estimation of the average particle thickness contributed by the RIgG molecules on the particle surface. This was obtained by subtracting the size of the PEGylated AuNPs from the sizes of the AuNP-PEG-RIgG conjugates printed in green (table 5.6). The fraction of the particle thickness contributed by RIgG molecules was obtained as the half the value of particle's diameter. This resulted to an average RIgG shell thickness of ~ 9 nm/2 i.e. 4.5 nm for all AuNP-PEG-RIgG conjugates. This value is strikingly within the range of values given for the hydrodynamic radius of RIgG []. Additionally this generally result supports the antibody orientation suggested in section 5.5.1.

Plasmon Position: The Plasmon bandwidth and position are influenced by the capping ligands on the particle surface [154-160]. The chemical interface damping (CID) was proposed to account for the dependent of those factors on the chemical nature of the ligand [161]. According to that report, the plasmon resonance of metallic nanoparticle is influenced by the electronic structure of the adsorbate molecules, whereby plasmon electrons are excited into the empty orbitals of the molecules causing changes of the particle's surface plasmon. This explains the absorption peak shifts when ligands are attachment onto particles during exchanged reactions. For most of the exchange experiment with thiolated PEG and its variants in this work, peak-shifts ranging within 1-3 nm were recorded. The behavior of the ligands was similar irrespective of the size of the AuNP core and the ligand length.

Zeta Potential, ζ : Particle's surface charge is an important factor influencing its stability, reactivity and other important colloidal properties like solubility and pH values.

Information on the behaviour of the particles' surface charge density can greatly enhance the nanoparticle conjugates applications. This factor of a colloidal particle is influence by the surface bound ions or ligands. The effect of PEG and antibody coatings on nanoparticle surface charge is discussed in this section. Focus is made on the effects of PEG ligand length, particle size and the covering species.

Three AuNP samples with PEG coatings having different lengths (HS-PEG-NH₂: MW; ~3 kDa, ~5 kDa, ~1 kDa) were prepared. The PEG ligands have head caps of thiol group on one end and amine group on the other. Another set of samples was prepared similar to above using same AuNP core particle and three PEGylated RIgG (HS-PEG-RIgG ligands from ~3 kDa, ~5 kDa and ~1 kDa PEG polymers). The products systems were analysed by Zeta Potential measurements. Results obtained were plotted against the ligand length as seen in figure 5.22.

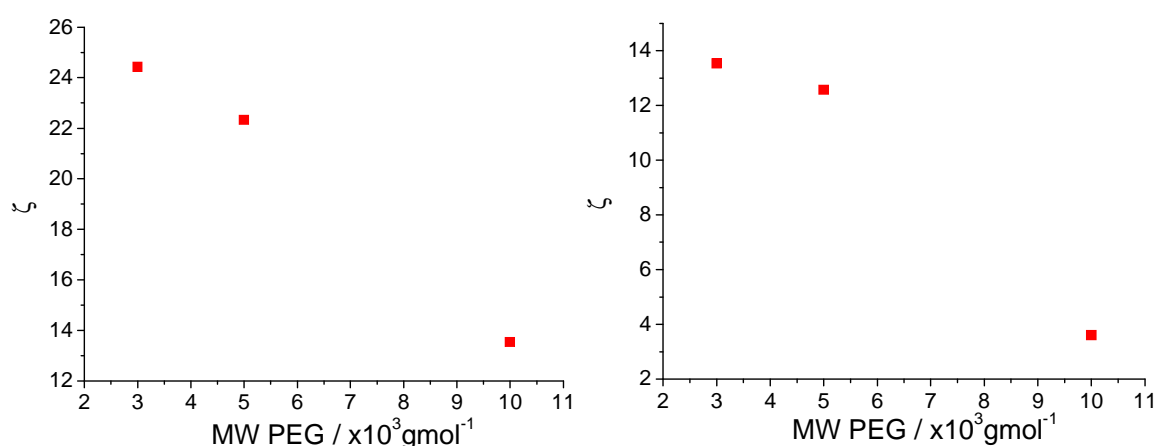


Figure 5.22: Results obtained by plotting the ζ -potential against the length of the ligands for AuNP-PEG-NH₂ systems (left) and AuNP-PEG-RIgG systems (right).

The results in figure 5.22 show changes of charge density of AuNPs as influenced by size of the PEG ligand on their surface. Both ligands HS-PEG-NH₂ and HS-PEG-RIgG exhibited similar behaviour. For both systems, the length of the PEG polymer proportionally increases with a reducing surface charge density represented by their zeta potentials.

In addition, the influence of particle size and the surface covering species on AuNP properties were further investigated. Two sets of four AuNP samples having Au core diameters of ~22 nm ~46 nm, ~52 nm and ~61 nm, and 5 kDa PEG ligands for the first and PEGylated RIgG for the second were prepared i.e. four AuNP-PEG-NH₂ samples and four AuNP-PEG-RIgG conjugates samples. After preparation, the functionalized samples and their corresponding citrate stabilized AuNP samples for controls were analysed by Zeta Potential measurements. Values obtained were plotted against the sizes of the core AuNP sizes as seen in figures 5.23, 5.24 and 5.25. Graph in figure 5.23 is the result of the citrate stabilised AuNPs, figure 5.24 is that of the PEGylated AuNPs (AuNP-PEG-NH₂) and figure 5.34 the AuNP-PEG-RIgG conjugates.

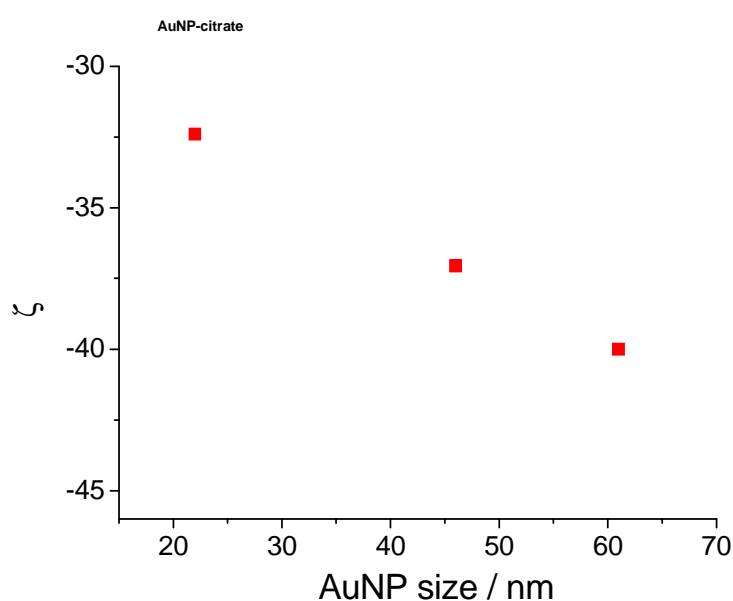


Figure 5.23: Plot of AuNP core sizes against the Zeta Potentials of citrate stabilized AuNP samples.

The charge changed from negative values of the citrate stabilized AuNP samples in figure 5.23 to positive values in figure 5.24 and 5.25 on ligand exchange with the PEG ligands. However, the behaviour of all three sets of particle systems of citrate stabilised AuNPs, PEGylated AuNPs and AuNP-PEG-RIgG conjugates was similar when the particle size was varied. The charge density varied directly with the size of the core particles for each of the ligands type. Changing the surface moiety from citrate, which has negative charges, to PEG ligand with amine functionality resulted in an inversion of the surface charges from negative to positive.

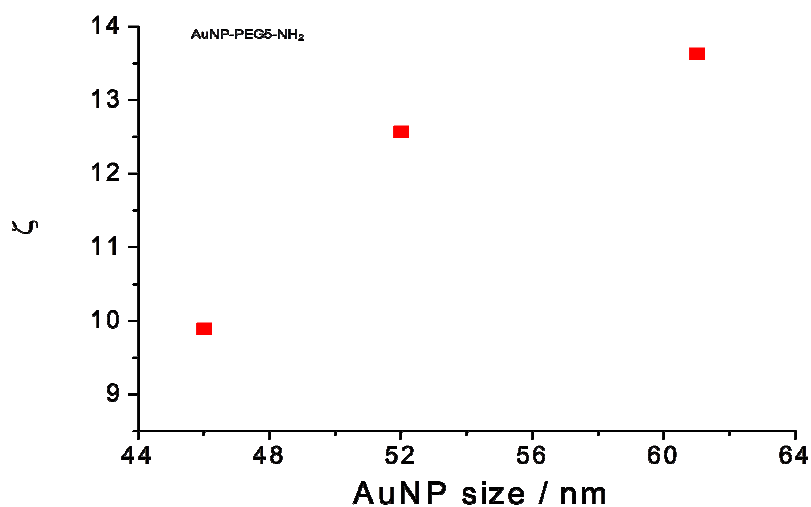


Figure 5.24: Plot of AuNP core sizes against the Zeta Potentials of AuNP-PEG-NH₂ samples. (Figure 5.25).

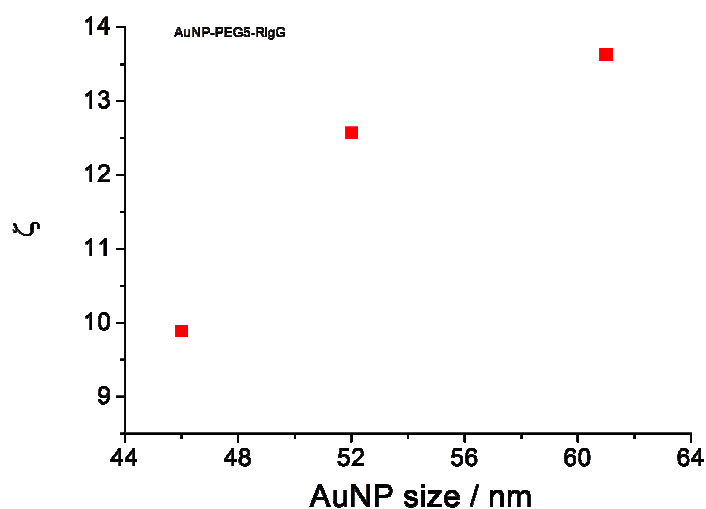


Figure 5.25: Plot of AuNP core sizes against the Zeta Potentials of AuNP-PEG-RlgG samples.

The Zeta potential (ξ) indicates the electric potential at the "slip plane". It is influenced by the thickness of the electrical double layer, the electrical charge in the Stern layer, and dielectrical constant [126].

The nature of the particle's surface changes after ligand exchange reactions of the citrate with thiolated PEG ligands. The resulting surface charge depends on the PEG ligands and their

capping functionalities (amine or antibody) used for their preparation. This explains the similar charges of the particles in each of the three sets of sample.

In general, ligand length and particle size obviously had significant effects on the particle charge density. The result in figure 5.22 shows a decreasing ξ value with increasing length of the PEG ligands. From Hückel's theory (equation 3.21 and 3.22), the size of a particle is inversely related to its ξ value [127]. This explains the behavior seen in figure 5.31 since increasing PEG length increases the particle size (hydrodynamic radius). For result shown in figure 5.23, 5.24 and 5.25, the ξ value increased with particle size. Also according to Hückel's theory (equation 3.21 and 3.22), the particle charge is directly proportional to the ξ . This suggests that the increased size of the particles seen in figure 5.23, 5.24, 5.25 resulted to increase of the surface charges, consequently increasing the ξ of the particles. This could be attributed to the fact that the larger particles accommodate more ligands (discussed in the next sections) which are the charge vectors.

5.5 AuNP surface coverage

The stabilizing strength of ligands could be affected by packaging and degree of coverage. Therefore it is necessary to understand the nature of particle's surface coverage and the factor influencing them.

In this section, results and detailed discussions on the surface coverage of gold nanoparticles systems investigated by different methods of analysis are presented. The influence of various factors like ligand length and core particle size on the coverage were investigated. This was done by preparing samples of AuNPs systems with 12 nm core sizes using the ligands; (i) thiolated PEG (HS-PEG-NH₂), (ii) PEGylated RIGG (HS-PEG-RIGG) and (iii) RIGG. The particle surface coverage for each ligand was analysed by the following methods:

- Dynamic Light Scattering (DLS) based calculations: Obtaining information on shell thickness by subtracting the metal core size from the hydrodynamic size of the particle system. This was then used to estimate the number of ligands employing a simple geometrical model which takes the ratios of ligand shell volumes and the spatial demands of the individual ligands into account.
- Bradford analysis (a quantitative colorimetric assay for protein concentration): After coupling (exchange) reaction, the unbound (excess) RIGG were quantified using this method. The obtained value of unbound RIGG was then subtracted from the total amount of RIGG used for the reaction, to acquire indirect information on the surface bound molecules.

The results were discussed together with the rough estimation obtained by the Lowest Coagulation Concentrations (LCC) measurements already presented in section 5.4.4.

While the discussions here in section 5.5 are based on coverage analysis of systems prepared with 12 nm Au core sizes and 3 kDa PEG ligands, the discussion in section 5.4.4 was based on systems having varying Au core sizes and PEG ligand weights. The concluding part of the section compares the results obtained by using different analytical methods.

5.5.1 DLS based calculation

Considering products of the particle preparations schematized in figure 5.11 and their resulting DLS-sizes presented in figure 5.12, the coverage of those AuNP systems could be calculated. This is done using values of the particle sizes and the values of ligand shell thickness estimated from the increase in particle radius. The samples were prepared from AuNPs with initial TEM core size of 12 nm and ~18 nm hydrodynamic sizes determined by DLS. The 3 kDa ligand, HS-PEG-NH₂ was used for the synthesis of the PEGylated RIgG ligands HS-PEG-RIgG. The DLS values represented by the volume statistics were generally used for all calculations, due to the reasons already mentioned in section 5.1.2.

The DLS-sizes of the prepared samples AuNP-PEG-NH₂, AuNP-PEG-RIgG, and AuNP-RIgG were ~29 nm, ~35 nm, and ~40 nm respectively. RIgGs contributed to the surface coverage (thickness) in the two latter cases resulting to average size increase of about 17 nm for AuNP-PEG-RIgG compared to citrate stabilized AuNPs, while AuNP-RIgG exhibited a size increase of ~22 nm.

According to a previous investigation based on liposome surfaces [147-149], hydrodynamic coating thickness of 5 kDa and 3 kDa PEG polymer were 13.2 nm and 7.3 nm respectively. From the preceding discussion, the particle diameter increased when 3 kDa ligands (HS-PEG-NH₂) were used for the preparation of AuNP-PEG-NH₂ is calculated as 8.5 nm [i.e. (29 nm - 12 nm)/2). This value is comparable to the calculated hydrodynamic coating thickness of the 3 kDa PEG polymer deposited on liposomes [149].

Assuming particle size (diameter) increase is caused by the ligand HS-PEG-RIgG used for sample (AuNP-PEG-RIgG) preparation and that this increase is considered to be equivalent to a monolayer of PEG-RIgG moiety around the core Au with diameter, d . The overall diameter of the particle system is given as D , as demonstrated in figure 5.26 i. This particle system comprises of the Au core (figure 5.26 ii) and the ligand shell (figure 5.26 iii).

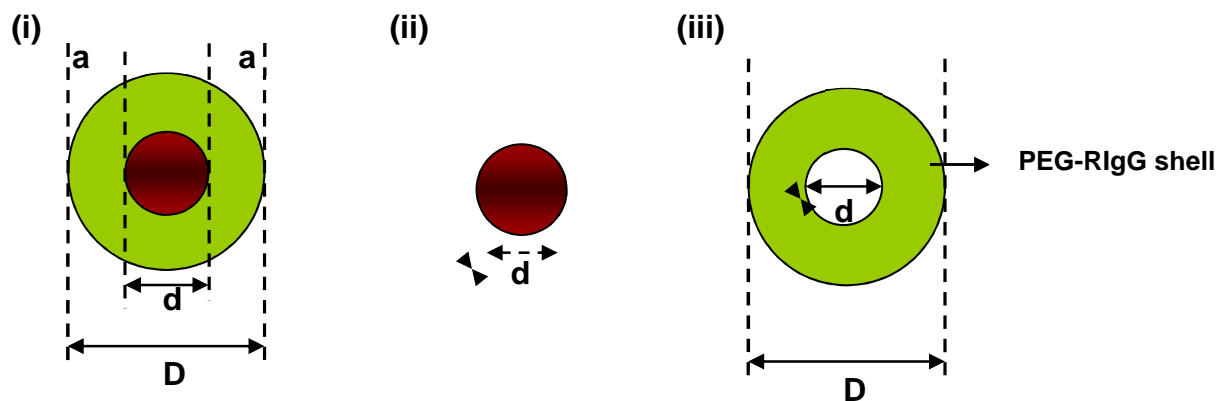


Figure 5.26: The monolayer of PEG-RIgG molecules formed around the nanoparticles with diameter, d . The overall diameter of the particle system is given as D (i). This particle system comprising the metallic core (ii) and the ligand shell (iii).

The volume of the PEG-RIgG shell, V_3 on the particle (figure 5.26, iii) is the difference between the total particle volume (figure 5.26, i) V_1 and the volume of Au core (figure 5.26, ii) V_2 , given by

$$V_3 = 0.5236(D^3 - d^3) \quad (5.1)$$

d is the diameter of the Au core obtained by TEM.

From the foregoing, the particle surface coverage of IRP3-RIgG could be calculated from the increased volume of the AuNP resulting from the deposition of IRP3-RIgG. If the hydrodynamic radius of IRP3-RIgG could be considered as the sum of that of RIgG (5.5 nm) alone and the hydrodynamic coating thickness of 3kDa PEG which was obtained as 7.3 nm. The diameter of the ligand is seen to be equivalent to the shell thickness. The value (7.3 nm + 5.5 nm) of the shell diameter d , is then given as 12.8 nm. Since the diameter of the Au core is 12 nm (TEM), we can fit these values into equation 3. The volume of the -PEG-RIgG shell V_3 obtained in this manner is 26,928.4 nm³. If we divide this value by the volume of PEG-IgG ligand obtained using the calculated hydrodynamic diameter of 12.8 nm, we have ~ 26, which is the number of IgGs per AuNP. This value is in remarkable agreement with the result of Bradford assay, by which ~27 IgGs per AuNP was obtained.

Due to the larger thickness of the IgG-shell in case of the electrostatically coupled IgG, the estimated number of IgG per AuNP in this sample was somewhat larger, i.e. ~ 43 .

Orientation of RIgG on AuNP surface: After conjugation of PEG-RIgG to AuNP, the particle size increased due to the PEG-RIgG deposited onto the particle surface. The RIgG is linked via the PEG polymer to the AuNP surface. Because RIgG has a rigid and compact structure while the PEG is flexible and comparably negligible in size, the increased covering shell is proportional to a value added by the RIgG dimensions.

RIgG has a “Y” shaped structure with a molecular mass of 166 kDa and dimensions 10 nm (length) x 2 nm (width) x 7 nm (height) [150]. The orientation of RIgG on the AuNP surface predicted from the particle DLS size increase can be one of the four possibilities demonstrated in figure 5.27.

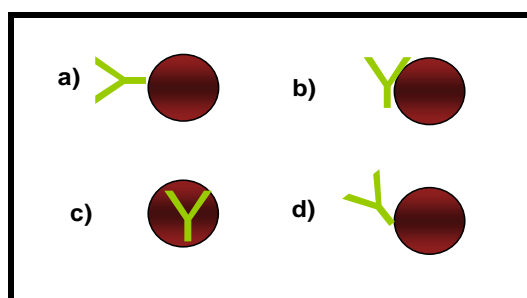


Figure 5.27: Supposed orientations of covalently coupled RIgG on AuNP surface.

If RIgG is oriented vertically to the nanoparticle surface as seen in figure 5.27a, a size increase of about 7 nm due to the RIgG dimension could be expected on full surface coverage. Horizontal orientation of RIgG on the nanoparticle surface as in figure 5.27b, results to a size increase of about 10 nm, on the other hand, when it lies totally flat on the nanoparticle surface as in figure 5.27c, the increase is approximately 2 nm. The orientation in 5.27d should results to a size increase with a value between 2 nm and 7 nm. This theoretical approach was practically investigated and obtained results are presented in table 5.7 with a follow up discussion below.

Table 5.7: The analysis of results obtained by DLS measurements of AuNP-PEG-RIgG conjugates synthesized using 4 different Au core sizes.

Sample (Au core/nm)	DLS	
	Volume / nm	PDI
AING1 (22)	23,67	0,23
AING1-IRP5-RIgG	51,52	0,12
Diameter increase	27,85	
AING4 (46)	43,58	0,16
AING4-IRP5-RIgG	63,88	0,17
Diameter increase	20.03	
AING5 (52)	48,25	0,18
AING5-IRP5-RIgG	78,88	0,17
Diameter increase	30.63	
AING6 (61)	55,17	0,20
AING6-IRP5-RIgG	80,17	0,15
Diameter increase	25,00	

The results in table (5.7) above were obtained by the analysis of AuNP-PEG-RIgG conjugates synthesized using 4 different Au core sizes. Average particle diameter increase due to the ligand coverage of about 25.88 nm was calculated from the 4 systems. This gives a shell thickness of 12.94 nm, since this is half the value obtained for the total diameter increase. If we subtract the hydrodynamic diameters of the 5 kDa PEG ($d = 8.5$ nm) from this value, we obtain the RIgG layer thickness which is 4.44 nm. This value suggests an orientation of the RIgG molecules on the particle surface closely related to that illustrated in Figure 5.27d. This suggests that the IgG is oriented in vertically tilted position to the particle surface. This orientation of the RIgG is reasonable considering the fact that the glycan moiety on the RIgG to which PEG molecule is directly attached is located at halfway distance up the Fc segment of the antibody.

5.5.2 LCC method

This section could be seen as an extended discussion of the preceding section 5.4.4 since those results obtained for the LCC analysis were also used here for the coverage calculations.

The minimum (lowest) coagulation concentrations of 2.6×10^1 nmol/mL for HS-PEG-NH₂, 2.6×10^{-1} nmol/mL for RIgG and 2.6×10^{-2} nmol/mL for HS-PEG-RIgG respectively were found in section 5.4.4. These were the ligand concentrations able to sufficiently stabilize 2.6×10^{-3} nmol/mL (12 nm diameter) citrate stabilized AuNPs solution in 1xPBS buffer.

These values could be logically used as parameters to determine the coverage of the 12 nm AuNP for each of the ligands by estimating the ligand/AuNP ratios in each of the samples. 100 μ L (18nM, 12 nm diameter) citrate stabilized AuNPs solution were used for each exchange reaction i.e. 2.6×10^{-3} nmol/mL AuNPs. Consequently,

- i.) having 2.6×10^1 nmol/mL of HS-PEG-NH₂ ligand for the stabilization of 2.6×10^{-3} nmol/mL AuNP, a ligand/AuNP ratio of 11,300 was obtained.
- ii.) using 2.6×10^{-1} nmol/mL RIgG ligand for the stabilization of 2.6×10^{-3} nmol/mL AuNP, a ligand/AuNP ratio of 113 was obtained.
- iii.) And using 2.6×10^{-1} nmol/mL HS-PEG-RIgG ligand for the stabilization of 2.6×10^{-3} nmol/mL AuNP, a ligand/AuNP ratio of 11 was obtained as number of molecules covering the particle surface. This is in close agreement with the value obtained by S Kumar [86] who used coverage estimation strategies involving dyes.

If we assume quantitative binding of the HS-PEG-RIgG ligand to the AuNP, we can conclude that at the lowest coagulation concentration the AuNP surface is covered by ~11 RIgG. This value is somewhat lower than the ratio ~26 RIgGs per AuNP, determined using the DLS measurements reported above. However, the DLS measurements were carried out with AuNP-PEG-RIgG samples, which were prepared with 1000-fold molar excess of HS-PEG-RIgG ligands. Thus, in case of the DLS measurements it is reasonable to assume saturation of the AuNP surfaces with -PEG-RIgG ligands in contrast to the lowest coagulation concentration conditions where saturation of the AuNP surface is most likely not achieved.

5.5.2.1 Particle core size and ligand length

To investigate the ligand length effect on particles' coverage, different nanoparticles with varying sizes were used for sample preparations and the results of their analysis are discussed in this section.

Repeated set of experiments for the coverage investigation using the LCC method were carried out by varying both the ligand length and particle size. For easy analysis, the calculated coverage is presented as footprint, which is defined as the number of particles' surface atoms covered by one ligand molecule. A summary of experimental results are presented in table 5.8 and table 5.9 and a detailed discussion with graphical representations are presented in the succeeding paragraphs.

5. RESULTS AND DISCUSSION

Table 5.8: Summary of PEG ligand coverage values obtained for different particle systems to elaborate the influence of ligand length and particle size. The LCC method of ligand coverage analysis was used.

		Diameter(nm)/ Surface atoms	Ligand/AuNP	Surface atoms/ Ligand	nm ² / Molekül
G1	PEG-3	22/19116	654	29	2.33
G4	PEG-3	46/84729	13158	6	0.51
G5	PEG-3	52/108431	37037	3	0.23
G6	PEG-3	61/149458	63211	2	0.18
G1	PEG-5	22/19116	6536	3	0.23
G4	PEG-5	46/84729	26316	3	0.25
G5	PEG-5	52/108431	37037	3	0.23
G6	PEG-5	61/149458	63211	2	0.18
G1	PEG-10	22/19116	3268	6	0.47
G4	PEG-10	46/84729	13158	6	0.51
G5	PEG-10	52/108431	37037	3	0.23
G6	PEG-10	61/149458	31606	5	0.37

Table 5.9: Summary of PEG-RIgG ligand coverage values obtained for different particle systems to elaborate the influence of ligand length and particle size. The LCC method of ligand coverage analysis was used.

	Diameter (nm)/ Surface atoms	Ligand	RIgG/ AuNP	Surface atoms/RIgG	nm ² / Molekül
G1	22/19116	PEG-3-RIgG	6	3186	247.82
G4	46/84729	PEG-3-RIgG	25	3389	269.09
G5	52/108431	PEG-3-RIgG	35	3098	244.33
G6	61/149458	PEG-3-RIgG	59	2533	197
G1	22/19116	PEG-5-RIgG	12	1593	126.26
G4	46/84729	PEG-5-RIgG	48	1765	137.1
G5	52/108431	PEG-5-RIgG	68	1595	124.48
G6	61/149458	PEG-5-RIgG	116	1288	100.37
G1	22/19116	PEG-10-RIgG	12	1593	125.16
G4	46/84729	PEG-10-RIgG	49	1729	135.91
G5	52/108431	PEG-10-RIgG	69	1572	123.4
G6	61/149458	PEG-10-RIgG	117	1277	99.5

From tables 5.8 and 5.9, the coverage represented as footprint for all the particle systems with similar PEG ligands (HS-PEG3-NH₂, HS-PEG5-NH₂ or HS-PEG10-NH₂,) are comparably identical irrespective of the Au core size. The result is the sum total surface atoms for all particles in sample solutions. From those values the value for a single particle was deduced and the results are presented graphically in figure 5.28. It shows a plot of the particle diameter against the deduced surface atoms per ligand for each of the ligand systems. Their values ranged within 2-6 atoms/ligand for HS-PEG3-NH₂, 3 atoms/ligand for HS-PEG5-NH₂ and 6 atoms/ligand HS-PEG10-NH₂. Similar analysis was done for the ligands with RIgG caps and presented in figure 5.29.

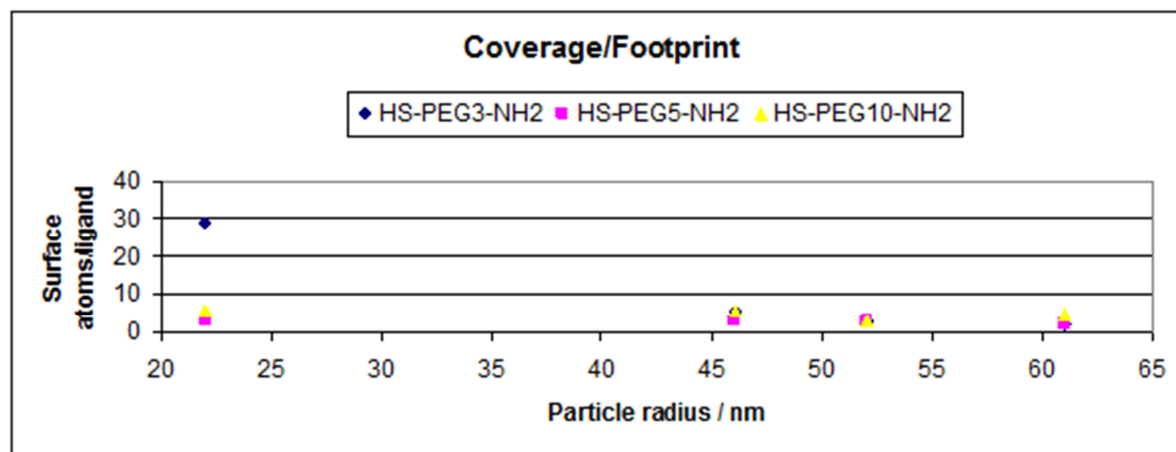


Figure: 5.28: The footprints of HS-PEG-NH₂ ligands for different particle of varying sizes.

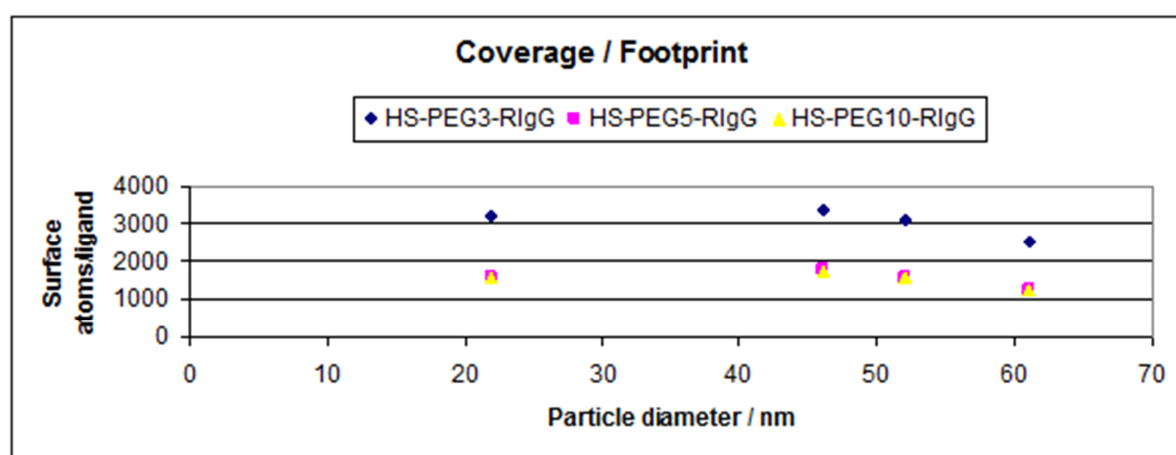


Figure: 5.29: The footprints of HS-PEG-RIgG ligands for different particle of varying sizes.

An exceptional behavior was exhibited by AuNP-PEG3-NH₂ systems with the smallest particle diameter of 22 nm. This system had a footprint of 29 atoms/molecule.

For the PEGylated RIGG ligands (HS-PEG3-RIGG, HS-PEG5-RIGG or HS-PEG10-RIGG), similar observations were made. The coverages/footprints for all the particle systems with same PEG-RIGG ligands are also comparably similar, all having values of approximately 3000 atoms/ligand for these HS-PEG3-RIGG systems, approximately 1500 atoms/ligand for each of HS-PEG5-NH₂ and HS-PEG10-RIGG. An exceptional behavior was exhibited again by AuNP-PEG3-RIGG systems with the smallest PEG ligand length (MW, 3 kDa) showing with a value double the coverage values of their counterparts with PEG5-RIGG and PEG10-RIGG ligands. This exceptional behavior could be attributed to “Bulky Cap” effect earlier discussed. A steric effect from RIGG cap or charged –NH₂ cap depending on ligand. Remarkably, this anomaly was only observed for all the systems having HS-PEG3-RIGG coverage and Au core sizes of 22 nm. This anomaly is more pronounced with the bulky RIGG caps than the charged –NH₂ caps.

Since charge and steric factors have been found to influence the packaging on particle surface, a further step was taken to investigate the influence of the anchoring end group (dentate) of the PEG ligand by using a homemade tridentate thiol PEG ligand (HS3-PEG1-OH) with very shorter PEG chain (MW, 1 kDa) and a non-charged hydroxyl cap. This ligands with three thiol groups (3 dentate) were synthesized in a one-step reaction using commercially available polyethylene oxide monoacrylate as described in our previous publication [152]. The results obtained for the footprints of this ligand on varying particle sizes are shown in figure 5.28 below.

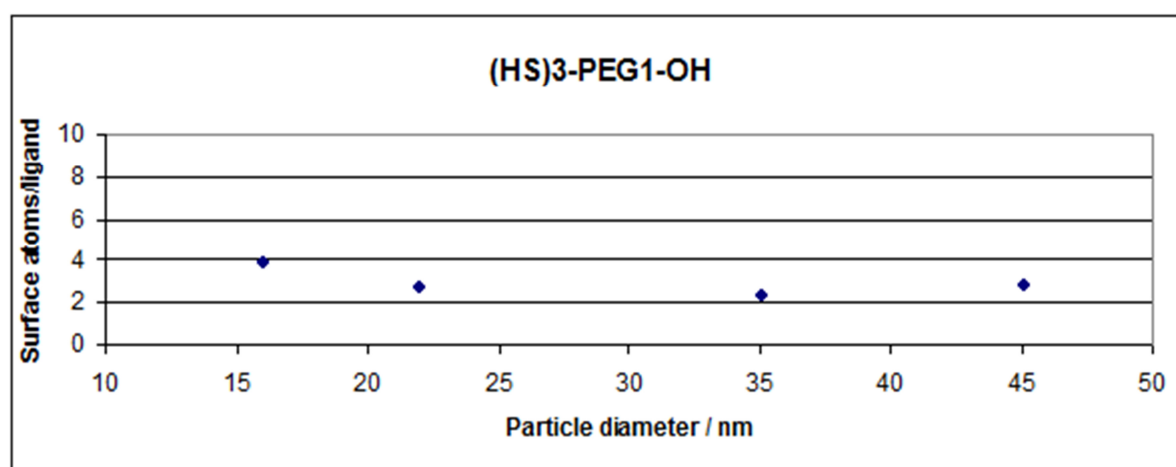


Figure: 5.30: The footprints of HS3-PEG1-OH ligand for different particle of varying sizes

The coverages/footprints for all the particle systems with the HS3-PEG-OH ligand are also comparably similar, having values approximately 3 atoms/ligand. In this case also packaging was not affected by the particle size and the ligand length.

5.5.3 Bradford method

The discussion in this section is based on experiments done using 12 nm AuNP (16 nM) and PEG-RIgG ligands whose solution protein concentrations were previously determined by Bradford protein quantification procedure described in the experimental section. Figure 5.31 shows the optical absorption spectra of solutions of RIGG concentration series after treatment with the protein reactive dye (Roti-Nanoquant). Figure 5.32 is the standard curve obtained by plotting the ratio of the optical absorptions (figure 5.31) at 590 nm to that at 450 nm (OD_{590}/OD_{450}) against their respective RIGG concentration.

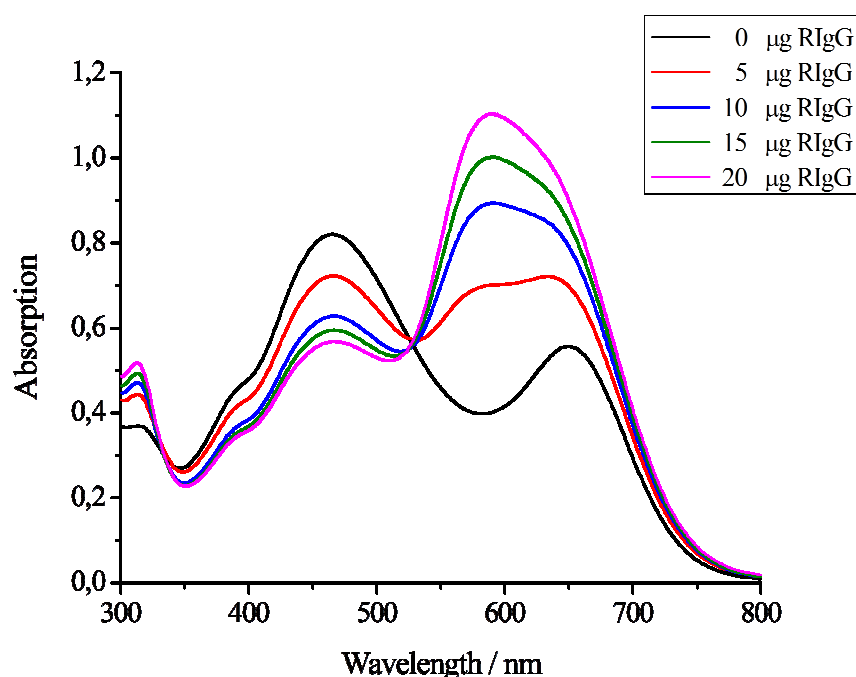


Figure 5.31: Absorption curves from solution series of RIGG concentration after reaction with Roti-Nanoquant.

In the absence of protein molecules, the reagent molecules exists in equilibrium condition of their neutral states with absorption peak at 650 nm and the cationic states with peak at 450 nm. This is the case of the solution having 0 μg RIgG in figure 5.31. The dye molecule on interacting with protein amines becomes deprotonated as shown below, to give the anionic states with absorption at a wavelength of 590 nm. The proportion of the different states could be estimated by their absorption peaks and the resulting values related to the concentration of the protein in solution.

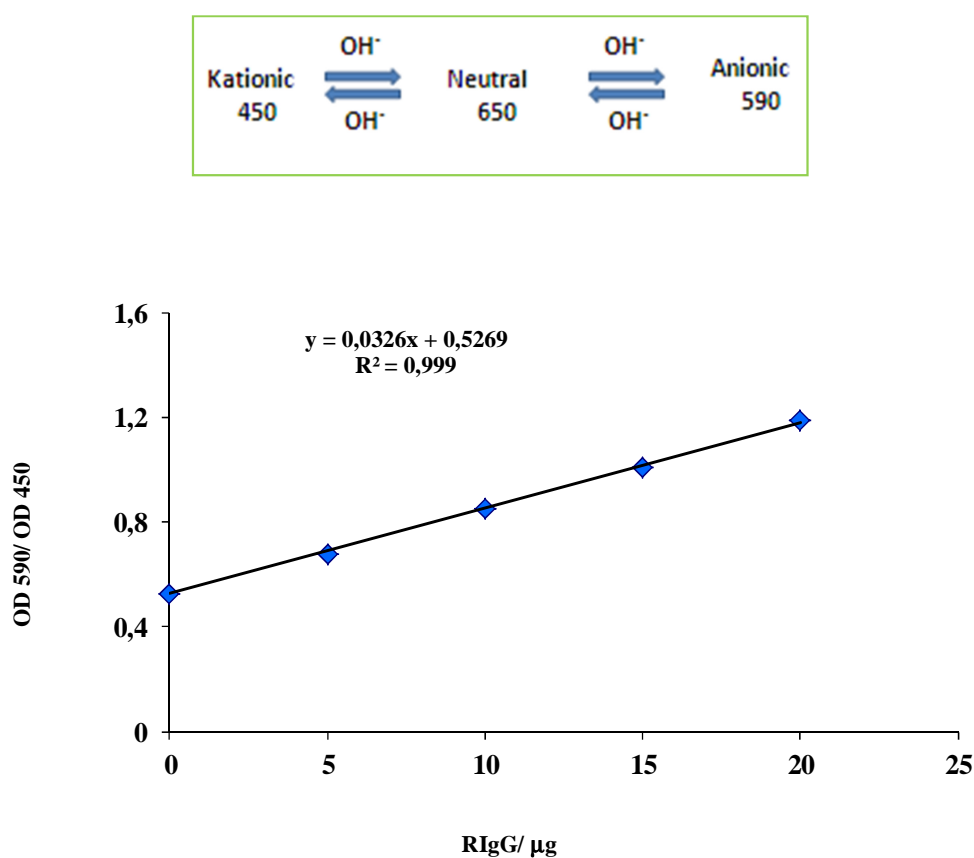


Figure 5.32: Standard curve obtained by plotting the ratios of the optical absorptions OD590/OD450 (from the curves in figure) against the respective RIgG concentration solution.

After a successful exchange reaction of citrate stabilised 12 nm AuNP with the ligand PEG-RIgG, surface bound ligands were quantified using the Bradford protein quantification procedure [132, 151]. The coated AuNPs were separated from the supernatant after each exchange reaction by centrifugation. Subsequently, the supernatants were analysed for protein

concentration by using a modified protocol of Bradford's method. This involved the use of the Roti-Nanoquant reagent as described in the experimental section of this thesis.

The number of surface RIgG molecules was calculated by subtracting the determined RIgG concentration in the supernatant from the initial RIgG concentration of the solutions (HS-PEG3-RIgG, HS-PEG5-RIgG, HS-PEG10-RIgG) used for exchange reaction. The obtained values were divided by the number of AuNP used for exchange to obtain the coverage. Table 5.10 shows the results obtained.

Table 5.10: The number of RIgG linked to each nanoparticle obtained by Bradford method, for PEG3-RIgG, PEG5-RIgG, PEG10-RIgG.

Sample	Surface RIgG μg	RIgG/AuNP	Coverage nmol/cm^2	Coverage (Surface atoms/RIgG)
AuNP-PEG3-RIgG	62,306132	27	9.9	206
AuNP-PEG5-RIgG	92,8160633	41	15.0	136
AuNP-PEG10-RIgG	94,2560182	42	15.4	133

The number of RIgG on each particle surface obtained for the samples AuNP-PEG5-RIgG and AuNP-PEG10-RIgG is similar (47 RIgG molecules/AuNP) but that for AuNP-PEG3-RIgG is lower with 27 RIgG molecules/AuNP. The reason for this behaviour is the already introduced “Bulky Cap” effect,.

5.5.4 LCC vs Bradford

The excess ligand used for exchange reaction during LCC investigations is low compared to the high ligand excess used during Bradford method. This suggest that for LCC, the low excess condition result to a minimal coverage, where the particle surfaces are not fully covered by the ligand. To achieve a full coverage, a larger excess of ligand is required, which is the case in the Bradford analysis.

To prove this coverage difference for both methods, the samples prepared with HS-PEG5-RIgG whose coverage has been investigated using LCC method in table 5.10, were analyzed again for their coverage by using the Bradford method. In this way, similar particle system

achieved with the ligand HS-PEG5-RIgG for the two methods (LCC and Bradford) could be investigated for their coverage. The coverage values obtained for each of the systems using both methods are summarized in table 5.11 below.

Table 5.11: Surface coverage for four AuNP sizes as determined by LCC and Bradford method.

	LCC RIgG/AuNP	Bradford RIgG/AuNP	Difference RIgG/AuNP	Particle Core size, TEM (nm)
AIN9G1-IRP5- RIgG	12	45	33	22
AIN9G4-IRP5- RIgG	48	112	64	46
AIN9G5-IRP5- RIgG	68	186	118	52
AIN9G6-IRP5- RIgG	116	360	244	61

With the result in table 5.11, a clear picture was obtained showing the surface coverages for four different AuNP sizes determined using two different analysis methods. While the number of RIgG/AuNP increases with increased particle core size for both methods (LCC and Bradford method), the values obtained using different methods for systems with similar ligand and particle size are different as elaborated by the plot in figure 5.33 below.

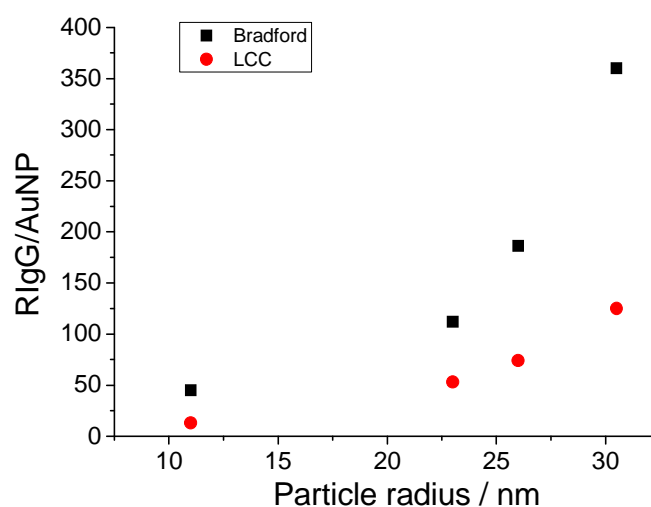


Figure 5.33: Comparison of the results for the particle size influence on coverage obtained by using the Bradford and LCC method.

The Bradford method yielded higher coverage values compare to the LCC method. This could be explained by the larger ligand excesses (approximately 1000 ligand excess) used for ligand exchanges during particle preparation in the Bradford method. For the LCC method ligand excess was only 113.

The differences in ligand concentration relative to the particles in reaction solution led to the difference coverage of the particles. Similar coverage values were observe for all preparation involving high ligand excesses in which cases, the particle surface attain full coverage.

5.6 Functionality tests of AuNP-RIgG conjugates

5.6.1 Immuno Blot Assays

The AuNP antibody conjugates (AuNP-PEG-RIgG) prepared from 11 nm AuNPs were tested for the antibody reactivity by using goat anti-rabbit IgG, G α RIgG directed against rabbit IgG, RIgG. This was done by dropping RIgG solutions five different spots on each of three NC-membranes (figure 5.34). Moving from left to right in a clockwise direction on each membrane, each of spots 1-5 was initially treated with 100 μ L solution of RIgG (spot 1), mixtures of RIgG and G α RIgG (spot 2 – spot 4) and G α RIgG (spot 5). The free binding spaces were subsequently blocked with BSA. The three NC-membranes at this stage prepared by the same procedure were incubated in different particle solutions. Figure 5.34 shows the photographs of the membrane after incubation in: (a) AuNP-PEG-RIgG solution, (b) in AuNP-PEG-NH₂ solution and (c) in citrate stabilised AuNP solution. The spots on the membranes were finally inspected by eye for red colour appearance.

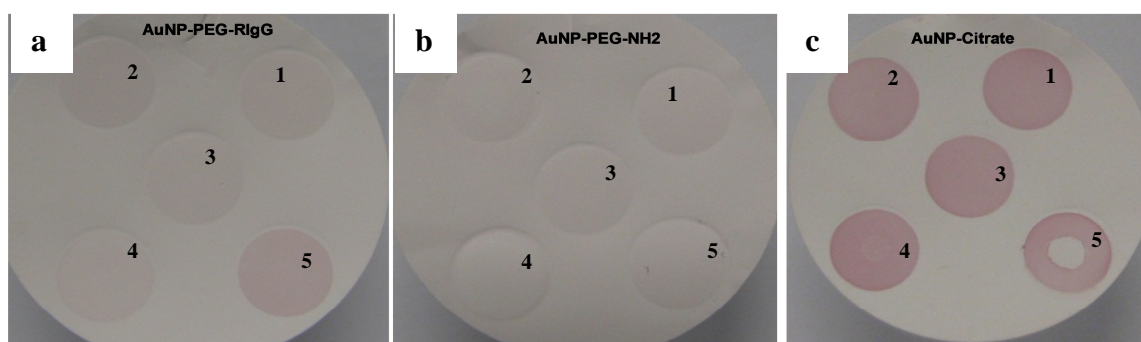


Figure 5.34: NC membranes with five spots of antibodies which were incubated in AuNP-PEG-RIgG solution (a), in AuNP-PEG-NH₂ solution (b) and in citrate stabilised AuNP solution (c).

This reactivity test systems, AuNP-PEG-RIgG, PEGylated AuNP (AuNP-PEG-NH₂) and citrate stabilized AuNPs showed remarkably different behaviour. Where G α RIgG was present in spots immobilized on the NC-surface, it is intended to interact with its reaction partner RIgG on the conjugate or particle. The interaction between the immobilised G α RIgG and AuNP-RIgG conjugates results in appearance of red colour on NC-membrane on the spot with G α RIgG. This is evident by the photograph on the left in figure 5.34. There was no colour

appearance on the other spots with RIgG or RIgG/GαRIgG mixture (1-4) on this first membrane. The intention of using the spots with IgG mixtures was to show varying colour intensity proportional to the ratio of GαRIgG/RIgG. Unfortunately the results did not show this trend, suggesting that there were no free GαRIgGs molecule in the mixtures of IgGs.

For the second NC-membrane (middle) incubated in the PEGylated AuNP solution, no red colour on the spots was observed as expected, while red spots appeared on all the NC-membrane spots incubated in the citrate stabilised AuNP solution. This result is likewise expected since proteins are known to interact electrostatically with citrate stabilised AuNPs and for the PEGylated particle without RIgG on their surfaces, no interaction on the spots. An open question was why the citrate stabilized particle while interacting with IgG, did not also interact with BSA used for blocking the rest membrane surface. One wonders if the varying isoelectric points (pI) of both molecules (BSA has pI 4.7 and IgG has pI 6.5 [162]) could be a reason.

The experiment above was repeated with little variation. The positions of the GαRIgG and RIgG were exchanged. GαRIgG was in this case attached to the AuNP to form AuNP-GαRIgG conjugates and RIgG molecules were immobilized on the membrane. The loading of the NC-membrane was done like before but this time the spots have varying amounts of RIgG to ensure varying colour intensities proportional to the RIgG concentration after incubation with AuNP-GαRIgG conjugates. Figure 5.35 shows the appearance of the membrane after incubation and washing.

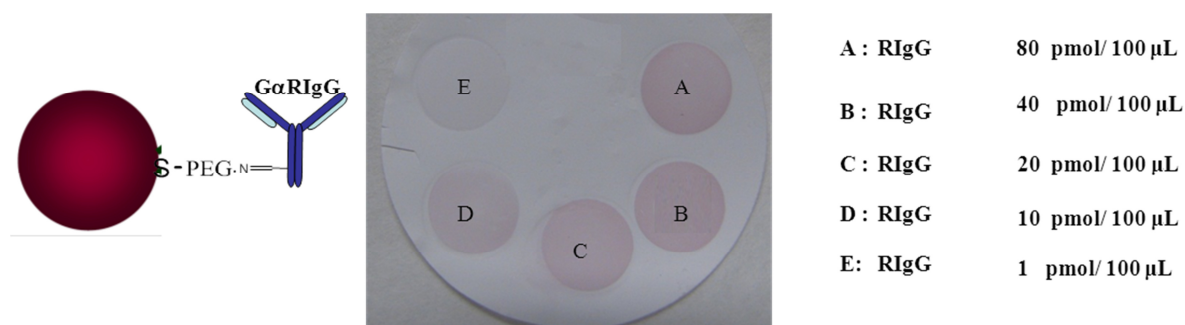


Figure 5.35: NC membranes with spots of containing complexes formed by the reaction between immobilized RIgG (quantity as seen on the left) and AuNP-PEG-GαRIgG conjugates after incubation.

The NC membrane shown in figure 5.35 was prepared with 100 μ L solution containing 80 pmol RIgG (spot A), 40 pmol RIgG (spot B), 20 pmol RIgG (spot C), 10 pmol RIgG (spot D), and 1 pmol RIgG (spot E). The complex formation from the reaction of the immobilised RIgG with the AuNP-PEG-G α RIgG conjugates resulted in red coloured spots. The colour intensity diminished with reducing RIgG concentrations on the spot. No colour appearance was observed on the spot with the lowest concentration, suggesting a lower limit of detection in the range of \sim 10 pmol.

Densitometric analysis was additionally done on the nitrocellulose membrane in figure 5.35. This was performed using Quantity One software (Biorad). The count density of each spot versus the immobilized protein is shown in figure 5.36. The relative binding of AuNP-G α RIgG to immobilized RIgG over the concentration range up to 80 pmol/spot could be elaborated.

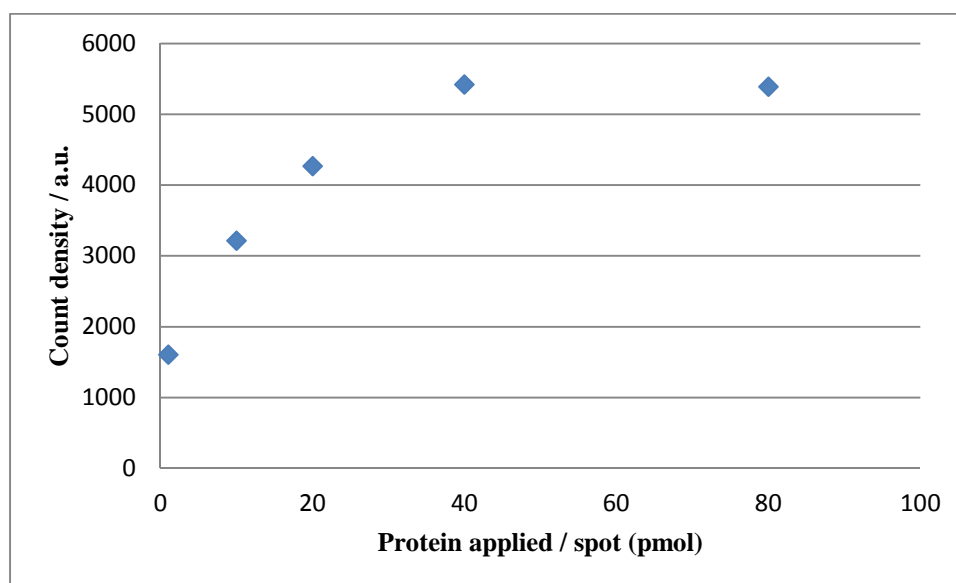


Figure 5.36: The curve shows the relative count density (binding) of AuNP-Antibody conjugates to antigen dosed spots on nitrocellulose membrane over the concentration range of 1 to 80 pmol/spot.

The plot of signal count density versus the amount of antigen (protein on spots) shows the AuNP-G α RIgG conjugates binding (interaction) which increased with the RIgG concentration. The signal count density plot shows a near linear relationship up to 40 pmol/spot protein. Increased concentration above 40 pmol/spot protein resulted to no further count increase. This suggests that the antigen binding capacity of the nitrocellulose membrane

is maximally exhausted for spot at protein load of 40 pmol. The observed conjugate binding at concentration as low as 1.0 pmol was not possible on simple inspection with the eyes. For each spot, the membrane binding capacity calculated in section 4.3 from producer's information is 21 μg IgG/Spot which is 0.13 pmol/Spot. This should normally be the maximum capacity of the spot, but the value obtained in figure 5.36 is two orders of magnitude larger. This difference could be attributed to variation in the conditions at which the tests were carried out.

5.6.2 Effect of particle size on sensitivity

Here, influence of the nanoparticle size on the colour effect (optical properties) which could boost sensitivity of the AuNP-PEG-RIgG conjugates for LFIA application was investigated. This is a study of the behaviour of conjugates with varying core Au sizes in detecting the presence of a given quantity of analyte on the NC-membrane. Citrate stabilized AuNPs with varying sizes, 22 nm, 46 nm, 52 nm and 61 nm diameter, were used for exchange reactions with HS-PEG-RIgG ligands (previously prepared from the 5 kDa PEG polymer). The product conjugates were used in dot blot analysis. For this immune test, 10 mL of each conjugate sample were used. The solutions contain comparable concentrations of the conjugates. The smallest sized particles, AuNP-PEGG1-RIgG ($\sim 14 \times 10^{-12}$ particles) having approximately twice the concentrations of AuNP-PEGG4-RIgG ($\sim 9.0 \times 10^{-12}$ particles) and AuNP-PEGG5-RIgG ($\sim 9.0 \times 10^{-12}$ particles) whose concentration on the other hand are approximately twice that of AuNP-PEGG6-RIgG ($\sim 4.6 \times 10^{-12}$ particles). In table 5.12 all necessary information of the preparation, like the size of core particles used, ligand concentration etc. are presented. After the preparation of the conjugates as described, four NC-membrane sheets are then spotted with solutions of GaRIgG containing varied concentrations as done before. But this time the solutions are prepared with amounts as seen in table 5.12.

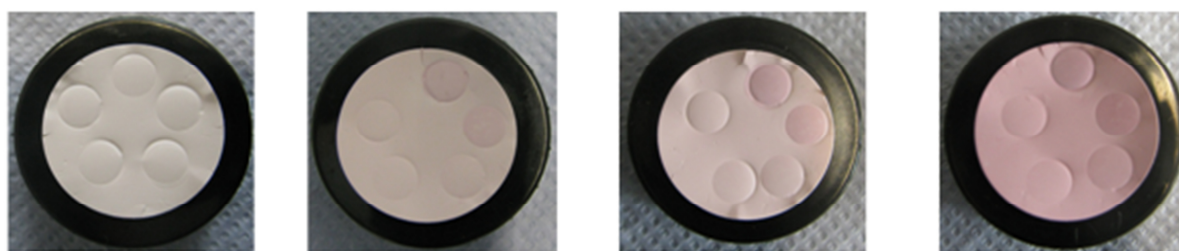


Figure 5.37: Test results for the reaction of conjugates solutions with $\sim 14 \times 10^{-12}$ particles (AuNP-PEGG1-RIgG), $\sim 9.0 \times 10^{-12}$ particles (AuNP-PEGG4-RIgG and AuNP-PEGG5-RIgG) and $\sim 4.6 \times 10^{-12}$ particles (AuNP-PEGG6-RIgG) on NC- membrane spotted with solution having GaRIgG concentrations as given on the left column of table 5.12 used for immune test.

Table 5.12: A tabular representation of the result shown in figure 5.38, summarizing the test results as colour intensity for the reaction of conjugates solutions with $\sim 14 \times 10^{-12}$ particles (AuNP-PEGG1-RIgG), $\sim 9.0 \times 10^{-12}$ particles (AuNP-PEGG4-RIgG and AuNP-PEGG5-RIgG) and $\sim 4.6 \times 10^{-12}$ particles (AuNP-PEGG6-RIgG) with NC- membrane spotted solution having concentration as given on the left column of the table used for immune test.

	Conjugate solution (10mL)				
GaRIgG (Amount spotted on NC-membrane)	AuNP core diameter (nm)	22	36	52	61
		AuNP- PEGG1-RIgG (230 pM)	AuNP- PEGG4- RIgG (148 pM)	AuNP- PEGG5- RIgG (150 pM)	AuNP- PEGG6- RIgG (76 pM)
60.0 pmol		-			?
6.0 pmol		-			?
0.6 pmol		-	-		?
60.0 fmol		-	-	-	?
6.0 fmol		-	-	-	?

From figure 5.37 and its corresponding table 5.15 above, there was no spot with red colour appearance for the conjugates with the smallest particle sizes (22 nm, AuNP-PEGG1-RIgG). Even though the concentration was twice or four times that of the other conjugate solutions. While conjugates from 46 nm and 52 nm diameter particles (AuNP-PEGG4-RIgG and AuNP-PEGG5-RIgG) showed colour changes on the spots loaded with G α RIgG, there was very high background red coloration for conjugates having 61 nm Au core size (AuNP-PEGG6-RIgG). The reaction of both conjugates AuNP-PEGG4-RIgG and AuNP-PEGG5-RIgG were visible on the NC-membrane at G α RIgG concentrations as low as 6.0 pmol analyte/spot. Light colour appearance is seen even at 0.6 pmol/spot for AuNP-PEGG5-RIgG discernable on the photograph.

These results prove that the size of the AuNP influences the optical sensitivity of the conjugates. Conjugates with larger core particles (46 nm and 52 nm diameter) exhibited most visible signals after the reaction with the antigens on NC-membrane. Particles larger than 52 nm seemed to be inappropriate candidates for this application, as undesirable background staining emerges. This result supports the theoretical finding of El-Sayed [29] who related particles optical absorption and scattering to the particle size. He theoretically demonstrated that AuNP has its largest absorption component with minimum scattering of the optical extinction at particle sizes of 40 nm diameter.

5.6.3 Liquid phase reactivity of conjugates

In the previous sections, the activity of AuNP-antibody conjugates were studied in a heterogeneous set up. A reaction partner was immobilized on a solid phase (NC-membrane) and the other is in solution. In this section, the investigation that follows centres on reactivity of conjugates with their antigens in a homogeneous set up. Here both reaction partners are in liquid phase. To do this, DLS measurements was employed to monitor conjugate size increase promoted interacting partners subsequently attached to their surfaces. This process of attachment due to interaction was also demonstrated using TEM image.

5.6.3.1 DLS analysis

Citrate stabilized AuNPs with hydrodynamic sizes of 13 nm were used for the preparation of RIgG conjugates. Products were subjected to further reaction with their appropriate reaction, GaRIgG. A solution of GaRIgG was prepared and added to the sample in an excess. This mixture was incubated for two hours at room temperature. After incubation, the complex product and a control AuNP-PEG-RIgG conjugate solution were characterized by DLS measurements using the citrate stabilized particles as reference. Figure 5.38 shows the measurement results.

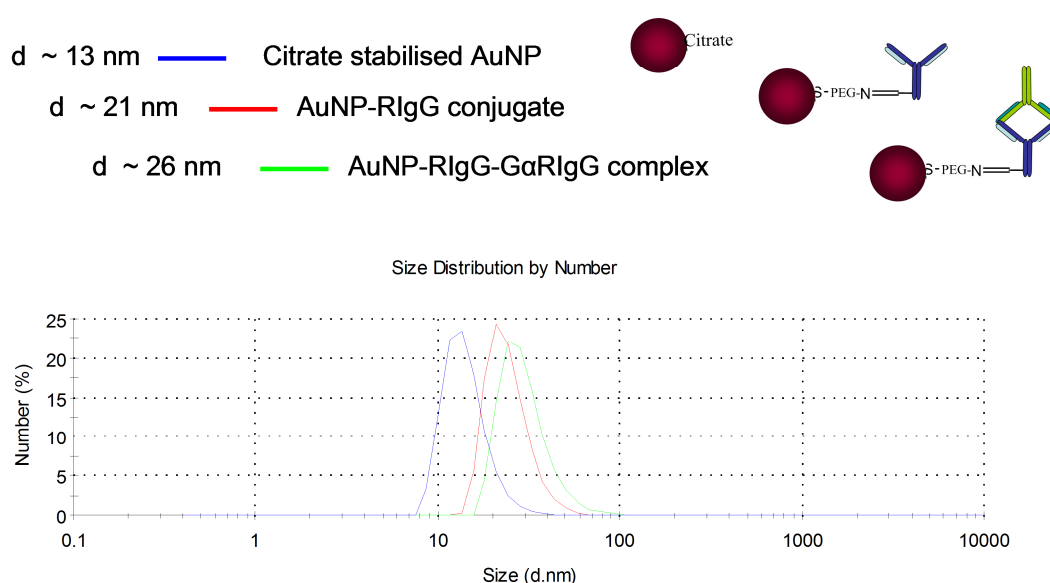


Figure 5.38: Result of DLS measurements (number statistics) of the complex product and the AuNP-RIgG conjugate using the citrate stabilized particles as control.

The measurement result in figure 5.38 shows an increased size of the 13 nm citrate stabilized AuNPs after the formation of conjugate with PEGylated RIgG on conjugate synthesis. The products are 21 nm sized particle conjugates with size increase of about 8 nm. This size increase is a confirmation of an added layer of RIgG on the previous citrate covered particles. Interestingly, a further size increase from the conjugate size to a product size of 26 nm was observed after the reaction of the conjugates with GaRIgG. This suggests an additional covering layer as contributed by the molecules of GaRIgG additionally attached to the particle surface on interacting with the RIgG on the surface.

5.6.3.2 TEM analysis

The intention of the analysis discussed in this section was to investigate the liquid phase formation of aggregates by antibody antigen interaction of two systems. To distinguish between the reacting counterparts systems on imaging by TEM, each of two antibodies with affinity for each other was coupled to gold nanoparticles having differing sizes. For this purpose, AuNP with quite distinguishable sizes of 13 nm and 37 nm were used. The TEM image after mixing the two conjugate solutions is shown in figure 5.40.

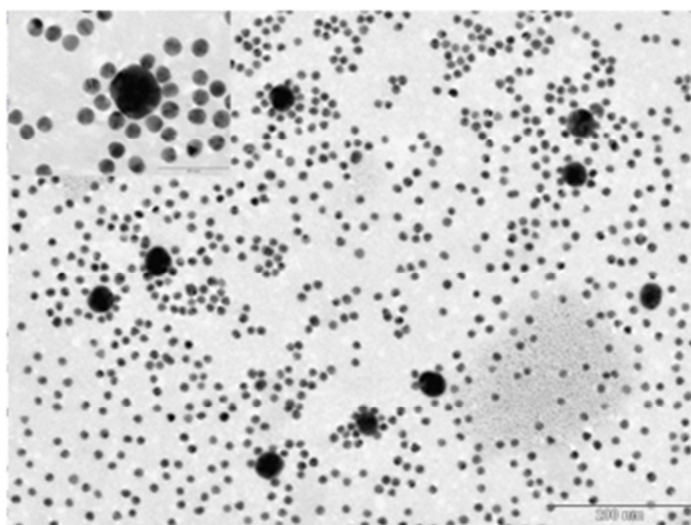


Figure 5.39: TEM image of sample prepared by mixing AuNP conjugates with different antibodies coupled to their surfaces. Gold nanoparticle of differing sizes, 11 nm and 37 nm diameter AuNP were coupled to RIgG and GaRIgG respectively.

The evident of antigen-antibody reactions are the aggregate formations, which could be clearly seen in figure 5.39. The inset shows an enlarged section of the image. The conjugates with smaller Au core particles which are in large excess form a layer on the surface of the larger particles. This is a clear evident of the antigen-antibody interaction of the conjugates in solution.

6. CONCLUSION

The fabrication of LFIA using AuNP as optical sensor is, in the past, based on AuNP-antibody conjugates prepared by physical attachments of the antibodies on the AuNP surface. In this thesis, the coupling of AuNP to antibodies via their Fc-glycan moiety using thiolated PEG ligands having varied molecular weights as linkers was carried out. This is done to obtain covalently coupled conjugates as means for achieving higher stability and better coverage of the AuNP by IgGs having orientations on the particle surface suitability for LFIA performance enhancement. Starting by using a modified seeded-growth protocol for the synthesis of 10 nm to over 60 nm citrate stabilized AuNPs, varieties of conjugates having varying AuNP core sizes with varying PEG linkers lengths, were successfully synthesized. The obtained products were characterized and their various properties were studied. Accordingly, investigations of the influence of the AuNP core size and the influence of linker length on various conjugates properties necessary for their LFIA application were carried out. The investigations that followed were made to exploit means of achieving optimized LFIA systems on the AuNP basis. Focus was on improving the performance of the conventional test systems by the use of chemically and nanotechnologically based methods.

The synthesis of the conjugates were done using citrate stabilized AuNP and rabbit IgG (RIgG) or goat anti-rabbit IgG (G α RIgG) depending on the intended investigation. For instance, for tests involving conjugates' immune reactivity, the G α RIgG was attached to the particle surface while the RIgG was used as antigen immobilized on NC-membrane, attached on particles' surfaces or just present in solution. To cut down cost, RIgG was mostly conjugated to AuNP for use in experiments involving coverage and stability investigations since their costs are comparable lower than that for G α RIgG.

Results obtained showed that systems with longer PEG linker lengths have higher stabilities. In other words, stability increases with linker length. The covalently coupled AuNP antibody conjugates were stable in ionic environment as high as 4M NaCl solution without any observable change in optical properties when investigated with the UV-Vis spectrometry.

The coverage of the particles investigated was found to be affected by the ligand's length but almost constant with varying core particle's size. Although an anomaly character was observed for the 3 kDa PEG linker on particles with smaller size ($d \sim 10$ nm). In most cases where this linker was used for conjugate of small size particles, they exhibited high

instability. This was attributed to the “Bulky Cap” effect discussed in section 5.4.4 of this thesis.

While ligands with longer PEG chains occupied larger surface area on the AuNP, they showed reduced ligand/particle ratios values proportional to the length of the PEG linker.

LFIA are based on accumulation concept, where test samples flow along the nitrocellulose membrane via capillary action. Depending on the presence of analytes in the sample, the AuNP conjugate could become bound onto the membrane after antigen-antibody reactions. In this way, they accumulate at the test line or zone as red colored particles. The analytes (reaction partners) are thus detected at low concentration. In this work, the gold nanoparticle antibody conjugates showed very good antigen-antibody activity and were capable to detect analytes which were immobilized on NC-membrane. They were found to detect antigen concentrations as low as 6 pM concentration. There is every tendency to push this limit lower by additional investigations involving adjustments and fine-tuning of parameters. Specifically, one of the parameters that could be finely tuned is the particle size for optimal optical performance. Results in this thesis show that the larger particles above 60 nm resulted in high background reactions (colouring) on the NC-membrane during the dot blot test. An improvement could be achieved, if this effect could be taken care of, so that particles in the bigger size denominations could successfully be tested for this purpose.

7. REFERENCES

- [1] Eustis S. and El-Sayed M.A., *Chemical Society Reviews*, **2006**, 35, 209.
- [2] Daniel M. C., Astruc D., *Chemical Reviews* **2004**, 104, 293.
- [3] Liz-Marzán L. M., *Langmuir*, **2006**, 22, 32.
- [4] Link S and El-Sayed M A, *J. Phys. Chem. B*, **1999**, 103, 4212.
- [5] Nie S., Emory S. R. *Science*, **1997**, 275, 1102.
- [6] Rosi N. L. et al., *Science*, **2006**, 312, 1027.
- [7] Sperling R. A. et al., *J. Chem. Soc. Rev.*, **2008**, 37, 1896.
- [8] Grzelczak M., et al., *Chem. Soc. Rev.* **2008**, 37, 1783.
- [9] West J. L., Halas N. J., *Annual Review of Biomedical Engineering*, **2003**, 5, 285.
- [10] Pavlov V. et al., *Journal of the American Chemical Society*, **2004**, 126, 11768.
- [11] Raschke G. et al., *Trends in Optics and Photonics*, **2004**, 96.
- [12] Posthuma-Trumpie G. A., Korfván J., Amerongen A., *Anal. Bioanal. Chem.*, **2009**, 393, 569.
- [13] Peruski A. H., Peruski L. F. Jr., *Clinical and diagnostic lab. immunology*, **2003**, 10, 506.
- [14] Ayong L. S. et al. *Trop. Med. Int. Health*, **2005**, 10, 228.
- [15] Delmulle B. S. et al., *J. Agric. Food Chem.*, **2005**, 53, 3364.
- [16] M. Mettler et al., *J. Clinl. Microbiol.*, **2005**, 43, 5515.
- [17] Hoffman T. J. et al., *Journal of Nuclear Medicine*, **1996**, 37, 850.
- [18] Hoffman T.J., T.P. Quinn, W.A. Volkert, *Nucl Med Biol*, **2001**, 28, 527.
- [19] Karra S.R. et al., *Bioconjug. Chem*, **1999**, 10, 254.
- [20] Hu F. et al., *Nuclear Medicine and Biology*, **2002**, 29, 423.
- [21] David S. Hage, *Methods in Molecular Biology*, **2000**, 147, 69.
- [22] Billman J. H., Diesing A. C., *J. Org. Chem.*, **1957**, 22, 1068.

- [23] Kreibig U., Vollmer M., *Optical Properties of Metal Clusters* Springer, Berlin, **1995**.
- [24] Prashant K. J., El-Sayed M A., *J. Phys. Chem. C* **2008**, *112*, 4954.
- [25] Kelly K. L. et al. *J. Phys. Chem. B* **2003**, *107*, 668.
- [26] El-Sayed M. A., *Acc Chem Res*, **2001**, *34*, 257.
- [27] Link S., El-Sayed M. A., *Int Rev Phys Chem*, **2000**, *19*, 409.
- [28] Link S, El-Sayed M. A., *Annu Rev Phys Chem*, **2003**, *54*, 331, 668.
- [29] Jain P.K et al., *J Phys Chem B*, **2006**, *110*, 7238.
- [30] Underwood S, Mulvaney P, *Langmuir*, **1994**, *10*, 3427.
- [31] Ghosh S. K., Nath S., Kundu S., Esumi K., Pal T., *J Phys Chem B* **2004**, *108*, 13963.
- [32] Rechberger W. et al., *Opt. Commun*, **2003**, *220*, 137.
- [33] Jain P.K, Qian W, El-Sayed MA, *J Phys Chem B*, **2006**, *110*, 136.
- [34] Jain P. K., Eustis S, El-Sayed MA, *J Phys Chem B*, **2006**, *110*, 18243.
- [35] Su K. H. et al., *Nano Lett*, **2003**, *3*, 1087.
- [36] Storhoff J. J. et al., *J Am Chem Soc*, **2000**, *22*, 4640.
- [37] Mie G., *Ann. Phys.* **1908**, *25*, 377.
- [38] Kerker, M., *The Scattering of Light and Other Electromagnetic Radiation*; Academic Press: New York, **1969**.
- [39] Bohren C. F., Huffman D. R., *Absorption and Scattering of Light by Small Particles*, Wiley, New York, **1983**.
- [40] Mulvaney, P., *Langmuir* **1996**, *12*, 788.
- [41] Kittel, C., *Introduction to Solid State Physics*, Wiley, New York, **1996**.
- [42] Kopitzki, K., *Einführung in die Festkörperphysik*, 3.Ed. 184. **1993**, BG Teubner Verlag.
- [43] Ashcroft, N.W., Mermin N.D., *Solid State Physics*, International edition, 17.
- [44] Papavassiliou G. C., *Prog. Solid State Chem.*, **1980**, *12*, 185.

- [45] Kreibig, U.; Vollmer, M. *Optical Properties of Metal Clusters*, Springer, Berlin, **1995**.
- [46] Bohren, C. F., Huffman, D. R., *Absorption and Scattering of Light by Small Particles*, Wiley-Interscience, New York, **1983**.
- [47] Hulst, H.C.v.d., *Light Scattering by Small Particles*, **1981**, Dover Publications.
- [48] Jain K. P., Huang X., El-sayed I. H., *Plasmonics*, **2007**, 2, 107.
- [48] Arruebo M., Valladares M., González-Fernández Á., *Journal of Nanomaterials*, **2009**, 1.
- [50] Bennett C., Konigsberg W. H., Edelman G. M., *Biochemistry*, **1970**, 9, 3181.
- [51] Lesk A. M., Chothia C., *Journal of Molecular Biology*, **1982**, 160, 325.
- [52] Siskind G.W., *Uremia Investigation*, **1984**, 8, 179.
- [53] Bell D. A., Hahn B., Harkiss G., *Lupus*, **1992**, 1, 335.
- [54] Burton D. R., Gregory L., Jefferis R., *Monographs in Allergy*, **1986**, 19, 7.
- [55] Alberts B., Johnson A., Bray D., *Molecular Biology of the Cell*, Taylor and Francis, London, UK, **1989**.
- [56] Kabat E. A., Wu T. T., Bilofsky H., *The Journal of Biological Chemistry*, **1977**, 252, 6609.
- [57] Kabat E. A., *Advances in Protein Chemistry*, **1978**, 32, 1.
- [58] Mizuochi T., Taniguchi T., Shimizu A., Kobata A., *J Immunol*, **1982**, 129, 2016.
- [59] Rademacher T. W, Dwek R. A. *Progress in Immunology* **1983**, 5, 95.
- [60] Rademacher T. et al., *Biochem. Soc. Trans.*, **1982**, 11, 132.
- [61] Diesenhofer et al., *J. Biochemistry*, **1981**, 20, 2361.
- [62] Sutton B. J., Phillips D. C., *Biochem. Soc. Trans.*, **1983**, 11, 130.
- [63] Kornfeld R., Keller J., Baenziger J., S. Kornfeld, *J. Biol. Chem.*, **1971**, 246, 3259.
- [64] Kohn J., *An immunochromatographic technique. Immunology* **1968**. 15, 863.
- [65] Posthuma-Trumpie G. A., Korf J., van Amerongen A., *Anal. Bioanal. Chem.*, **2009**, 393, 569.
- [66] Ayong, L.S. et al. *Trop. Med. Int. Health*, **2005**, 10, 228.

- [67] Delmulle B.S., et al., *J. Agric. Food Chem.* **2005**, 53, 3364.
- [68] Mettler, M et al., *J. Clin. Microbiol.* **2005**, 43, 5515.
- [69] Peruski A. H., Peruski L. F. Jr., *Clinl and diagnostic laboratory immunology*, **2003**, 10, 506.
- [70] Posthuma-Trumpie, G. A., Korf, J., van Amerongen, A. *Anal. Bioanal. Chem.* **2009**, 393, 569.
- [71] Ahmadi, T. S. et al., *Science* **1996**, 272, 1924.
- [72] Turkevich J., *Gold Bull*, **1985**, 18, 86.
- [73] Turkevich, J., Stevenson, P. C.; Hillier, J. *J. of Phy. Chem.* **1953**, 57, 670.
- [74] Narayanan R., El-Sayed M. A., *J. Phys. Chem., B* **2005**, 109, 12663.
- [75] Sun, Y.; Xia, Y., *Science*, **2002**, 298, 5601, 2176.
- [76] Frens, G., *Nature, Physical Science*, **1973**, 241, 20.
- [77] Wilson O. M. et al., *Phy. Rev. B* **2002**, 66, 224301.
- [78] Mayer A. B. R., Mark J. E., *European Polymer Journal*, **1998**, 34, 103.
- [79] Hostetler, M. J. et al., *Langmuir* **1998**, 14, 17.
- [80] Pillai Z. S., Kamat, P. V., *J. Phys. Chem. B*, **2004**, 108, 945.
- [81] Cassagneau T., Fendler J. H., *J.Phys. Chem. B*, **1999**, 103, 1789.
- [82] Richter, R. S., *Advanced Materials*, **2000**, 12, 507.
- [83] Lin, C. S., Khan, M. R.; Lin, S. D., *J. of Colloid and Interface Sci.*, **2005**, 287, 366.
- [84] Schmid, G., *Chem. Rev.*, **1992**, 92, 1709.
- [85] S K Balasubramanian et al., *Biomaterials*, **2010**, 31, 9023.
- [86] Kumar S, Gandhi K S, Kumar R, *Ind Eng Chem Res*, **2007**, 46, 3128.
- [87] Keating C. D., Kovalski K. M., Natan M. J., *J. Phys. Chem. B*, **1998**, 102, 9404.
- [88] Chen Y. H., Nickel U., *J. Chem. Soc.* **1993**, 89, 2479.
- [89] Christopher Roos, M., *Advanced Materials*, **1999**, 11, 9, 761.
- [90] Kamat, P. V., Shanghavi, B., *J. Phys. Chem. B*, **1997**, 101, 7675.

- [91] Johnson S. R., Evans S. D., Brydson R., *Langmuir*, **1998**, *14*, 6639.
- [92] Badia A., et al., *Langmuir* **1996**, *12*, 1262.
- [93] Brust, M. et al., R., *Chemical Communications*, **1994**, *7*, 801.
- [94] Pellegrino, T. et al., *Small*, **2005**, *1*, 48.
- [95] Sperling R. A., et al., *Adv. Funct. Mater.*, **2006**, *16*, 943.
- [96] Hong R. et al., *J. Am. Chem. Soc.* **2006**, *128*, 1078.
- [97] Tkachenko A. G. et al., *J. Am. Chem. Soc.*, **2003**, *125*, 4700.
- [98] Tkachenko A. G. et al. *Bioconjugate Chem.*, **2004**, *15*, 482.
- [99] Sokolov K et al., *Technol Cancer Res Treat.*, **2003**, *2*, 491..
- [100] Elghanian R. et al., *Science*, 1997, *277*, 1078.
- [101] Collings, A. F., Caruso, F. *Reports Progress Physics*, **1997**, *60*, 1397.
- [102] Rao, S. V., Anderson, K. W., Bachas, L. G. *Microchim. Acta*, **1998**, *128*, 127.
- [103] Scouten, W. H. et al., *Trends Biotechnol.*, **1995**, *13*, 178.
- [104] Faulk W. P., Taylor G. M., *Immunochemistry*, **1971**, *8*, 1081.
- [105] Hayat M., Coll. Gold: Principles, Mtds, Applications. Academic, San Diego, CA, 1989.
- [106] Mukherjee P, Sastry M, Kumar R, *Phys. Chem. Com.*, **2000**, *4*, 15.
- [107] Beesley, J. *Coll. Gold*, A new perspective for cytochemical marking. Royal Microscopical Society Handbook No 17; Oxford University Press: Oxford, U.K., **1989**.
- [108] Bruchez M. Jr., Moronne M., Gin P., Weiss S., Alivisatos A. P., *Science* **1998**, *281*, 2013.
- [109] Sondi I., Siiman O., Koester S., Matijevic E., *Langmuir*, **2000**, *16*, 3107.
- [110] Soukka T., Harma H., Paukkunen J., Lovgren T., *Anal. Chem.*, **2001**, *73*, 2254.
- [111] Xu C et al., *J. Am. Chem. Soc.*, **2004**, *126*, 3392.
- [112] Caruso F. *Adv. Mater.*, **2001**, *13*, 11.
- [113] Droz E., et al., *J. Vacuum Sci. Technol. B*, **1996**, *14*, 1422.

- [114] Ghosh S. S., Kao P. M., McCue A. W., Chappelle, H. L. *Bioconj. Chem.*, **1990**, 1, 71.
- [115] O'Shannessy D. J., Quarles R. H., *J. Immunol. Methods*, **1987**, 99, 153.
- [116] Fasman, G. D. *Practical Handbook of Biochemistry and Molecular Biology*, **1989**, CRC Press, Boca Raton, Florida, 13.
- [117] Hermanson G. T., *Bioconjugate Techniques*. New York: Academic Press; **1996**.
- [118] Ebelle R. et al., *Clinical Immunology*, **2002**, 105, 141.
- [119] Aslam M, Dent A. H., *Bioconjugation: protein coupling techniques for the biomedical sciences*. Houndsmills, Macmillan Publishers; **1999**.
- [120] Wong S. S., *Chemistry of protein conjugation and crosslinking*,. Boca Raton, FL, CRC Press, **1991**.
- [121] Loun, B., Hage, DS, *Anal. Chem.*, **1994**, 66, 3814.
- [122] Ghose T. I., Blair A. H., Kulkarni P. N., *Methods Enzymol.*, **1983**, 93, 280.
- [123] Mohr P., Holtzhauer M., Kaiser, G., *Immunosorption Techniques Fundamentals and Applications*, 1st ed., 40. Akademie Verlag, Berlin, **1992**.
- [124] Ruhn P. F., Garver S., Hage D. F., *J. Chromatogr. A*, **1994**, 669, 9.
- [125] Berne and Pecora, *Dynamic Light scattering*, John Wiley, **1975**.
- [126] Hunter, R. J., *Foundations of Coll. Science*, Oxford University Press, **1989**, 1.
- [127] Henry D. C. *Proc Roy Soc*, **1931**, 133A, 10.
- [128] Templeton, A. C.; Wuelfing, W. P.; Murray, R. W. *Acc. Chem. Res.* **2000**, 33, 27.
- [129] N. G. Bastús, *Ph.D. Thesis*, Universitat de Barcelona, Barcelona, Spain, **2008**.
- [130] Haiss W. et al., *Anal. Chem.* **2007**, 79, 4215.
- [131] Kuma S., Aaron J., Sokolov K., *Nature Protocols*, **2008**, 3, 314
- [132] Jacobsen N. W., Dickinson R. G., *Analytical Chemistry*, **1974**, 46, 298.
- [133] Bradford M.M., *Anal. Biochem.*, **1976**, 72, 248.

- [134] Meyer et.al., *Biochim. Biophys. Acta*, **1965**, 107, 144.
- [135] Bohren, C. F., Huffman, D. R., *Absorption and scattering of light by small particles*, Wiley, New York, **1983**.
- [136] Link S., El-Sayed M. A., *J. Phys. Chem B*, **1999**, 103, 8410.
- [137] Jacobsen N. W., Dickinson R. G., *Analytical Chemistry* **1974**, 46, 298.
- [138] Hill R. J., *Phys. Rev. E*, **2004**, 70, 051406.
- [139] Jans H, Lui X, Austin L, Maes G, Huo Q., *Anal. Chem.*, **2009**, 81, 9425.
- [140] Imberechts H et al., *J. Nanopart. Res.*, **2008**, 10, 143.
- [141] Napper D., Netchey A., *J. Colloid Interf. Sci.*, **1971**, 37, 528.
- [142] van Oss C., *Annu. Rev. Microbiol.*, **1978**, 32, 19.
- [143] Abuchowski A., Van Es T., Palczuk N., Davis F., *J. Biol. Chem.*, **1977**, 252, 3578.
- [144] Hermanson G. T., *Bioconjugate Techniques*, **2008**, 24.
- [145] Jans H. et al., *Anal. Chem.*, **2009**, 81, 9425.
- [146] Stakenborg T. et al., *J Nanopart Res*, **2008**, 10, 143.
- [147] Hackley V. A., et al., *Langmuir*, **2010**, 26, 10325.
- [148] Reghan J. H., *Phys. Rev. E*, **2004**, 70, 051406.
- [149] Cohen J. A., Khorosheva V. A., *Colloids and Surfaces*, **2001**, 195, 113.
- [150] Marc et al., *J Neuroscience*, **1995**, 15, 5106.
- [151] Niess, U., *J Bacteriol*, **2004**, 186, 3640.
- [152] Thiry M. et al., *America. Chem. Society*, **2011**, 5, 4965.
- [153] Pease, L. F., et al., *J.Phys. Chem. C* **2007**, 111, 17155.
- [154] Link S., El-sayed M. A., *Reviews in Physical Chemistry*, **2000**, 19, 409.
- [155] Henglein A., **1993**, *J. phys. Chem.*, 97, 8457.
- [156] Mulvaney P., *Langmuir*, **1996**, 12, 788.

- [157] Kreibig U., Genzel U., *Surf. Sci.*, **1985**, 156, 678.
- [158] Kreibig U., Gartz M., Hilger A., *Ber. Bunsenges. Phys. Chem.*, **1997**, 101, 1593.
- [159] Persson N. J., *Surf. Sci.*, **1993**, 281, 153.
- [160] Linnert T., Mulvaney P., Henglein A., **1993**, *J. Phys. Chem.*, 97, 679.
- [161] Vollmer M. et al., *Phys. Rev.*, **1993**, 48, 18178.
- [162] Wu et al. *J. Microcolumn Separations*, **2001**, 13, 322.

Risks and Safety Statements:

Chemicals

Chemical [Hazard Codes]	Risk Statements	Safety Statements
Diethylether [F+, Xn]	R 12-19-22-66-67	S 9-16-29-33
Ethanol [F]	R 11	S 7-16
Ethyl Acrylate [F,Xn]	11-20/21/22-36/37/38-43	9-16-33-36/37
Gold (III) chloride [Xi]	R 36/37/38	S 26-36
Gold (III) chloride trihydrate [C]	R 34-43	S 26-27-36/37/39-45
Calcium carbonate [Xi]	R 36/37/38	S 22-26
Methanol[F, T]	R 11-23/24/25-39	S 7-16-36/37-45
Sodium azid [T+, N]	R 28-32-50/53	S 28.1-45-60-61
Sodiumborohydride [T, F]	R 15-24/25-35	R 14.2-26-36/37/39-43.6-45
Sodium carbonate [Xi]	R 36	S 22-26
Sodiumcyanoborohydride [F, C]	R 15-32-34	S 26-36/37/39-43-45
Sodium hydroxide [C]	R 45	S 26-37/39-45
Sodium phosphate [C]	R 34	26-36/37/39-45
Sodium (meta)periodate [O,Xn]	8-22-36/37/38	26
Sulfuric acid [C]	R 35	S-26-30-45
Hydrogen Chloride [C]	R 34-37	S 26-36/37/39-45
Pentaerythritol tetrakis(3-mercaptopropionate) [Xi]	R 36/37/38	R 26-36
Purpald [Xi]	R 36/37/38	S 26-36
Tetrabutylammonium bromide [Xi]	R 36/37/38	S 26-36
Tetraoctylammoniumbromid [Xi]	R 36/37/38	S 26-36
Toluene [F, Xn]	R 11-38-48/20-63-65-67	S 36/37-46-62

Hazard Codes

B	Biohazard
C	Corrosive
E	Explosive
F	Highly Flammable
F+	Extremely Flammable
Xn	Harmful
Xi	Irritant
N	Dangerous for the environment
O	Oxidizing
R	Radioactive
T	Toxic
T+	Very Toxic

R-Phrases

R1 : Explosive when dry

R2 : Risk of explosion by shock, friction, fire or other source of ignition

R3 : Extreme risk of explosion by shock, friction, fire or other source of ignition

R4 : Forms very sensitive explosive metallic compounds

R5 : Heating may cause an explosion

R6 : Explosive with or without contact with air

R7 : May cause fire

R8 : Contact with combustible material may cause fire

R9 : Explosive when mixed with combustible material

R10: Flammable

R11: Highly flammable

R12: Extremely flammable

R13: Extremely flammable liquefied gas

R14: Reacts violently with water

R15: Contact with water liberates highly flammable gases

R16: Explosive when mixed with oxidizing substances

R17: Spontaneously flammable in air

R18: In use, may form flammable/explosive vapor-air mixture

R19: May form explosive peroxides

R20: Harmful by inhalation

R21: Harmful in contact with skin

R22: Harmful if swallowed

R23: Toxic by inhalation

R24: Toxic in contact with skin

R25: Toxic if swallowed

- R26: Very toxic by inhalation
- R27: Very toxic in contact with skin
- R28: Very toxic if swallowed
- R29: Contact with water liberates toxic gas
- R30: Can become highly flammable in use
- R31: Contact with acids liberates toxic gas
- R32: Contact with acids liberates very toxic gas
- R33: Danger of cumulative effects
- R34: Causes burns
- R35: Causes severe burns
- R36: Irritating to eyes
- R37: Irritating to respiratory system
- R38: Irritating to skin
- R39: Danger of very serious irreversible effects
- R40: Possible risk of irreversible effects
- R41: Risk of serious damage to eyes
- R42: May cause sensitization by inhalation
- R43: May cause sensitization by skin contact
- R44: Risk of explosion if heated under confinement
- R45: May cause cancer
- R46: may cause heritable genetic damage
- R47: May cause birth defects
- R48: Danger of serious damage to health by prolonged exposure
- R49: May cause cancer by inhalation
- R50: Very toxic to aquatic organisms
- R51: Toxic to aquatic organisms
- R52: Harmful to aquatic organisms

R53: May cause long-term adverse effects in the aquatic environment

R54: Toxic to flora

R55: Toxic to fauna

R56: Toxic to soil organisms

R57: Toxic to bees

R58: May cause long-term adverse effects in the environment

R59: Dangerous to the ozone layer

R60: May impair fertility

R61: May cause harm to the unborn child

R62: Possible risk of impaired fertility

R63: Possible risk of harm to the unborn child

R64: May cause harm to breast-fed babies

R65 Harmful: may cause lung damage if swallowed

R66 Repeated exposure may cause skin dryness or cracking

R67 Vapors may cause drowsiness and dizziness

R68 May cause irreversible effects

Combinations of R-Phrases

R14/15: Reacts violently with water liberating highly flammable gases

R15/29: Contact with water liberates toxic, highly flammable gas

R20/21: Harmful by inhalation and in contact with the skin

R20/21/22: Harmful by inhalation, in contact with the skin and if swallowed

R20/22: Harmful by inhalation and if swallowed

R21/22: Harmful in contact with the skin and if swallowed

R23/24: Toxic by inhalation and in contact with the skin

R23/24/25: Toxic by inhalation, in contact with the skin and if swallowed

R23/25: Toxic by inhalation and if swallowed

R24/25: Toxic in contact with the skin and if swallowed

R26/27: Very toxic by inhalation and in contact with the skin

R26/27/28: Very toxic by inhalation, in contact with the skin and if swallowed

R26/28: Very toxic by inhalation and if swallowed

R27/28: Very toxic in contact with the skin and if swallowed

R36/37: Irritating to eyes and respiratory system

R36/37/38: Irritating to eyes, respiratory system and skin

R36/38: Irritating to eyes and skin

R37/38: Irritating to respiratory system and skin

R42/43: May cause sensitization by inhalation and skin contact

R48/20: Harmful: danger of serious damage to health by prolonged exposure through inhalation

R48/20/21: Harmful: danger of serious damage to health by prolonged exposure through inhalation and in contact with the skin

R48/20/21/22: Harmful: danger of serious damage to health by prolonged exposure through inhalation, in contact with the skin and if swallowed

R48/20/22: Harmful: danger of serious damage to health by prolonged exposure through inhalation and if swallowed

R48/21: Harmful: danger of serious damage to health by prolonged exposure in contact with skin

R48/21/22: Harmful: danger of serious damage to health by prolonged exposure in contact with skin and if swallowed

R48/22: Harmful: danger of serious damage to health by prolonged exposure if swallowed

R48/23: Toxic: danger of serious damage to health by prolonged exposure through inhalation

R48/23/24: Toxic: danger of serious damage to health by prolonged exposure

through inhalation and in contact with the skin

R48/23/24/25: Toxic: danger of serious damage to health by prolonged exposure through inhalation, in contact with the skin and if swallowed

R48/23/25: Toxic: danger of serious damage to health by prolonged exposure through inhalation and if swallowed

R48/24: Toxic: danger of serious damage to health by prolonged exposure in contact with skin

R48/24/25: Toxic: danger of serious damage to health by prolonged exposure in contact with skin and if swallowed

R48/25: Toxic: danger of serious damage to health by prolonged exposure if swallowed

R50/53: Very toxic to aquatic organisms, may cause long term adverse effects in the aquatic environment

R51/53: Toxic to aquatic organisms, may cause long term adverse effects in the aquatic environment

R52/53: Harmful to aquatic organisms, may cause long term adverse effects in the aquatic environment

R68/20: May cause irreversible effects by inhalation

R68/21: May cause irreversible effects in contact with skin

R68/22: May cause irreversible effects if swallowed

R68/20/21: May cause irreversible effects by inhalation and in contact with skin

R68/20/22 May cause irreversible effects by inhalation and if swallowed

R68/21/22 May cause irreversible effects in contact with skin and if swallowed

R68/20/21/22 May cause irreversible effects by inhalation, in contact with skin and if swallowed

S-Phrases

S1 : Keep locked up

S2 : Keep out of reach of children

S3 : Keep in a cool place

S4 : Keep away from living quarters

S5 : Keep contents under.....(appropriate liquid to be specified by the manufacturer)

1 ... water

2 ... kerosene

3 ... paraffin oil

S6 : Keep under.....(inert gas to be specified by the manufacturer)

1 ... nitrogen

2 ... argon

3 ... carbon dioxide

S7 : Keep container tightly closed

S8 : Keep container dry

S9 : Keep container in a well ventilated place

S12: Do not keep the container sealed

S13: Keep away from food, drink and animal feedstuffs

S14: Keep away from..... (incompatible material to be indicated by the manufacturer)

1 ... reducing agents, heavy metal compounds, acids, alkaline

2 ... oxidizing and acidic substances and heavy metal compounds

3 ... iron

4 ... water and alkaline

5 ... acids

6 ... alkaline

7 ... metals

8 ... oxidizing and acidic substances

9 ... flammable organic substances

10 .. acids, reducing agents and flammable materials

11 .. flammable substances

S15: Keep away from heat

S16: Keep away from sources of ignition - No Smoking!

S17: Keep away from combustible material

S18: Handle and open container with care

S20: When using do not eat or drink

S21: When using do not smoke

S22: Do not breathe dust

S23: Do not breathe gas/fumes/vapor/spray (appropriate wording to be specified
by the manufacturer)

1 ... gas

2 ... vapor

3 ... spray

4 ... fumes

5 ... vapor/spray

S24: Avoid contact with the skin

S25: Avoid contact with eyes

S26: In case of contact with eyes, rinse immediately with plenty of water and seek
medical advice

S27: Take off immediately all contaminated clothing

S28: After contact with skin, wash immediately with plenty of.....(to be specified by
the manufacturer)

1 ... water

2 ... water and soap

3 ... water, soap, and polyethylene glycol 400, if available

4 ... polyethylene glycol 300 and ethanol (2:1), then water and soap

5 ... polyethylene glycol 400

6 ... polyethylene glycol 400, then cleaning with water

7 ... water and acidic soap

S29: Do not empty into drains

S30: Never add water to this product

S33: Take precautionary measures against static discharges

S34: Avoid shock and friction

S35: This material and its container must be disposed of in a safe way

1 ... through treatment with 2% sodium hydroxide

S36: Wear suitable protective clothing

S37: Wear suitable gloves

S38: In case of insufficient ventilation, wear suitable respiratory equipment

S39: Wear eye/face protection

S40: To clean the floor and all objects contaminated by this material use (to be specified by the manufacturer)

S41: In case of fire and/or explosion do not breath fumes

S42: During fumigation /spraying wear suitable respiratory equipment (appropriate wording to be specified by the manufacturer)

S43: In case of fire, use....(indicate in this space the precise type of fire fighting equipment. If water increases the risk, add "never use water")

1 ... water

2 ... water and powder extinguishing agent

3 ... powder extinguishing agent, do not use water

4 ... carbon dioxide, do not use water

6 ... sand, do not use water

7 ... metal extinguishing agent, do not use water

8 ... sand, carbon dioxide, or powder extinguishing agent, do not use water

S44: If you feel unwell, seek medical advice (show the label where possible)

S45: In case of accident or if you feel unwell, seek medical advice immediately
(show the label where possible)

S46: If swallowed, seek medical advice immediately and show the container or
label

S47: Keep at temperature not exceeding °C (to be specified by the
manufacturer)

S48: Keep wetted with (appropriate material to be specified by the
manufacturer)

S49: Keep only in the original container

S50: Do not mix with... (to be specified by the manufacturer)

1 ... acids

2 ... alkaline

3 ... strong acids, strong alkaline, heavy metals and their salts

S51: Use only in well ventilated areas

S52: Not recommended for interior use on large surface areas

S53: Avoid exposure - obtain special instructions before use

S54: Obtain the consent of pollution control authorities before discharging to
waste-water treatment plants

S55: Treat using the best available techniques before discharge into drains or the
aquatic environment

S56: Do not discharge into drains or the environment, dispose to an authorised
waste collection point

S57: Use appropriate containment to avoid environmental contamination

S58: To be disposed of as hazardous waste

S59: Refer to manufacturer/supplier for information on recovery/recycling

S60: This material and/or its container must be disposed of as hazardous waste

S61: Avoid release to the environment. Refer to special instructions/ material safety data sheet

S62: If swallowed, do not induce vomiting: seek medical advice immediately and show the container or label

S63: In case of accident by inhalation: remove casualty to fresh air and keep at rest

S64: If swallowed, rinse mouth with water (only if the person is conscious)

Combinations of S-Phrases

S1/2: Keep locked up and out of reach of children

S3/9: Keep in a cool, well ventilated place

S3/7/9: Keep container tightly closed in a cool, well ventilated place

S3/14: Keep in a cool place away from..... (incompatible materials to be indicated by the manufacturer)

1 ... reducing agents, heavy metal compounds, acids, alkaline

2 ... oxidizing and acidic substances and heavy metal compounds

3 ... iron

4 ... water and alkaline

5 ... acids

6 ... alkaline

7 ... metals

8 ... oxidizing and acidic substances

S3/9/14: Keep in a cool, well ventilated place away from. (incompatible

materials to be indicated by the manufacturer)

- 1 ... reducing agents, heavy metal compounds, acids, alkaline
- 2 ... oxidizing and acidic substances and heavy metal compounds
- 3 ... iron
- 4 ... water and alkaline
- 5 ... acids
- 6 ... alkaline
- 7 ... metals
- 8 ... oxidizing and acidic substances

S3/9/49: Keep only in the original container in a cool, well ventilated place

S3/9/14/49: Keep only in the original container in a cool, well ventilated place away from.

(incompatible materials to be indicated by the manufacturer)

- 1 ... reducing agents, heavy metal compounds, acids, alkaline
- 2 ... oxidizing and acidic substances and heavy metal compounds
- 3 ... iron
- 4 ... water and alkaline
- 5 ... acids
- 6 ... alkaline
- 7 ... metals
- 8 ... oxidizing and acidic substances

S3/14: Keep in a cool place away from.....(incompatible materials to be indicated by the manufacturer)

S7/8: Keep container tightly closed and dry

S7/9: Keep container tightly closed and in a well ventilated place

S7/47: Keep container tightly closed and at a temperature not exceeding °C (to be specified by the manufacturer)

S20/21: When using do not eat, drink or smoke

S24/25: Avoid contact with skin and eyes

S27/28 Take off immediately all contaminated clothing. After contact with skin, wash immediately with plenty of(to be specified by the manufacturer)

S29/35 Do not empty into drains. This material and its container must be disposed of in a safe way.

S29/56: Do not empty into drains: dispose of this material and its container to hazardous or special waste collection point

S36/37: Wear suitable protective clothing and gloves

S36/37/39: Wear suitable protective clothing, gloves and eye/face protection

S36/39: Wear suitable protective clothing and eye/face protection

S37/39: Wear suitable gloves and eye/face protection

S47/49: Keep only in the original container at a temperature not exceeding °C
(to be specified by the manufacturer)

ACKNOWLEDGEMENTS

I am indebted to many people who helped me through this journey of graduate studies. Foremost, I would like to express my profound gratitude to Prof. Dr. Horst Weller, who gave me the opportunity to work and enabled this successful thesis in his group. This journey could not be possible without his financial support and the various discussions with him that helped to finish this thesis.

I owe special debt of gratitude to my closer research advisor Dr. Tobias Vossmeier for his kind and helpful supervision. I could not have enjoyed a better supervision enriched with friendship, patience, constant encouragement and unending enthusiasm for efficiency. I will always remember that door you opened to this important career.

Prof. Dr. Moritz Hans-Ulrich, Prof. Dr. J. A. C. Broekaert and Dr. Mrs. Brita Werner for readily accepting to referee this thesis.

I am grateful to Dr. Theo Schotten and Katja Werner for giving me the opportunity to work with them in the interdisciplinary projects with CAN GmbH Hamburg.

Practical and research students whom I enjoyed time with in the lab and hours of fruitful discussion. It was all interesting, giving and taking from you; Inga Reimer, Alexandra Bey, Dino Behn, Hendrik Schlicke, Baldur Schroeter who contributed so much time and effort to the work in the laboratory.

A million thank to those brilliant scientist: K. Boldt, M. Thiry, Hendrik Schlicke, Jan H. Schröder for their efforts that successfully yielded publications. I am grateful for the opportunity to be part of it all.

This thesis could not have been completed without the support of the friendly workers in the working group of Prof. Dr. Horst Weller, who assisted me in diversified ways; Dr. Kathrin Hoppe for the helpful dispositions, Andreas Kornowski and Mrs. Sylvia Bartholdi-Nawrath for the assistance with TEM, Mrs. Almut Barck and Petra Schulz for always being so nice and friendly, Mrs. Beate Kreutzer und Mrs. S. Zeckert for those rescuing moments whenever there was bureaucratic needs and Mr. Frank Bürli for all the assistance. My debt of gratitude extends to other colleagues and doctorate students. Ulli Tromsdorf, Andjana Panicker, Sebastian Sanders, Florian Schulz and Mona Nagel among other group members who made my time in the working group a fulfillment.

Michael Sartor is greatly indebted for being a friend “in did and in need” all through the time. The readiness to read this thesis together with Florian Schulz and the help translating the abstract are greatly appreciated.

All through the entire process, the support of my family was steadfast. The daily grind was made bearable with the support and the motivation enjoyed from my wife Margret, son Noah, daughter Alicia and Mom Catherine. Their understanding was, all through fantastic!

Personal data:

First Name:	Michael
Last Name:	Ijeh
Middle Name:	Onuwa
Residence:	Reinckeweg 7, 22399 Hamburg
Date of Birth:	25.03.70
Place of Birth:	Otolokpo, Delta State, Nigeria
Marital Status:	Married, 2 Children
Nationality:	German

Post Graduate studies:

01.11.2009 – 30.11.2011	PhD student in Prof. Horst Weller's working Group, Physical Chemistry Department, University of Hamburg. Topic of Thesis: Covalent gold nanoparticle-antibody conjugates for sensitivity improvement in LFIA.
-------------------------	--

University Studies:

2007-2008	Master thesis in Prof. Horst Weller's working group, Physical Chemistry Department, University of Hamburg. Topic of Thesis: Fabrication of gold nanoparticle films on flexible polyethylene substrates and a study of their electrical properties.
2004-2007	Studies at the Department of Chemistry, University of Hamburg.
1987-1991	Bachelor Studies Dept. of Biochemistry Bendel State University, Ekpoma, Nigeria.

Educational Background:

1987	JAMB (Joint Admissions and matriculation Board).
1982-1987	St. Anthony's College Ubulu-uku, Delta State, Nigeria.
1976-1982	Azagba Primary School Otolokpo, Delta State, Nigeria.

Work Experience in Nigeria:

1991-1992	Nigerian National Youth Service Corps (NYSC)
1993-1998	Assistant Manager YMS, Management Consultants, Ikeja Lagos

Work Experience in Germany:

01.11.2009 – 30.11.2011	Researcher Scientist University of Hamburg Instructor/supervisor of research groups of undergraduate students at the physical chemistry institute of the University
01.11.2008 – 30.09.2009	Center for Applied Nanotechnology (CAN), Hamburg (scientific worker)

Further Work Experience in Germany:

01.04.07 – 01.03.08	State and University Library, Hamburg.
18.06.02 – 01.09.03	Firma WAW (Assist. Worker)
01.01.02 – 01.03.02	Firma Kasten Meyer (Assist. Worker)
15.03.99 – 31.03.00	Firma Leurs, (Assist. Worker)

Publications:

1. **M Ijeh**, T. Vossmeier and H. Weller, Highly stable and orientationally coupled gold nanoparticle antibody conjugates for sensitivity improvement in LFIA, *Manuscript TechConnect World Nanotech Conference, Boston*, **2011**, ISBN 978-1-4398-7138-6 Vol. 3, 197-200.
2. M. Thiry, K. Boldt, M. S. Nikolic, F. Schulz, **M Ijeh**, A. Panicker, T. Vossmeier, H. Weller, Fluorescence properties of hydrophilic semiconductor nanoparticles with tridentate polyethyleneoxide ligands, *ACS Nano*, **2011**, 5 (6), 4965.
3. Hendrik Schlicke, Jan H. Schröder, Martin Trebbin, **M Ijeh**, Horst Weller, and Tobias Vossmeier, Freestanding films of crosslinked gold nanoparticles prepared via layer-by-layer spin-coating, *Nanotechnology*, **2011**, 22, 305303.
4. German Research Association (DFG) Project: A Report of feasibility study on the fabrication of gold nanoparticle based LFIA for point-of-care diagnosis of the viral tropical disease, Chikungunya-Fieber, **2009**.
5. T. Vossmeier, C. Stolte, **M. Ijeh**, A. Kornowski, H. Weller, Networked Gold-Nanoparticle Coatings on Polyethylene: Charge Transport and Strain Sensitivity, *Adv. Funct. Mater.*, **2008**, 18, 1611.
6. **M Ijeh**, Tobias Vossmeier and Horst Weller, Synthesis, surface analysis and functionality tests of highly stable, site-specific coupled gold nanoparticle antibody conjugates for LFIA improvements. (on press)

Talks:

- Oral Presentation at the international Nanotech Conference (NSTI) in Boston, Massachusetts, USA, Juni **2011**.
- Various internal Präsentations

Declaration

I declare that there was no previous attempt made towards the acquiring of a doctorate degree and that this thesis has not been previously submitted to another academic institution.

Hamburg, November, 2010

.....

Michael Ijeh

I affirm that the above thesis was independently completed by me and that materials herein taken directly or indirectly from external sources were properly marked as such.

Hamburg, November, 2010

.....

Michael Ijeh

.....

Hiermit erkläre ich, dass vorher keine weiteren Promotionsversuche unternommen worden sind, oder an einer anderen Stelle vorgelegt wurden.

Hamburg, November, 2010

.....

Michael Ijeh

Eidesstattliche Versicherung

Hiermit erkläre ich an Eides Statt, dass die Vorlegende Dissertationsschrift selbständig und allein von mir unter den angegebenen Hilfsmitteln angefertigt wurde.

Hamburg, November, 2010

.....

Michael Ijeh